Hermann Luís Lebkuchen

Dynamic Response and Pitch Damper Design for a Moderately Flexible, High-Aspect Ratio Aircraft

Joinville, Brazil

2015

Hermann Luís Lebkuchen

Dynamic Response and Pitch Damper Design for a Moderately Flexible, High-Aspect Ratio Aircraft

Trabalho de Conclusão de Curso apresentado como requisito parcial para obtenção do título de bacharel em Engenharia Aeroespacial no Centro de Engenharias da Mobilidade da Universidade Federal de Santa Catarina, Campus de Joinville.

Universidade Federal de Santa Catarina – UFSC

Centro de Engenharias da Mobilidade

Bacharelado em Engenharia Aeroespacial

Supervisor: Prof. Gian Ricardo Berkenbrock, Dr.

Co-supervisor: Alexander Hamann, Dipl.-Ing.

Prof. Robert Luckner, Dr.-Ing.

Joinville, Brazil

2015

Hermann Luís Lebkuchen

Dynamic Response and Pitch Damper Design for a Moderately Flexible, High-Aspect Ratio Aircraft/ Hermann Luís Lebkuchen. – Joinville, Brazil, 2015-

142 p. : il. (algumas color.) ; 30 cm.

Supervisor: Prof. Gian Ricardo Berkenbrock, Dr.

Trabalho de Conclusão de Curso – Universidade Federal de Santa Catarina – UFSC
Centro de Engenharias da Mobilidade
Bacharelado em Engenharia Aeroespacial, 2015.

1. Aeroelasticity. 2.Aeroservoelasticity. 3.Unsteady Aerodynamics. 4.Structural Dynamics. 5.Ground Vibration Tests. 6.Integrated Models. 7.Flight Dynamics. 8.Flight Control. 9. Pitch Damper. I. Supervisor: Prof. Dr. Gian Ricardo Berkenbrock. Co-Supervisor: Dipl.-Ing. Alexander Hamann, Prof. Dr-Ing. Robert Luckner. II. Universidade Federal de Santa Catarina. III. Centro de Engenharias da Mobilidade. IV. Engenharia Aeroespacial V. Title: Dynamic Response and Pitch Damper Design for a Moderately Flexible, High-Aspect Ratio Aircraft

CDU 02:141:005.7

Hermann Luís Lebkuchen

Dynamic Response and Pitch Damper Design for a Moderately Flexible, High-Aspect Ratio Aircraft

Trabalho de Conclusão de Curso apresentado como requisito parcial para obtenção do título de bacharel em Engenharia Aeroespacial no Centro de Engenharias da Mobilidade da Universidade Federal de Santa Catarina, Campus de Joinville.

Trabalho aprovado. Joinville, Brazil, 04 de Dezembro de 2015:

Prof. Gian Ricardo Berkenbrock, Dr.
Orientador

Prof. Antônio Otaviano Dourado, Dr.
Membro 1

Prof. Rafael Gigena Cuenca, MSc.
Membro 2

Joinville, Brazil
2015

To my family and all my professors.

Acknowledgements

Firstly, I would like to express my whole-heartedly thanks to my parents that gave me full support to keep my studies and always motivated me to look forward. Besides that, I would like to express my sincere and special thanks to all of you that in somehow contributed with my education and supported me to achieve the development of this work, specially:

- to the fellow students Cassiano Tecchio and Bruno Backes at Universidade Federal de Santa Catarina, where I had the opportunity to daily meet you guys and share interesting ideas, specially about computational fluid dynamics and aeroacustics;
- to Prof. Dr.ª Viviane Lilian Soethe and Prof. Dr. Gian Ricardo Berkenbrock at Universidade Federal de Santa Catarina in Joinville-SC, who in my point of view are an unwavering example of kindness and partnership in the relation professor-student;
- to Prof. Dr. Carlos Eduardo de Souza, who advised me during my research about parameters fitting techniques for aeroelastic models at Instituto de Aeronáutica e Espaço in São José dos Campos-SP and next gave me the opportunity to internship at company AeroEst, where the preliminary design of an simplified unmanned aerial vehicle to aeroelastic research was carried out;
- to Prof. Dr. Flávio Silvestre, who indicated me to the Institut für Luft- und Raumfahrt at the Technische Universität Berlin (TU Berlin), Fachgebiet Flugmechanik, Flugregelung und Aeroelastizität (FMRA), where I had the opportunity to know interesting people and to increase my technical skills. I had a great time in Berlin and there I developed the most part of this work;
- to Prof. Dr.-Ing. Robert Luckner, Dipl.-Ing. Alexander Hamann and Dipl.-Ing. David Bieniek at TU Berlin and Prof. Dr.-Ing. Wolf-Reiner Krüger at TU Berlin and also at Deutsches Zentrum für Luft- und Raumfahrt (DLR) in Göttingen. Your orientation, patience, willingness to cooperate and interesting to share your vast knowledge in disciplines like flight mechanics, flight control, aeroelasticity, aerodynamics, among others was of great importance for me;

At last I acknowledge all of my family, friends, professors and people that directly or indirectly helped me to complete this work and accompanied me though my life. Any omission in this brief text does not mean lack of gratitude.

"Eppur si muove"
(Galileo Galilei.)

Abstract

This work presents the dynamic response of a slightly flexible hight-aspect-ratio aircraft in time domain and the design of a pitch damper controller to augment pitch moments. The methodology adopted in this work extends the rigid body equations of motion and consider the effects of structural flexibility on the aircraft flight dynamics. The aircraft equations of motion are linearized and a flight control system to augment the pitch rate is designed. Firstly, the methodology to model a slightly flexible hight-aspect-ratio aircraft in time domain is revised. The mean axes reference frame is presented to situate the aircraft in time and space. Next, in order to consider the flexibility effects in the flight dynamics, the linearized structural dynamics in modal coordinates as well as the traditional modal superposition technique are briefly explained. The aerodynamic theory adopted in the methodology is also revised, where the incremental aerodynamic theory with the unsteady strip theory formulation in the time domain based on the Wagner function is described. The equations of motion are written by adding the flexible with rigid body terms. The methodology has been implemented at TU Berlin resulting in the software FlexSim, which was used in this work. Moreover, the linearized equations of motion in state space formulation and the decoupling to model the longitudinal aircraft dynamics are given to design the pitch damper. The controller gains are calculated following the frequency and damping values presented in the flying qualities for piloted aircrafts given by the American Military Specifications MIL-F-8785C. Two aircraft are investigated in this work. The first one is the motor glider Stemme S15, which is referred in this work as the reference aircraft. Since the Stemme S15 has its wing structural properties redesigned without changes in geometry. The Stemme S15 had its name changed to Ecarys ES15. Due this fact, the flight dynamic model is updated, comprehending the second aircraft model. The utility aircraft Ecarys ES15 is investigated using two configurations: with and without attached pods at wing. The structural properties of the aircraft are obtained by means of a linear interpolation of ground vibrations test data (GVT). The results compare the flight dynamic responses of aircraft's rigid body model and the flexible model. The comparison gives the flight dynamic angle rates in pitch, roll and yaw after an input step in aircraft's elevator and rudder controls. Furthermore, the modal amplitudes are also presented and the effects of longitudinal and lateral controls on the excitation of the vibrational modes is shown. The pitch damper is implemented and the variation of system roots is depicted. Besides that, the controller gains for the two aircraft models. The results compare the responses of the rigid aircraft model and the flexible aircraft models to step inputs in elevator and rudder.

Key-words: Aeroelasticity; Aeroservoelasticity; Unsteady Aerodynamics; Structural Dynamics; Ground Vibration Tests; Integrated Models; Flight Dynamics; Flight Control; Pitch Damper.

Resumo

O presente trabalho tem como objetivo investigar a resposta dinâmica de uma aeronave moderadamente flexível com alta razão de aspecto no domínio do tempo e projetar um controlador de resposta de arfagem. Primeiramente, a metodologia aplicada nesse trabalho para modelar os efeitos elásticos da aeronave é revisada. O sistema de coordenadas dos eixos médios é apresentado para situar a aeronave no tempo e espaço. Em seguida, as equações de dinâmica estrutural em coordenadas modais bem como a técnica de superposição modal são brevemente revisadas. Na sequência a teoria aerodinâmica incremental com formulação não estacionária baseada na teoria das faixas é apresentada no domínio do tempo com a função de Wagner. O equacionamento apresentado na revisão da metodologia foi implementado pela TU Berlim no software FlexSim, o qual é utilizado no presente trabalho com o intuito de automatizar a análise aeroelástica. Ademais, com a linearização das equações do movimento o sistema de equações é reescrito na forma de espaço de estados e o sistema de controle é apresentado. As equações linearizadas de primeira ordem são então desacopladas e reescritas para o movimento longitudinal. A aproximação com dois graus de liberdade para o período curto é dada e um sistema de controle em malha fechada é definido. A frequência e o amortecimento das qualidades de voo requeridas para projetar o controlador são definidas com base na especificação militar americana MIL-F-8785C. Duas aeronaves são investigadas no trabalho. A primeira aeronave é o motoplanador Stemme S15, que é considerado como aeronave de referência, devido ao mesmo ser investigado na literatura para validação da metodologia utilizada no presente trabalho. A segunda aeronave é a Ecarys ES15, fruto de modificações nas propriedades estruturais da longarina e da superfície da asa da aeronave Stemme S15. Duas configurações da aeronave Ecarys ES15 são investigadas: com e sem pods fixados na parte inferior da asa. As propriedades estruturais da Ecarys ES15 são obtidas com ensaios de vibração em solo. Os resultados do ensaio são interpolados linearmente sobre toda a geometria da aeronave para consideração dos efeitos elásticos. Os resultados apresentados comparam as respostas dinâmicas das duas aeronaves com modelos de corpo rígido e flexível da estrutura. As variações das velocidades de rolamento, arfagem e guinada são plotadas com comandos no profundor e leme para representar a resposta dinâmica . Além disso, as amplitudes modais são representadas e a relação entre as superfícies de comando e a excitação de modos de vibração simétricos e não simétricos é comentada. Finalmente, o controlador de resposta de arfagem é implementado e os ganhos são calculados. A influência dos efeitos de flexibilidade nas raízes do sistema de equações, bem como na resposta dinâmica são apresentados e a relevância da consideração dos efeitos elásticos da estrutura é justificada.

Palavras-chaves: Aeroelasticidade; Aeroservoelasticidade; Aerodinâmica não Estacionária; Dinâmica Estrutural; Testes de Vibração em Solo; Modelos Integrados; Dinâmica de Voo; Controle de Voo; Controlador de Arfagem.

List of Figures

List of Tables

List of abbreviations and acronyms

MIL	United States Military Standard
FAA	Federal Aviation Administration
TUB	Technische Universität Berlin
FMRA	Fachgebiet Flugmechanik, Flugregelung und Aeroelastizität
EC	Ecarys
CG	Center of Gravity
CM	Center of Mass
MATLAB	Matrix Laboratory
MAC	Mean aerodynamic chord
GVT	Ground Vibration Test
EMA	Experimental Modal Analysis
OMA	Operational Modal Analysis
FEM	Finite Element Model
FCS	Flight Control System
DGOF	Degrees of Freedom
EOM	Equations of Motion
LAPAZ	Luft-Arbeits-Plattform-für-die-Allgemeine-Zivilluftfahrt
EFRE	Europäischer Fonds für regionale Entwicklung
TAS	True air speed
CFD	Computational Fluid Dynamics
SAC	Structure-Aerodynamic Coupling
TUHH	Technische Universität Hamburg-Harburg
HTP	Horizontal tail plane

VTP	Vertial tail plane
CAD	Computer Aided Design
CR	Cruise Flight
RB	Rigid-body
S	Symmetric
A	Asymmetric

List of symbols

Latin Characters:

a	number of degrees of freedom of the discrete structural system
$\mathbf{A}$	system's matrix in state space formulation
$\mathbf{A}_{mod}$	modified system's matrix in state space formulation due to feedback control
b	half wing span
b	in chapter 2, also used as half airfoil's length
$\mathbf{B}$	system's input matrix in state space formulation
c	airfoil's chord
$\bar{c}$	mean aerodynamic chord
$C(k)$	Theodorsen's function (k means reduced frequency)
C	origin of the fixed reference frame in chapter 2
$\mathbf{C}$	system's output matrix in state space formulation
D_{rigid}	aerodynamic drag in subsection 2.1.3
$\mathbf{D}$	structural damping matrix
$\mathbf{D}$	system's feedforward matrix in state space formulation
D	dissipation function
dm	differential element of mass
H	flight altitude
$H_{operational}$	aircraft's operational ceiling
I_x, I_y, I_z	moments of inertia in roll, pitch and yaw axis
I_{yz}, I_{xz}, I_{xy}	products of inertial in roll, pitch and yaw axis
$\mathbf{J}$	inertia tensor
j	imaginary unity, $\sqrt{-1}$

$\mathbf{K}$	stiffness matrix
k	reduced frequency in chapter 2
k	also used in index as counter
$k_{\eta q}$	controller gain from elevator to pitch rate in pitch damper design
$k_{\eta \alpha}$	controller gain from elevator to attack angle in pitch damper design
L_{rigid}	used in Equation 2.37 as lift force
L	Lagrangian, $L = T - U$
L, M, N	used in chapter 3 as the aerodynamic moment components in roll, pitch and yaw axis
L	used in section 3.2 as the aircraft's fuselage length
ℓ^C	circulatory portion of lift per unit span
ℓ^{NC}	non circulatory portion of lift per unit span
$\mathbf{M}$	mass matrix
m	aircraft's mass in chapter 3
m	in chapter 2 used as profile's pitching moment per unit span
m^C	circulatory airfoil's pitching moment per unit span at elastic axis
m^{NC}	non circulatory airfoil's pitching moment per unit span at elastic axis
m_{empty}	aircraft's mass in empty configuration
m_{PL}	aircraft's payload mass
m_{total}	aircraft's mass full filled
n_α	aircraft's load factor response to attack angle in g's per radian
n_e	used as number of chosen elastic modes
$\mathcal{O}_l$	origin of the inertial reference frame
O_M	origin of the mean axes reference frame
$\mathbf{p}$	position vector of a structural element dm relative to the origin of the body reference frame
$\mathbf{p}_d$	elastic displacement of the mass element dm

p, q, r	roll, pitch and yaw angular rates
$\mathbf{p}_r$	position of the mass element dm of the undeformed structure in relation to the point C and elastic displacement $\mathbf{p}_d$
q	vector of the physical coordinates of the discrete elastic system
Q_{rigid}	used in Equation 2.37 as aerodynamic force in $z-$direction
Q	in chapter 2 used for the downwash at the profile's $3/4-$chord position
$\mathbf{Q}_\eta$	vector of generalized forces on the elastic DGOF
$\mathbf{R}$	position vector of the origin of the lifting surface's local body coordinate system relative to the aircraft CG
$\mathbf{R}_0$	position of the aircraft centre of gravity relative to the origin of the inertial reference frame
r_M	distance between the origin of the fixed and the floating reference frames
S	reference wing's area
s	non dimensional time defined in semi-chord traveled lengths
$S(K)$	Sear's function
t	time
T	kinetic energy in subsection 2.1.3
T	
u, v, w	used in chapter 2 as the velocity components in roll, pitch and yaw axis
$\mathbf{u}$	system's input or control vector
U	undisturbed flow velocity
U_G	gravitational potential energy
U_S	deformation energy
V	flight velocity in section 2.3
V_{TAS}	true air speed
$\mathcal{V}$	aircraft's volume
$w_{3/4}$	x -position of the three-quarter-chord point on the local body reference frame

X, Y, Z	aerodynamic force components
$\mathbf{x}$	system's state vector in state space formulation
$\dot{\mathbf{x}}$	system's derivative of the vector with respect to time in state space formulation
$\mathbf{y}$	system's output vector in state space formulation

Greek Characters

α	angle of attack
β	sideslip angle
$\boldsymbol{\beta}$	modal structural damping matrix
δ	control deflection in section 2.2
$\boldsymbol{\epsilon}$	strain tensor
η	elevator command surface
η_e	tracking error
η_F	thrust command
η_k	flaps command
$\boldsymbol{\eta}$	column vector of modal amplitudes, $[\boldsymbol{\eta_1}, \boldsymbol{\eta_2}, \boldsymbol{\eta_3}, \ldots, \boldsymbol{\eta_{n_e}}]^T$
$\bar{\boldsymbol{\eta}}$	vector of modal amplitudes
$\boldsymbol{\eta_k}$	amplitude of the k-th elastic modal shape
$\boldsymbol{\gamma}$	modal stiffness matrix
$\boldsymbol{\Lambda}$	eigenvector matrix of the undamped structural eigenvalue problem
$\bar{\boldsymbol{\Lambda}}$	matrix of eigenvectors of the n_e chosen elastic modes
$\boldsymbol{\mu}$	modal mass matrix
$\boldsymbol{\omega}$	aircraft angular velocity vector relative to the aircraft CG
$\boldsymbol{\omega}_{C/M}$	angular velocity of the reference frame fixed on the undeformed structure relative to the mean axes
ω_{n_k}	natural frequency of the k-th elastic mode
$\omega_{n_{PH}}$	phugoid frequency

$\omega_{n_{SP}}$	short period frequency
$\omega^*_{n_{SP}}$	modified short period frequency (with pitch damper)
ψ, θ, ϕ	Euler's angles from yaw, pitch and roll
Φ	Wagner's Function
$\mathbf{\Phi}$	matrix of elastic modal shapes
$\bar{\mathbf{\Phi}}$	matrix of modal shapes of the n_e chosen elastic mode
$\boldsymbol{\sigma}$	stress tensor
ξ	aileron command
ζ	rudder command
ζ_{n_k}	$k-$th damping of the undamped structural eigenvalue
ζ_{PH}	phugoid damping
ζ_{SP}	short period damping
ζ^*_{PH}	modified phugoid damping
ζ^*_{SP}	modified short period damping

Contents

1 Introduction

1.1 Contextualization

The design of an aircraft is a complex iterative task that involves requirements, sizing, trade studies and analysis to end up with a final concept (CHIOZZOTTO, 2013). Diverse groups work together in order to design all necessary systems to assure that a flight vehicle is capable to fulfill the requirements and perform its flight envelope without compromise safety factors. Among all fields involved into the aircraft design, the disciplines of propulsion, avionics, flight tests, control, aerodynamic and structures work together to find the best design solution available. One of the disciplines that came up as a source of problems in moder aircraft design is the aeroelasticity (DOWELL, 2014).

As defined in Bisplinghoff e Ashley (2013) the aeroelasticity is the discipline that involves the interaction between aerodynamic, inertial and elastic forces. Besides that, if the airplane structure were perfectly rigid, no aeroelastic problems would exist. Modern flight vehicle structures are in most cases very flexible, which is the source of aeroelastic problems. One of the first documented aeroelastic problem in airplane design, according to Bisplinghoff e Ashley (2013) and Fung (2002), dates from the World War I with the biplane military bomber Handley Page 0/400. This aircraft experienced violent oscillations at fuselage and tail surfaces. After that, with the development of the monoplane wing Fokker D-8, problems involving the aircraft's wing like torsion-bending divergence and flutter, loss of aileron effectiveness and changes in load distribution were experienced. With the development of aeronautic industry, the flight speed was increased and aeroelastic problems were even more evidenced, creating the necessity to better understand what kind of physical effects were happening. In the aircraft design history, the aeroelastic phenomenon raised in the aeronautic history as a source of problem (SILVESTRE, 2012). Livne (2003) states that nowadays the consideration of aeroelasticity since the first steps of the aircraft design can bring many benefits like costs reduction, performance improvements, lower weight structures and the ability to explore new concepts.

Collar (1946) represented the aeroelastic phenomena by means of a triangle. Each vertex of this triangle illustrates one of the forces related with aeroelastic phenomena. The forces are: aerodynamic, inertial and elastic. The representation of aeroelasticity by means of the Collar's diagram displays not only static but also dynamic problems. The classical Collar's diagram, presented in Figure 1, can be also expanded to a pyramid in order to account for control forces, in this case the aeroelasticity is commonly defined as aeroservoelasticity (WRIGHT; COOPER, 2015). Barbarino et al. (2011) and Silvestre e Pagliole (2007) state that during the last decades of aeronautic research development, the flexibility of structures has been increased due the adoption of new materials and multidisciplinary optimization methods, such as composites in association

with tailoring techniques, in order to design lighter and strengthen structures. Furthermore, since the flexibility effects may also change the aircraft geometry and consequently the loads distributions, to consider the effects of flexibility into the flight mechanics and control design becomes a substantial task (LOOYE, 2008).

Figure 1: The aeroelastic triangle of forces with addition of control forces.

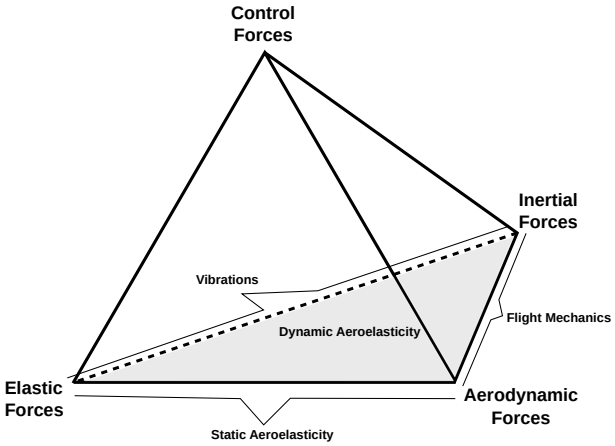

Source: Adapted from (WRIGHT; COOPER, 2015), pg 20 and 202.

Traditionally, the flight mechanics and aeroelasticity are treated aside of each other as presented in Etkin e Reid (1998) and Nelson (1998) for applications to performance, handling qualities and control analysis. For this case, the airplane is assumed as a rigid-body, without consideration of elastic degrees of freedom (DGOF). However, when the structure has significant effects of flexibility, the rigid body frequencies get closer to the frequencies of the elastic DGOF, so that the difference between frequencies of rigid-body and elastic modes is reduced (WASZAK; SCHMIDT, 1988).

The interaction between aeroelasticity and flight mechanics is implemented through the aerodynamic loading and mass distribution. When the aircraft perform dynamic maneuvers, the aerodynamic loading change due to the structural displacements in the volume, modifying the mass distribution and consequently the center of gravity (CG) and moments of inertia. The alteration of aircraft's CG position and moment of inertia modify the aircraft flight dynamic response (WASZAK; DAVIDSON; SCHMIDT, 1987a). The usage of integrated models represents an extension of the rigid body dynamics with the consideration of structural flexibility and mass distributions effects. Milne (1968) started the investigation of flight dynamics of aeroelastic vehicles considering three DGOF, after that CAVIN III e Dusto (1977) used the mean axes references frame to derive the equations of motion of a flexible aircraft using Lagrangian Mechanics, where the structure was represented with finite element models. Moreover, Waszak, Davidson e Schmidt (1987a) and Waszak, Davidson e Schmidt (1987b) simplified the expressions working with the linearized mean axes considering small displacement of the structure. The consideration of small displacements means that the structure displacements are much smaller than the displacement of the aircraft's center of gravity and the linear structural dynamics can be used without losing real

physical characteristics (SILVESTRE; PAGLIOLE, 2007). The formulation derived by Waszak e Schmidt (1988) has been given the ability to implement the model in real time man-in-the-loop simulations, which is adequate to flight simulators. The formulation published by Waszak e Schmidt (1988) was revised by Silvestre e Pagliole (2007) and Looye (2008).

This work makes use of the methodology developed by Silvestre (2012). Silvestre applied the formulation derived by Waszak e Schmidt (1988) and revised by (SILVESTRE; PAGLIOLE, 2007) in time domain for a slightly flexible, hight-aspect ratio aircraft in incompressible flight. The structural dynamic was modeled with Lagrangian Mechanics, with the eigenvectors added by ground vibration tests or finite element models. The incremental unsteady aerodynamic forces were implemented by using the corrected Prandtl-Glauert lifting line and the strip theory based on the Wagner function. This methodology is a suitable way to model the integrated dynamics of the slightly flexible aircraft and to obtain the aircraft linearized equations of motion in order account and design the flight control system (FCS). The methodology developed by Silvestre (2012) was implemented in MATLAB® and had as results the development of the software *FlexSim*. The linearized aircraft equations of motion can be written in the state space arrangement, which is suitable to design feedback controllers to improve flight qualities.

The department of Flight Mechanics, Flight Control and Aeroelasticity (FMRA) at Technische Universität (TU) Berlin developed a flight control system for the utility aircraft Stemme S15, as presented by Silvestre (2013), Kaden B. Boche (2013). The aircraft can be operated automatically, including take off and landing. In this context, a flight dynamic model of the flexible aircraft was built with the methodology developed by Silvestre (2012). The usage of this methodology requires the elastic properties of the aircraft, which can be obtained by a finite element model or by a ground vibration test (GVT). The geometry of the wing of Stemme S15 remained unchanged while the structural properties have been modified. Besides that, the aircraft was renamed as Ecarys (EC) ES15. The modifications were performed in the aircraft's wing spar and shell, modifying the wing's mass, bending stiffness and torsional stiffness in comparison to the previous version. For this reason the flight dynamic model has to be updated with the elastic properties of the aircraft EC ES15.

The aircraft dynamic response is required in order to design the flight control laws. Traditionally only the aircraft's rigid body dynamics with 6 DGOF is considered when the control laws are implemented, such as presented by Mila (2013) for an aircraft with negative sweep angle. However, the effects of structure elasticity have influence on the aircraft's flight dynamics and consequently on the controller design. So that, the influence of the aircraft's structural flexibility on the flight control system is an field of research. One of the aircraft's controllers is the pitch damper. The pitch damper acts on the aircraft's longitudinal plane and stabilizes commanded pitch angles. This controller can improve not only the command response but also the flight qualities for the short period rigid body motion. In this case the flight qualities requirements for manned aircrafts must be defined in order to have satisfactory values of damping

and frequency.

1.2 Objective

In face of the concepts of aeroelasticity and aeroservoelasticity, the importance to consider the structural flexibility effects into the aircraft flight mechanics and the new wing structural properties of the utility aircraft presented above, the general objective of this work is given as follows:

General Objectives

- Update of the existing flight dynamic model developed at TU Berlin with the properties of the aircraft EC ES15 using the in-house software FlexSim. Furthermore, a pitch damper shall be designed to augment the short period of the EC ES15;

Based on the main objectives, the specific objectives are presented in the following.

Specific Objectives

- Literature study on the subjects of flight dynamic model of elastic aircrafts, flying qualities and flight control systems;
- Transformation of the GVT eigenvectors and eigenvalues into structural input data for FlexSim. With the aircraft structural behavior and the aerodynamic strip models, the flight dynamics shall be simulated with the in-house FlexSim and the rigid body and flexible models response of the EC ES15 and the Stemme S15 compared;
- The definition of the damping and frequency for the pitch damper shall follow the flight quality requirements given in MIL-F-8785C (1980) for the short period motion. An algorithm that computes pitch damper parameters for adjusting the flight dynamic characteristics according to the requirements shall be implemented. The controller augmentation shall be compared for the rigid and flexible aircraft;

1.3 Overview

The structure of this work is depicted as follows:

- chapter 2 - Methodology:
  - Equations of Motion of Slightly Flexible Aircraft: First, the representation of the aircraft in time and space by means of the mean references axes is introduced, next the

classic modal superposition technique for structural dynamics is presented. Further, the elastic equations of motion are written with Lagrangian mechanics, which relates the kinetic and potential energies with the generalized forces.

  - Unsteady Aerodynamic: The incremental unsteady aerodynamic based on the potential theory is shortly presented. The lift force and pitch moment expressions for a profile undergoing arbitrary motion in incompressible flow, the use of *Theodorsen*, *Wagner* and *Küssner* functions are also briefly introduced;
  - Flight Control System (FCS): The linearized equations of motion in state-space formulation are given. The system's matrix, system's input matrix, output state vector with longitudinal and lateral motion properties and control vector are defined. The longitudinal approximation and rigid-body characteristic motions are introduced. The short period approximation as well as the aircraft's flight dynamic qualities and the pitch damper implementation are later presented;

- chapter 3 - Models:

  - Flight Simulation Model: Briefly introduction about the non-linear high-fidelity flight simulation model developed at TU Berlin with MATLAB® Simulink for the utility aircraft Stemme S15;
  - Aircraft: General properties of the aircraft EC ES15.
  - Aeroelastic Model: Both structural properties of the aircraft Stemme S15 and EC ES15 with and without pods are given.
  - Linear interpolation of modal shapes from ground vibration tests (GVT) data and the construction of the readable input file to FlexSim are carried out;

- chapter 4 - Results and Discussion:

  - Flight dynamic response: The effects of structural flexibility are presented for the stationary trimmed flight. Next, the flight dynamic response of the aircrafts Stemme S15 and EC ES15 with and without pods are compared presenting the pitch rates of the rigid body and flexible structural modes for a step input of 1^{o} in the elevator and rudder. Furthermore, the modal amplitudes and changes in altitude are also presented;
  - Pitch damper: The frequency and damping are defined and the the equations of motion to longitudinal and short period approximations are depicted. The pitch damper results are given comparing the aircraft models with rigid body and flexible structural properties; and

- chapter 5 - Conclusions:

  - The conclusions achieved with the development of this work are presented, followed by final remarks and the proposed future works.

2 Methodology

This work applies the methodology developed by Silvestre (2012) with the objective to simulate the dynamics of slightly flexible, hight-aspect-ratio aircraft in the time domain. The subsection 2.1.1 introduces the mean axes reference frame to situate the aircraft in time and space. Further in subsection 2.1.2, the linear structural dynamics in the modal coordinates followed by the Lagrangian Mechanics are introduced. Based on the floating reference frame and modal coordinates, the equations of motion of flexible aircraft are presented in subsection 2.1.3. Next, the section 2.2 depicts the unsteady incremental aerodynamic formulation to consider the changes in loads caused by structure deformations. In subsection 2.3.4 the linearized equations of motion in state space formulation are introduced. The desired damping and frequency following the military flight qualities MIL-F-8785C are given according to the aircraft's flight phase, level of flight and flight envelope. Further, the pitch damper implementation is carried out with the longitudinal and short period approximations.

2.1 Equations of Motion of Slightly Flexible Aircraft

2.1.1 Mean Axes Reference Frame

Before starting to derive the aircraft differential equations of motion, it is first necessary to define an appropriate and secure foundation on which to build the models. The foundation means a mathematical framework where the equations of motion can be developed in order to represent the aircraft in time and space (COOK, 2012). In flight mechanics literature such as Etkin e Reid (1998) and Hull (2007), the aircraft is modeled as a rigid body with fixed engines, an aft tail and a right-left plane of symmetry. With such model the diagram of forces in symmetric flight comprehend in thrust, lift, drag and weight acting at the aircraft center of gravity (CG). This type of reference frame is called "fixed reference frame".

The approach of rigid body is suitable when the elastic effects are not significant for the analysis or the structure has high stiffness properties. However, when the structural displacements change the aircraft volume $\mathcal{V}$, and consequently its center of gravity and moment of inertia, the flight dynamic response is affected (SILVESTRE; PAGLIOLE, 2007). Thus, the consideration of flexibility effects on the aircraft's dynamic response becomes an important issue. Assuming the aircraft as an elastic body, it changes its form due loads during the flight and the concept of body reference frame must be extended. Waszak e Schmidt (1988) assert that " *during the process of developing equations of motion of any unconstrained elastic system, inertial coupling can occur between the rigid-body degrees of freedom (DGOF) and the elastic DGOF unless a appropriate choice for the local body-reference coordinate is used*". In this case, the body reference frame is

not essentially defined with a fixed point but can also have a relative motion in relation to the CG. These words define the "floating reference frame".

Different body reference frames were defined such as the mean axes reference frame, the principal axes reference frame, the body reference frame fixed on a physical point of the deformable body, among others (SILVESTRE, 2012). The methodology applied in this work makes use of the mean axes reference frame. The justification of the use of this reference system is that it simplifies significantly the kinetic energy expression in Lagrange equations, which are going to be present further in subsection 2.1.2.

In Figure 2 the fixed reference frame fixed on the undeformed structure and the mean axes floating reference frame are illustrated. The undeformed aircraft is presented by dashed lines and the fixed reference frame is fixed on point C. The full lines depict the deformed aircraft, where the mean axes are represented floating out of the aircraft surface. In Figure 2 an infinitesimal element of mass dm is shown. An arrangement of vectors correlate the fixed and the mean axes reference frames. The vector $\mathbf{p}_r$ represents the position of the mass element dm of the undeformed structure in relation to the point C and $\mathbf{p}_d$ the deformation vector. The vector $\mathbf{r}_M$ gives the distance between the origin of the fixed and the floating reference frames. Finally the vector $\mathbf{p}$ is the resultant vector, which represents the distance between the mass elementdm of the deformed structure in relation to the mean axes center O_M. The index $_M$ is related to the floating and the index $_C$ to the fixed reference system.

Based on the statements presented above, the mean axes can be mathematically defined. The mean axes is a floating reference frame where the linear and angular momenta, due to elastic deformation, are zero at every instant (WASZAK; SCHMIDT, 1988). Hence, the Equation 2.1 is written.

$$\underbrace{\int_{\mathcal{V}} \frac{\delta \mathbf{p}}{\delta t} dm}_{\text{elastic linear moment}} = \underbrace{\int_{\mathcal{V}} \mathbf{p} \times \frac{\delta \mathbf{p}}{\delta t} dm}_{\text{elastic angular moment}} = \mathbf{0} \tag{2.1}$$

The integration term $\int_{\mathcal{V}}$ is performed over the entire aircraft volume $\mathcal{V}$. As given in Equation 2.1, the elastic linear and angular moment are both equal the vector null, $\mathbf{0}$. Based on the vector relations in Figure 2, the Equation 2.2 is written.

$$\mathbf{p} = \mathbf{p}_r + \mathbf{p}_d - \mathbf{r}_M \tag{2.2}$$

Replacing the Equation 2.2 in Equation 2.1, results in:

$$\int_{\mathcal{V}} \frac{\delta(\mathbf{p}_r + \mathbf{p}_d - \mathbf{r}_M)}{\delta t} dm = \int_{\mathcal{V}} (\mathbf{p}_r + \mathbf{p}_d - \mathbf{r}_M) \times \frac{\delta(\mathbf{p}_r + \mathbf{p}_d - \mathbf{r}_M)}{\delta t} dm = \mathbf{0} \tag{2.3}$$

Waszak e Schmidt (1988) defines the following assumptions in order to simplify the derivation:

Figure 2: Mean axes reference body frame for a slightly flexible aircraft and vectors of the wing deformation

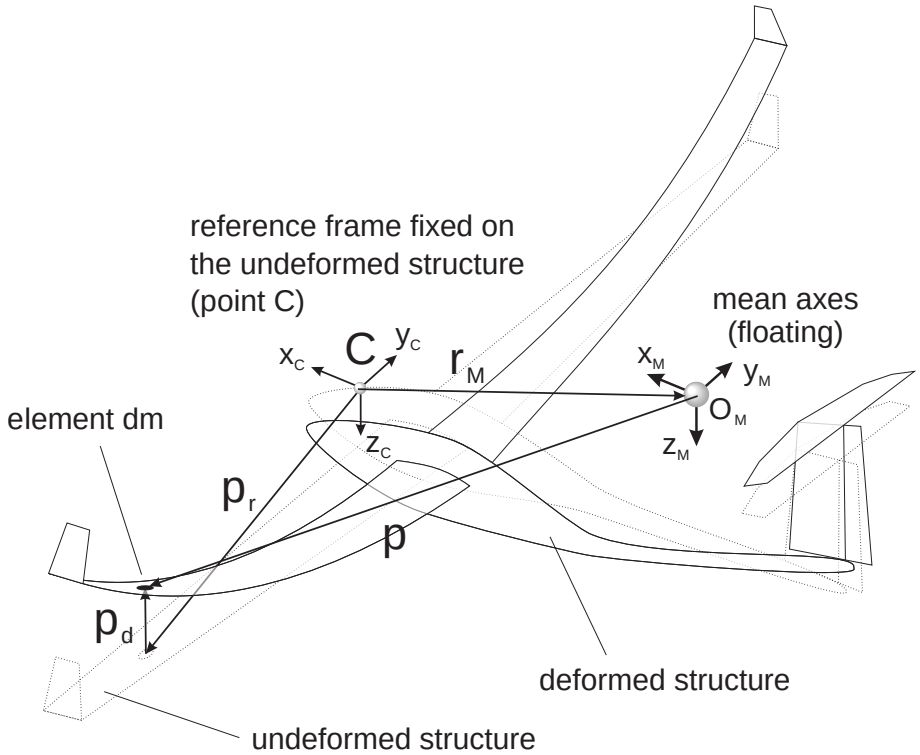

Source: Silvestre (2012), p.10.

1. The structural deformation is sufficiently small, such that linear elastic theory is valid;
2. A set of normal vibrations modes are assumed to be available;
3. The mean axes O_M are rotating relative to inertial space with angular velocity $\boldsymbol{\omega}_{C/M}$ and each mass element is treated as a mass point;
4. The structural deformation is assumed to be small or the displacement and rate are collinear

According to the assumptions given by Waszak e Schmidt (1988), it is possible to consider that the undeformed aircraft CG located on the fixed reference frame C and the instantaneous CG due elastic deformations located at O_M are coincident. Moreover, the float reference frame is located at aircraft instantaneous CG and remains stationary relative to the undeformed structure (SILVESTRE, 2012).

2.1.2 Structural Dynamics

The structural dynamics concerns with the behavior of structures subjected to dynamic loading. According to Thorby (2008), the discipline is an extension of traditional dynamic problems where not only the body motion is considered, but also its elasticity properties. In traditional dynamic analysis the aspects of kinematics and kinetics are considered and the body

is defined as rigid: the "rigid-body". However, in the structural dynamics the analysis is extended considering the bodies' elasticity, in other words the "elastic-body". The literature Rao (2011) presents the analysis of vibrations in mechanical systems starting with single degree-of-freedom (DGOF) until the multi DGOF systems. With interest in multi DGOF systems, two special cases are presented: the free vibration, with or without damping, and the response to an external applied load.

The methodology applied in this work uses the modal superposition technique to model the aircraft's structural dynamics. The modal superposition technique consists to transform the differential equation of motion into the modal base of the associated conservative system (BISMARCK-NASR, 1999). A conservative system is defined by (YOUNG; FREEDMAN, 2011) as a system where the work done by an external force has the following characteristics:

- the work is independent of path;
- is equal to the difference between the final and initial values of energy function; and
- is completely reversible.

The transformation into the modal base is the mean advantage to adopt this technique due the fact that it decoupled the modes of vibration and reduces considerably the number of equations involved when writing the elastic displacement $\mathbf{p}_d$ (see Figure 2). In addition to that, the modal basis satisfies the linearized mean axes constraints presented in the subsection 2.1.1, as well as the coupled elastic and flight mechanical equations of motion (SILVESTRE, 2012).

In subsection 2.1.3, the EOM of a discrete elastic mechanical system of n DGOF will be presented. The Lagrangian mechanics simplify the formulation when the structural dynamics is formulated with generalized coordinates (RAO, 2011). Considering the aircraft structure as a continuous system with discrete elements, each one with its 6 DGOF. So that, the system of equations comprehends a total of a DGOF. Assuming linear elasticity, the $2nd$-order equations are given in Equation 2.4.

$$\mathbf{M}\ddot{\mathbf{q}} + \mathbf{D}\dot{\mathbf{q}} + \mathbf{K}\mathbf{q} = \mathbf{F}(t) \tag{2.4}$$

In Equation 2.4 the terms $\mathbf{M}$, $\mathbf{D}$ and $\mathbf{K}$ are mass, viscous damping and stiffness system matrices, respectively. The matrices are square and its dimension is related with the number of DGOF of the system, resulting in dimension $a \times a$. The term $\mathbf{F}$ on the right side is the vector of extern distributed forces acting on the system , which has dimension $a \times 1$.

The modal superposition technique is introduced by following Bismarck-Nasr (1999). In doing so, the modal superposition technique transforms the differential EOM (see Equation 2.4) into the modal base of the conservative system. The conservative associated system is obtained

when the viscous damping is assumed to be equal zero, what means $\mathbf{D} = \mathbf{0}$. Considering the condition of free vibrations, the Equation 2.4 is rewritten in Equation 2.5.

$$\mathbf{M}\ddot{\mathbf{q}} + \mathbf{K}\mathbf{q} = \mathbf{0} \tag{2.5}$$

The solution of Equation 2.5 gives a vector with a eigenvalues ς_k and a matrix with a eigenvectors $\mathbf{\Lambda}_k$, where $k = 1, 2, \ldots, a$. In order to solve the general problem in Equation 2.5, the transformation to the modal base is performed using the relation given in Equation 2.6.

$$\mathbf{q}(t) = \mathbf{\Lambda}\boldsymbol{\eta}(t) \tag{2.6}$$

According to Equation 2.6, the term $\boldsymbol{\eta}(t)$ with dimension $a \times 1$ is the column vector of the modal amplitudes, also known as "modal response" or "generalized coordinates" (SILLER, 2004). So that, applying the Equation 2.6 into the Equation 2.4, it results in Equation 2.7.

$$\mathbf{M}\mathbf{\Lambda}\ddot{\boldsymbol{\eta}}(t) + \mathbf{D}\mathbf{\Lambda}\dot{\boldsymbol{\eta}}(t) + \mathbf{K}\mathbf{\Lambda}\boldsymbol{\eta}(t) = \mathbf{F}(t) \tag{2.7}$$

Premultiplying both sides of Equation 2.7 by $\mathbf{\Lambda}^T$ it results in Equation 2.8.

$$\boldsymbol{\mu}\ddot{\boldsymbol{\eta}}(t) + \boldsymbol{\beta}\dot{\boldsymbol{\eta}}(t) + \boldsymbol{\gamma}\boldsymbol{\eta}(t) = \mathbf{Q}_\eta(t) \tag{2.8}$$

The terms represented by Greek letters in Equation 2.8 and the right side term $\mathbf{Q}_\eta$ read:

$\boldsymbol{\mu} = \mathbf{\Lambda}^T\mathbf{M}\mathbf{\Lambda}$	Generalized Mass Matrix
$\boldsymbol{\beta} = \mathbf{\Lambda}^T\mathbf{D}\mathbf{\Lambda}$	Modal Damping Matrix
$\boldsymbol{\gamma} = \mathbf{\Lambda}^T\mathbf{K}\mathbf{\Lambda}$	Generalized Stiffness Matrix
$\mathbf{Q}_\eta(t) = \mathbf{\Lambda}^T\mathbf{F}(t)$	Generalized Forces

The matrices $\boldsymbol{\mu}$ and $\boldsymbol{\gamma}$ are diagonal matrices due the orthogonality properties of the eigenvalues and eigenvectors of the associated conservative system. In this case, these matrices are called respectively generalized mass and generalized stiffness matrices (for more details see Rao (2011), chapter 6). The damping $\boldsymbol{\beta}$ can be approximately assumed by a diagonal matrix, because in aeronautical structures the damping effect, $\boldsymbol{\beta}\dot{\boldsymbol{\eta}}(t)$, is small compared with the inertial and stiffness ones. The coupling damping between the modes is neglected. Moreover, the differential equation of motion with generalized coordinates represented by Equation 2.8, gives a system of uncoupled equations of a single degree of freedom, except by the external forces and are given in this work by aerodynamic forces in section 2.2. The vector of generalized forces is represented by $\mathbf{Q}_\eta$. Addressing generalized terms in the Equation 2.8 gives Equation 2.9.

$$\boldsymbol{\mu}_{kk}\ddot{\boldsymbol{\eta}}_k + \boldsymbol{\beta}_{kk}\dot{\boldsymbol{\eta}}_k + \boldsymbol{\gamma}_{kk}\boldsymbol{\eta}_k = \mathbf{Q}_\eta(t) \qquad \text{with } \mathrm{k} = 0, 1, 2, \ldots, \mathrm{a} \tag{2.9}$$

Normalizing the Equation 2.9 by the generalized mass, it results in Equation 2.10.

$$\ddot{\eta}_k(t) + 2\psi_k\omega_{nk}\dot{\eta}_k(t) + \omega_{nk}^2\eta_k(t) = \frac{Q_{\eta_k}(t)}{\mu_k} \qquad \text{with k} = 0, 1, 2, \ldots, \text{a} \tag{2.10}$$

The solution of each equation of the system of equations presented in Equation 2.10 can be solved by applying the *Duhamel's* Integral (for more details see Bmop A.G. Parkinson (1969)). Another advantage of adopting the modal basis is justified when only a range of frequencies are of interest instead of the entire spectrum, for instance the low frequencies for integrated models. It restricts the analysis, so that just the investigated modes can be analyzed. This fact reduces the number of DGOF and speeds up the computational time (SILVESTRE, 2012). Considering the number of investigated modes equal to n_e, therefore n_e system equations in Equation 2.10 are considered.

Furthermore, the formulation with modal coordinates is adequate to update finite element models (FEM). When designers work with complex airplane configurations a FEM model is adopted in order to reduces not only the costs and time but also to provide an idea of the structural behavior before it be constructed. Due the fact that FEM is a representation of reality and does not account for damping effects, the validation and update of results with experimental tests may be performed with ground vibration test (GVT), experimental modal analysis (EMA) or operational modal analysis (OMA).

2.1.3 Elastic Airplane Equations of Motion

In this section the equations of motion of elastic airplane are presented following the references: Waszak, Davidson e Schmidt (1987a), Waszak, Davidson e Schmidt (1987b) and Waszak e Schmidt (1988).

Due the representation of the structural dynamics with Lagrangian mechanics, it is necessary to define the most appropriate generalized coordinates $\mathbf{q}$ (THORBY, 2008). The generalized coordinates describe the motion of the aircraft's instantaneous CG relative to the inertial reference frame written in the body reference frame (SILVESTRE, 2012). In this case, the vector of generalized coordinates is defined in Equation 2.11.

$$\mathbf{q}^T = (x_{CG}, y_{CG}, z_{CG}, \psi, \theta, \phi, \eta_1, \eta_2, \ldots, \eta_{ne}). \tag{2.11}$$

The terms (x_{CG}, y_{CG}, z_{CG}) in Equation 2.11 define the inertial position of the origin of the body-reference frame. They can be written as: $\mathbf{R}_{0|B^{(G)}} = (x_{CG}, y_{CG}, z_{CG})$, where the angles ψ, θ, ϕ are the Euler angles, and $(\eta_1, \eta_2, \ldots, \eta_{ne})$ are the modal amplitudes .

The Figure 3 illustrates the flying flexible aircraft in inertial and mean axes reference frames. The EOM are written in function of the vectors presented in Figure 3, thus the mass

Figure 3: Representation of a mass element dm in the flying flexible aircraft discretized by inertial and mean axes reference frames.

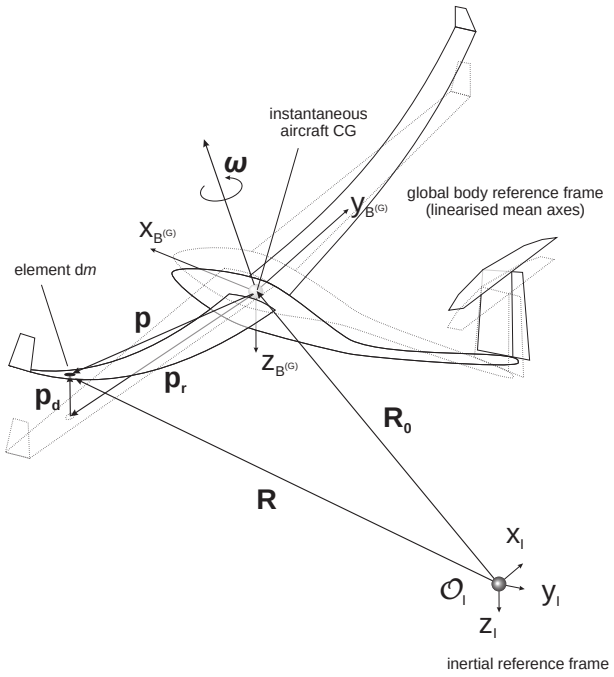

Source: Silvestre (2012), p.16.

element is defined relative to the aircraft's CG and the inertial reference frame. The vector $\mathbf{p}$ defines the position of the mass element relative to the aircraft's CG and by a vector $\mathbf{R}$ relative to the origin of the inertial reference frame. The vector $\mathbf{p}_r$ represents the position of the element of mass relative to CG of the rigid aircraft. Later, the vector $\mathbf{R}_0$ reads the position of the aircraft's CG relative to the origin of the inertial reference frame, $\mathcal{O}_l$. The term $\boldsymbol{\omega}$ is the angular velocity relative to the inertial reference frame.

Furthermore, the Lagrangian $L = T - U$ of the system relates the kinetic and potential energies with the generalized forces. Each one of these equations are presented in the next topics following the derivations presented by Waszak e Schmidt (1988), Silvestre e Paglione (2008) and Looye (2008).

The Kinetic Energy

In view of the above presented, the kinetic energy is given in Equation 2.12.

$$T = \frac{1}{2}\int_{\mathcal{V}} \frac{d\mathbf{R}}{dt} \cdot \frac{d\mathbf{R}}{dt} dm \tag{2.12}$$

In Equation 2.12 the vector $\mathbf{R}$, as illustrated in Figure 3, reads $\mathbf{R} = \mathbf{R_0} + \mathbf{p}$ and the

derivation of the position vector $\mathbf{R}$ by the time is given in Equation 2.13.

$$\frac{d\mathbf{R}}{dt} = \frac{d\mathbf{R_0}}{dt} + \frac{d\mathbf{p}}{dt} \tag{2.13}$$

Considering that the aircraft is moving relative to the inertial reference frame with angular velocity $\boldsymbol{\omega}$, and considering dm as a mass element, the time derivative of the position vector $\mathbf{R}$ relative to the inertial reference frame may be written as presented in Equation 2.14.

$$\frac{d\mathbf{R}}{dt} = \frac{d\mathbf{R_0}}{dt} + \frac{d\mathbf{p}}{dt} + \boldsymbol{\omega} \times \mathbf{p} \tag{2.14}$$

Hence, the kinetic energy in Equation 2.12 becomes:

$$\begin{aligned} T = \frac{1}{2}\int_{\mathcal{V}} \Bigg\{ & \frac{d\mathbf{R}_0}{dt} \cdot \frac{d\mathbf{R}_0}{dt} + 2\frac{d\mathbf{R}_0}{dt} \cdot \frac{\delta\mathbf{p}}{\delta t} + \frac{\delta\mathbf{p}}{\delta t} \cdot \frac{\delta\mathbf{p}}{\delta t} + \\ & 2\frac{\delta\mathbf{p}}{\delta t} \cdot (\boldsymbol{\omega} \times \mathbf{p}) + (\boldsymbol{\omega} \times \mathbf{p}) \cdot (\boldsymbol{\omega} \times \mathbf{p}) + 2(\boldsymbol{\omega} \times \mathbf{p}) \cdot \frac{d\mathbf{R}_0}{dt} dm \Bigg\}. \end{aligned} \tag{2.15}$$

The Equation 2.15 gives the kinetic energy of the body. The details about the expansion of each part of the integral terms in Equation 2.15 are not detailed in this work (see Silvestre (2012), Appendix A). Next, the following assumptions are considered to simplify the derivations:

1. The linearized constraints presented with the mean axes reference frame in subsection 2.1.1 are applied;
2. The aircraft structural density is assumed invariable with the deformations;
3. The inertia tensor $\mathbf{J}$, is assumed to be constant;

Hence, the kinetic energy expression given in Equation 2.15 can be simplified and rewritten in Equation 2.16.

$$T = \frac{1}{2}m\frac{d\mathbf{R}_0}{dt} \cdot \frac{d\mathbf{R}_0}{dt} + \frac{1}{2}\boldsymbol{\omega}^T\mathbf{J}\boldsymbol{\omega} + \frac{1}{2}\dot{\boldsymbol{\eta}}^T\boldsymbol{\mu}\dot{\boldsymbol{\eta}} \tag{2.16}$$

The potential energy equation, which comprehends the elastic strain and the gravitational potential energy is presented next.

The Potential Energy

The potential energy, denoted by U, is the sum of the elastic strain, U_S, and the gravitational potential energy, U_G. Therefore, U_G and U_S are derived.The gravitational potential energy is written in Equation 2.17.

$$U_G = -\int_{\mathcal{V}} \mathbf{R} \cdot \mathbf{G}\, dm = -\int_{\mathcal{V}} (\mathbf{R}_0 + \mathbf{p}) \cdot \mathbf{G}\, dm \tag{2.17}$$

The term $\mathbf{G} = [\ 0\ \ 0\ \ g\ ]^T$ is the gravitational acceleration vector written in the inertial reference frame. The methodology assumes $\mathbf{G}$ to be constant over the aircraft's volume, $\mathcal{V}$. According with the exposed, the position of the aircraft CG and center of mass (CM) are the same, i.e. $\mathbf{R}_{CG} = \mathbf{R}_{CM} = \mathbf{R}_0$. The potential energy in Equation 2.17 is rewritten in Equation 2.18.

$$U_G = -\left[\int_{\mathcal{V}} \mathbf{R}_0\, dm + \int_{\mathcal{V}} \mathbf{p}\, dm\right] \cdot \mathbf{G}. \tag{2.18}$$

Regarding the assumption of linear momenta adopted in subsection 2.1.1, the integral $\int_{\mathcal{V}} \mathbf{p}\, dm$ becomes null and the gravitational potential energy is defined in Equation 2.19.

$$U_G = -\left[\int_{\mathcal{V}} \mathbf{R}_0\, dm\right] \cdot \mathbf{G}. \tag{2.19}$$

Writing Equation 2.19 in the reference inertial frame, the vector $\mathbf{R}_0$ reads:

$$\mathbf{R}_0 = \mathbf{T}^T_{B\{G\}}[\ x_{CM}\ \ y_{CM}\ \ z_{CM}\ ]. \tag{2.20}$$

In Equation 2.20 the term $\mathbf{T}^T_{B\{G\}}$ means the transformation matrix. Based on the presented, the gravitational potential energy U_G is rewritten in Equation 2.21.

$$U_G = mg(x_{CM} sin\theta - y_{CM} cos\theta \sin\phi - z_{CM} \cos\theta \cos\phi). \tag{2.21}$$

The second portion of the potential energy is the elastic strain energy or deformation energy, U_S. This term uses the stress-strain relationship for an elastic linear continuum, where $\boldsymbol{\sigma}$ is the stress and $\boldsymbol{\epsilon}$ the strain tensor (BISMARCK-NASR, 1999). So that, the strain energy of the elastic mechanical system is defined in Equation 2.22.

$$U_S = \frac{1}{2}\int_{\mathcal{V}} \boldsymbol{\sigma}^T \boldsymbol{\epsilon}\, d\mathcal{V}. \tag{2.22}$$

For the linear case, Bismarck-Nasr (1999) defines the stress $\boldsymbol{\sigma}$ and strain $\boldsymbol{\epsilon}$ tensors as follows:

$$\boldsymbol{\sigma} = \mathbf{C}\boldsymbol{\epsilon}, \qquad \text{(Stress Tensor)}$$
$$\boldsymbol{\epsilon} = \mathbf{dq}. \qquad \text{(Strain Tensor)}$$

The stress and strain tensors have dimension 6×1 and the elasticity matrix $\mathbf{C}$, 6×6. The strain tensor, $\boldsymbol{\epsilon}$ is related with the vector $\mathbf{p}_d$ by means of the linear differential operator $\mathbf{d}$. So that, the Equation 2.22 is rewritten in Equation 2.23.

$$U_S = \frac{1}{2}\boldsymbol{\eta}^T\boldsymbol{\gamma}\boldsymbol{\eta} = \frac{1}{2}\boldsymbol{\eta}^T\boldsymbol{\mu}\boldsymbol{\omega}_n^2\boldsymbol{\eta}. \tag{2.23}$$

As defined in subsection 2.1.2, the term$\boldsymbol{\gamma}$ is the generalized stiffness, $\boldsymbol{\mu}$ the generalized mass, and $\boldsymbol{\omega}_n$ the diagonal matrix with the natural frequencies of elastic modes.

The Structural Dissipation

According to Bismarck-Nasr (1999), the viscous damping is considered, what means that the structural damping forces are linearly related with velocity vector of modal displacements ($\dot{\boldsymbol{\eta}}$). Thus, the variation in the dissipation matrix D caused by changes in velocity vector of modal amplitudes $\dot{\boldsymbol{\eta}}$ is given by:

$$D = \frac{1}{2}\dot{\boldsymbol{\eta}}^T\boldsymbol{\beta}\dot{\boldsymbol{\eta}}. \tag{2.24}$$

The Lagrangian Equations of Motion

The Lagrangian equations of motion are presented. The Lagrangian of the system L is defined as the difference between the total kinetic T and potential energy U in the system, which reads:

$$L = T - U. \tag{2.25}$$

Considering q_k as the $k-th$ generalized coordinate defined by the Equation 2.11. The Lagrangian EOM with k DGOF result in (RAO, 2011):

$$\frac{d}{dt}\left(\frac{\delta L}{\delta \dot{q}_k}\right) - \frac{\delta L}{\delta q_k} + \frac{\delta D}{\delta \dot{q}_k} = Q_k, \quad \text{for } k = 1, 2, \ldots, 6 + n_e \tag{2.26}$$

Replacing the Lagrangian of the system defined in Equation 2.25, the Kinetic energy with Equation 2.16, the potential energy with equation Equation 2.21 and 2.23, and the Equation 2.24 for the structural dissipation in the Equation 2.26, the EOM of a discrete elastic mechanical system with k DGOF are defined.

In Equation 2.26 the generalized forces Q_k for the $k-th$ DGOF is written. The Q_k is a moment if q_k is a rotational generalized coordinate. On the other hand, Q_k is a force if q_k is a

translational generalized coordinate. Even though, the term is typically referred as "generalized forces" (INMAN; SINGH, 2013). (SILVESTRE, 2012) asserts that Q_k is determined by means of the relationship between the Cartesian and generalized coordinate system with the following equation:

$$Q_k = \int_{\mathcal{V}} \mathbf{f}_{|l} \cdot \frac{\delta \mathbf{R}_{|l}}{\delta q_k} d\mathcal{A}, \quad \text{for} \quad k = 1, 2, \ldots, 6 + n_e. \tag{2.27}$$

The vector $\mathbf{f}_{|l}$ gives the external forces per unit area (for example: aerodynamic and propulsive forces), written in the inertial reference frame. The Equation 2.26 and Equation 2.27 are rewritten in the following system of equations given by Equation 2.28, Equation 2.29 and Equation 2.30.

$$\dot{\mathbf{V}}|_{B\{G\}} = -\boldsymbol{\omega}|_{B\{G\}} \times \mathbf{V}|_{B\{G\}} + \mathbf{T}|_{B\{G\}}\, \mathbf{G}|_l + \frac{1}{m}\mathbf{F}^{ext}|_{B\{G\}}, \tag{2.28}$$

$$\dot{\boldsymbol{\omega}}|_{B\{G\}} = -\mathbf{J}^{-1}\left(\boldsymbol{\omega}|_{B\{G\}} \times (\mathbf{J}\boldsymbol{\omega}|_{B\{G\}})\right) + \mathbf{J}^{-1}\mathbf{M}^{ext}|_{B\{G\}}, \tag{2.29}$$

$$\ddot{\boldsymbol{\eta}} = -\boldsymbol{\mu}^{-1}\boldsymbol{\beta}\dot{\boldsymbol{\eta}} - \boldsymbol{\mu}\boldsymbol{\gamma}\boldsymbol{\eta} + \boldsymbol{\mu}^{-1}\mathbf{Q}_{\eta}. \tag{2.30}$$

The EOM Equation 2.28 and Equation 2.29 are expanded in their components x, y and z, resulting in the following system of equations:

$$\dot{u} = \frac{X}{m} + rv - qw - g\sin\theta, \tag{2.31}$$

$$\dot{v} = \frac{Y}{m} - ru + pw + g\cos\theta\sin\phi, \tag{2.32}$$

$$\dot{w} = \frac{Z}{m} + qu - pv + g\cos\theta\cos\phi. \tag{2.33}$$

$$I_{xx}\dot{p} - I_{xy}\dot{q} - I_{xz}\dot{r} - I_{yz}(q^2 - r^2) - (I_{yy} - I_{zz})qr - p(I_{xz}q - I_{xy}r) = L, \tag{2.34}$$

$$-I_{xy}\dot{p} + I_{yy}\dot{q} - I_{yz}\dot{r} - I_{xz}(r^2 - p^2) - (I_{zz} - I_{xx})pr - q(I_{xy}r - I_{yz}p) = M, \tag{2.35}$$

$$-I_{xz}\dot{p} + I_{yz}\dot{q} - I_{xy}\dot{r} - I_{xy}(p^2 - q^2) - (I_{xx} - I_{yy})pq - r(I_{yz}pI_{xz}q) = N. \tag{2.36}$$

In the EOM, Equation 2.31 until Equation 2.36, the terms X,Y and Z are forces on the x, y and z axis, and L, M and N represent the corresponding moments around the CG. Due the fact that the elastic characteristics are taken in account, the Equation 2.31 until Equation 2.36 are finally rewritten with the additional forces and momenta terms resulting from the aircraft's structure deformations (HAMANN, 2014), resulting in:

$$\begin{bmatrix} X \\ Y \\ Z \end{bmatrix}_f = \begin{bmatrix} 1 \\ 0 \\ 0 \end{bmatrix} T + \begin{bmatrix} \cos\alpha & 0 & -\sin\alpha \\ 0 & 1 & 0 \\ \sin\alpha & 0 & \cos\alpha \end{bmatrix} \begin{bmatrix} -D_{Rigid} \\ Q_{Rigid} \\ -L_{Rigid} \end{bmatrix}_e + \begin{bmatrix} X_{Flex} \\ Y_{Flex} \\ Z_{Flex} \end{bmatrix}_f \tag{2.37}$$

$$\begin{bmatrix} L \\ M \\ N \end{bmatrix}_f = \begin{bmatrix} 0 \\ r_T \\ 0 \end{bmatrix} T + \begin{bmatrix} \cos\alpha & 0 & -\sin\alpha \\ 0 & 1 & 0 \\ \sin\alpha & 0 & \cos\alpha \end{bmatrix} \begin{bmatrix} L_{Rigid} \\ M_{Rigid} \\ N_{Rigid} \end{bmatrix}_e + \begin{bmatrix} L_{Flex} \\ M_{Flex} \\ N_{Flex} \end{bmatrix}_f \tag{2.38}$$

These additional flexible terms resulting from the structure's deformations are calculated applying the aerodynamic strip model presented in section 2.2.

2.2 Unsteady Incremental Aerodynamics in Incompressible Flow

The following sections will respectively present the reason why it is necessary to work with unsteady aerodynamic derivatives when analyzing more complex cases in aeroelasticity. Further, a brief introduction about the classical problems involving unsteady aeroelasticity, such as harmonic oscillations, abrupt change of attack angle and sharp-edged vertical gusts. Moreover, the incremental aerodynamics for an arbitrary motion is presented. The literatures that guide the content exposed in this section are Silvestre (2012), Bisplinghoff e Ashley (2013) and Fung (2002). For introduction remarks in fluid dynamics and aerodynamics the reader is referred, respectively, to Fox, McDonald e Pritchard (1985) and Anderson (2010).

2.2.1 Foreword to Unsteady Incremental Aerodynamics Theory

Bisplinghoff e Ashley (2013) starts the chapter 5, entitled "*Aerodynamic Tools for Incompressible Flow*", affirming that so many excellent books have been written on fluid dynamics but almost all limit themselves to the steady case. In addition, the phenomena of unsteady nature is important to aeroelasticians and need to be considered. Therefore, Silvestre (2012) introduces the phenomena stating the following: *"like every alteration in aircraft state, every elastic deformation of the aircraft structure during the flight is accompanied by a change in the external aerodynamic loads, what shall be called 'incremental aerodynamics "*.

As presented in chapter 1 by the Collar's Diagram (see Figure 1), the phenomena such as loss and reversal of aileron control and divergence refer to static aeroelastic problems. So that, Fung (2002) states that these phenomena can be easily solved with steady-state aerodynamic methodologies. However, when working with dynamic aeroelastic problems such as flutter, Fung (2002) asserts that steady aerodynamic derivatives cannot accurately represent the physics reality. In this case, as a matter of simplification, the quasi-steady aerodynamic derivatives may be used in first time as an initial approximation. Nevertheless, due the fact that flutter, for instance, comprehends in an oscillatory instability in a potential flow where neither separation nor strong shocks are involved (HEINZE, 2007), it becomes necessary to consider the unsteady aerodynamic case to have accurate results (FUNG, 2002).

2.2.2 Expressions for Lift Force and Pitching Moment

The expressions for lift force and pitching moment for a profile undergoing an arbitrary movement in an incompressible flow are presented. These expressions are the basis to define the incremental aerodynamic lift force and pitch moment due to arbitrary motions and elastic deformations

Figure 4: Definition of reference system and lengths in relation to the undeformed and deformed structure. The torsion and bending are represented by α and h, respectively. The angle δ is the control deflection.

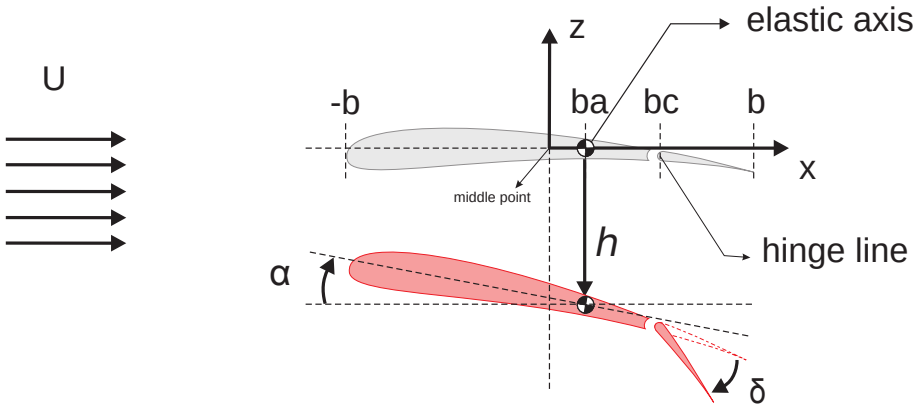

Source: adapted from Silvestre (2012), p.20.

The Figure 4 illustrates a chordwise rigid airfoil with chord equal $2b$; vertical translation h, positive downwards; angle of attack α and control surface angle δ, both positive clockwise, flying at velocity $\mathbf{U}$. The reference system is fixed at the non disturbed airfoil at the center of chord length. At the length ba, forward from the origin, the elastic axis is located. Also relative to the center at distance bc, the control surface hinge line is defined. The representation of the airfoil with positive attack and control surface angles illustrate the deflected case with torsion and bending components. Similar representations can be found at Bisplinghoff e Ashley (2013) and Theodorsen (1934).

The problem of an airfoil under arbitrary motion presented in Figure 4 was solved by Theodorsen (1934). Theodrosen solved definite integrals, which are identified as *Bessel* functions of the first and second kind of zero and first order. Moreover, the theory is based on potential flow and the *Kutta* condition (ANDERSON, 2010), which is equivalent to the conventional wing-section theory to the steady case (THEODORSEN, 1934). Modeling the flow, Theodorsen assumed perturbation potentials in source-skins-pairs to represent the non-circulatory flow and fulfill the Kutta condition (for more details see Anderson (2010), chapter 6), which states that the flow smoothly leaves the top and bottom surfaces of the airfoil at the trailing edge (ANDERSON, 2010). Furthermore, as presented by Silvestre (2012), Theodorsen added a vortex flow pattern composed by bound vortices and a wake of counter-vortices leaving the trailing edge with velocity $\mathbf{U}$. Regarding that the assumption of small-disturbance theory is considered, the potential flow

equation consists in solving the Laplace's equation:

$$\nabla^2 \boldsymbol{\phi}^{'} = \mathbf{0}. \tag{2.39}$$

As presented by Bisplinghoff e Ashley (2013), the movement of the airfoil given in Equation 2.40 is used as boundary conditions to solve Equation 2.39.

$$w = \frac{\delta z_a}{\delta t} + \mathbf{U}\frac{\delta z_a}{\delta x} = w_a(x,t); \quad \text{for } z = 0,\ -b \leq x \leq b. \tag{2.40}$$

In Equation 2.40 w is the velocity component in z direction, ϕ the velocity potential function, z_a the instantaneous displacement of the chordline and the index $_a$ means some position through the chordwise in relation to the reference system defined in Figure 4 (further mathematical derivations are given in Bisplinghoff e Ashley (2013), section 5.6.)

The derivation of Theodorsen (1934) had handled separately the circulatory and non circulatory portions of the flow. Due this fact, in the following equations the index $^{(NC)}$ is given for non circulatory and $^{(C)}$ for circulatory terms. Imposing the Kutta condition, applying Bernoulli's equation and integrating the pressure distribution over the airfoil, the expressions for lift force (ℓ) and pitch moment (m) about the profile's elastic axis (see Figure 4) can be determined. For an arbitrary motion these expressions read:

$$\ell = \ell^{(NC)} + 2\pi\rho U b Q \frac{\int_b^\infty \frac{x}{\sqrt{x^2-b^2}}\gamma_w(x,t)dx}{\int_b^\infty \sqrt{\frac{x+b}{x-b}}\gamma_w(x,t)dx}, \tag{2.41}$$

$$\ell^{(NC)} = \pi\rho b^2[\ddot{h} + U\dot{\alpha} - ba\ddot{\alpha}] + \ell_\delta^{(NC)}, \tag{2.42}$$

$$m = m^{(NC)} - 2\pi\rho U b^2 Q\left\{\frac{1}{2} - \left(a+\frac{1}{2}\right)\frac{\int_b^\infty \frac{x}{\sqrt{x^2-b^2}}\gamma_w(x,t)dx}{\int_b^\infty \sqrt{\frac{x+b}{x-b}}\gamma_w(x,t)dx}\right\}, \tag{2.43}$$

$$m^{(NC)} = \pi\rho b^2\left[U\dot{h} + ba\ddot{h} + U^2\alpha - b^2\left(\frac{1}{8}+a^2\right)\ddot{\alpha}\right] + m_\delta^{(NC)}, \tag{2.44}$$

The term γ_w, presented in Equation 2.41 and Equation 2.43, reads the strength of the wake of vortices leaving the profile. $\ell^{(NC)}$ and $m^{(NC)}$ are the noncirculatory portion of lift force and pitch moment, respectively. Fung (2002) states that the circulatory and noncirculatory portions of lift force may also be called "aparent mass" forces. The term Q presented also in Equation 2.41 and Equation 2.43 is a function defined by Theodorsen. The Theodorsen Function is defined in Equation 2.45.

$$Q = U\alpha + \dot{h} + b\left(\frac{1}{2} - a\right)\dot{\alpha} + Q_\delta. \tag{2.45}$$

The terms with index $_\delta$ in Equation 2.42, Equation 2.44 and Equation 2.45 write the dependencies of the surface control angle and are not represented in this work (for more details see Bisplinghoff e Ashley (2013) and Theodorsen (1934)). Further, in Equation 2.45 the term Q defines the boundary conditions of the airfoil's motion illustrated in Figure 4. Comparing Equation 2.40 and Equation 2.45 it is possible to state that $Q = -w_a$. Regarding the theory of oscillating airfoils, it can be consider that for bending (vertical translation, h) and pitching (attack angle, α) oscillations, the circulation about the airfoil is determined by the downwash velocity at the $3/4-$chord point ($w_{3/4}$) from the leading edge of the airfoil (FUNG, 2002), what means $a = +1/2$. It can be proved when replacing $a = 1/2$ in Equation 2.45. In this case, the term $b\left(\frac{1}{2} - a\right)\dot{\alpha}$ vanishes. Besides that, when $a = -1/2$ the dependency of the pitching moment m on the ratio integrals in Equation 2.43 vanishes.

2.2.3 Classical Problems Involving Incremental Aerodynamics

The classical problems represent the calculation of lift force and pitch moment for an airfoil undergoing known movements. The classical cases presented by the literature are the airfoil under the following motions: harmonic oscillations; abrupt change of attack angle; and subjected to a sharp-edged gust. Through the development of this methodologies to obtain the aerodynamic derivatives, important statements were formulated and the authors most known by their contribution are Theodorsen (1934), Wagner (1925), Küssner (1936) and Jones (1946).

Airfoil undergoing Harmonic Oscillations

The case of a thin airfoil undergoing harmonic oscillations was for many years one of the most investigated problems of all flutter prediction (BISPLINGHOFF; ASHLEY, 2013). Consider the airfoil oscillating in an harmonic motion with frequency ω (with phasor notation by the multiplication of all DGOF by $e^{j\omega t}$), Theodorsen solved the problem identifying the integrals in Equation 2.41 and Equation 2.43 as *Hankel* functions of the second kind and calculated then by means of $1st$ and $2nd$ *Bessel Functions* with the following definition:

$$C(k) = F(k) + jG(k). \tag{2.46}$$

Where, by following the derivation presented by Theodorsen (1934), the terms $F(k)$ and $G(k)$ are the first order and second order *Bessel Functions*, respectively. The terms in Equation 2.46 are a function of k, which means the *reduced frequency* or *Strouhal number*, a non dimensional frequency defined as:

$$k = \frac{b\omega}{U}. \tag{2.47}$$

The reduced frequency is the product of the profile's half chord b and the oscilation frequency ω divided by the undisturbed flow speed U. Placing the terms defined by Equation 2.46 and Equation 2.47 into Equation 2.41 and Equation 2.43, the lift and moment equation are rewritten in Equation 2.48 and Equation 2.49.

$$\ell = \ell^{(NC)} + 2\pi\rho U b Q C(k), \tag{2.48}$$

$$m = m^{(NC)} - 2\pi\rho U b^2 Q \left\{ \frac{1}{2} - \left(a + \frac{1}{2}\right) C(k) \right\}. \tag{2.49}$$

Regarding that Theodorsen's function is complex, the Equation 2.48 and Equation 2.49 have real and imaginary parts. The real part reads the physical forces while the imaginary ones the phase difference (SILVESTRE, 2012) (for further details and graphs see Silvestre (2012). For numerical values of $C(k)$ see Fung (2002). For the detailed mathematical derivations see Theodorsen (1934) and Bisplinghoff e Ashley (2013)).

Abrupt Change in Attack Angle

The second classic problem refers to an abrupt change of profile's angle of attack. Wagner (1925) investigated the circulatory lift generated after an abrupt change in attack angle. With the same initial approach presented in section 2.2, Wagner approximated the wake vortex flow pattern by means of given functions, whose coefficients were determined by considering the flow tangent to the airfoil and finite velocity at trailing edge. According to Wagner's approach, a function called "Wagner Function" represented by $\phi(s)$ was defined in order to describe how lift develops from the beginning of the motion until the rest position. Wagner's function is normally presented as a function of a non-dimensional quantity proportional to the non dimensional time s, defined as:

$$s = \frac{Ut}{b}. \tag{2.50}$$

The non-dimensional time given in Equation Equation 2.50 is a measure of semi-chords traveled by the wake of vortices leaving the profile trailing edge (SILVESTRE, 2012). As a result, a step is applied at rear aerodynamic center ($3/4-$chord position) for vertical translation, h, and attack angle, α. The circulatory portion of lift force and pitch moment read:

$$\ell^{(C)}_{Wagner} = 2\pi\rho U b(w_{3/4})\phi(s), \tag{2.51}$$

$$m^{(C)}_{Wagner} = -2\pi\rho U b^2(w_{3/4})\frac{1}{2} + 2\pi\rho U b^2(w_{3/4})\phi(s)\left\{ - \left(a + \frac{1}{2}\right) \right\}. \tag{2.52}$$

Wagner (1925) listed values for his function with s varying from 0 up to 20 (SILVESTRE, 2012). Aiming to have more flexibility to model this motion, Küssner (1936) reformulated the step function as a Fourier integral solving the problem in the frequency domain deriving Equation 2.53

$$\phi(s) = \sum_{n=0}^{\infty} \frac{s^n}{n!} A_n(s), \tag{2.53}$$

Bisplinghoff e Ashley (2013) stated that even with $\phi(s)$ listed by Wagner and derived from Fourier integral by Küssner, the most common usage of this function is by means of approximation functions. The model derived by Jones (1946) gives an accurate exponential approximation to the Wagner's Function. The Jone's exponential approximation is used in the methodology adopted in this work and it is written in Equation 2.55.

$$\phi(s) = 1 + A_1 e^{b_1 s} + A_2 e^{b_2 s}, \tag{2.54}$$

$$\phi(s) = 1 - 0.165 e^{-0.041 s} - 0.335 e^{-0.32 s}. \tag{2.55}$$

Sharp-Edged Gust

The wing's profile under a sharp-edged gust is another classical case. Fung (2002) defined that for an airfoil under a sharp-edged gust w must be equal an step function, what means that for $x < 0$, w vanishes and for $x > 0$ it is equal to a constant value, w_0. Additionally, this case is also known as Küssner's problem. According to Küssner's problem, the function entitled "Küssner Function" is defined in Equation 2.56.

$$\Psi(s) = \frac{2}{\pi} \int_0^{\infty} \frac{FG(k)}{k} sin(k) s \, dk, \tag{2.56}$$

The Equation 2.56 is frequently approximated by trial and error. A well spread approximation was proposed by Sears (1941) in Equation 2.57.

$$\Psi(s) = 1 - 0.5 e^{-0.13 s} - 0.5 e^{-s}. \tag{2.57}$$

The approximation functions presented in Equation 2.55 and Equation 2.57 were of great importance in the derivations carried out in subsection 2.2.4.

2.2.4 Incremental Aerodynamic Derivatives for an Arbitrary Motion

Until now the classical problems were presented, where the perturbation source was previously known as well as defined. Nevertheless, by practical situations it is desired to know how the incremental aerodynamic loads develops under airfoil's arbitrary motions. Therefore,

there are normally two directions from this point. The first one consist of to attack numerically the integral equation of the vortex sheet. The second one is to superpose infinitesimal steps in the downwash, having as a result the unsteady circulatory lift equal the sum over the time of all infinitesimal contributions. The result of this approach is known as Duhamel's integral. The second approach was adopted by the methodology used in this work and it is briefly introduced in the following paragraphs.

Figure 5: Representation of strip's geometry and Wagner function versus non-dimensional time as an introduction to derivate the unsteady aerodynamic equations for a general profile motion with h and α as DGOF.

(a) Geometry of the j-th strip without deflections and under a abrupt change in the angle of attack (AoA).

(b) Wagner's Function versus non-dimensional time for an incompressible flow.

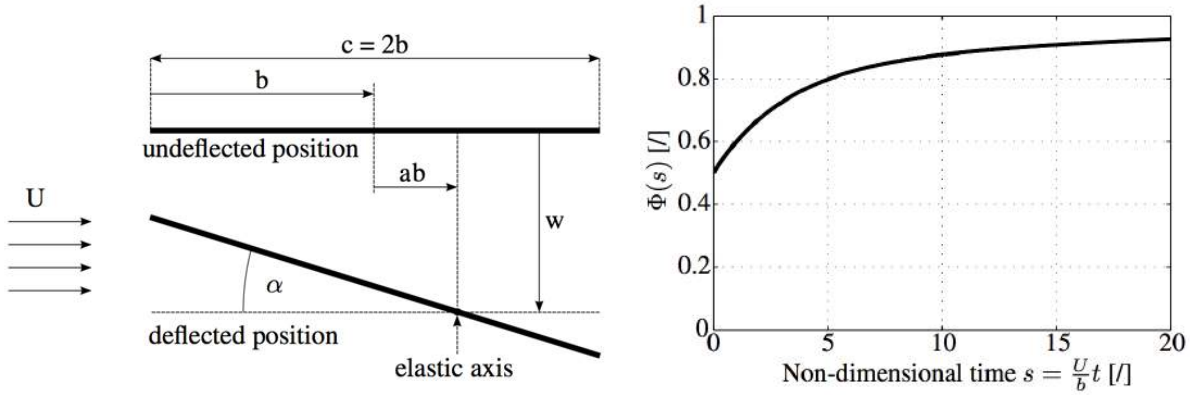

Source: Hamann (2014), p.3

In the Figure 4 a rigid airfoil under undeflected and deflected position from the beginning until its rest position was illustrated. The Figure 5a illustrates a simplification of what was previously presented. Wagner investigated the circulatory lift generated when an airfoil or a strip (in this case) undergoes an step in the angle of attack. For this case, the circulatory portion of lift force is calculated by the Equation 2.51. The Wagner function, ϕ, in relation to the non-dimensional time s, gives an interesting result for a general motion having two DGOF: h and α. For this case, the downwash over the airfoil is not uniform. The circulation for an arbitrary motion of such airfoil in this case is determined by the downwash velocity at $3/4-$chord point from the airfoil's leading edge (FÖRSCHING, 2013). The Figure 5b depicts the behavior of strip's lifting force with the nondimensional time s. Moreover, the Figure 5b shows that the lift force does not instantaneously follow the abrupt change in the angle of attack but develops it with a delay.

The circulatory lift was calculated by the sum over all infinitesimal contributions in non-dimensional time, s . The sum uses the Duhamel's integral, which is represented in Figure 6.

Figure 6: Representation of the Duhamel's integral. Superpositions of infinitesimal angle of attack steps.

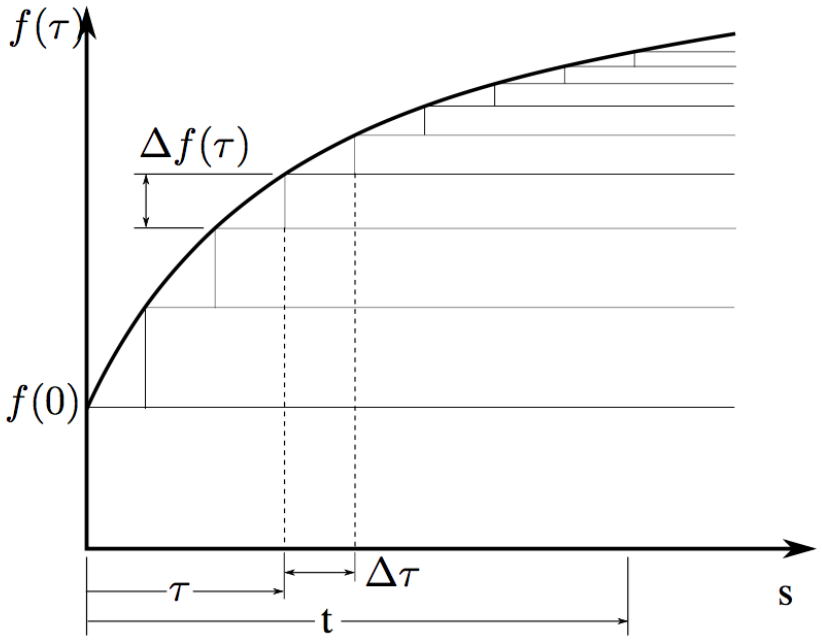

Source: Hamann (2014), p.3

By using this approach, the response to an unit-step function gives the Equation 2.58.

$$f(t) = f(t_0)A(t) + \int_{\tau=t_0}^{\tau=t} \frac{df}{dt}(\tau)A(t-\tau)d\tau. \tag{2.58}$$

The term τ in Equation 2.58 is the variable of integration, which for the inferior limit $\tau_0 = t_0$ and superior $\tau = t$. Now rewriting the Equation 2.58 for the strips theory definitions and considering the principle of superposition, which holds when w remains infinitesimal, the equations for lift force and moment read:

$$\ell^{(C)}(t) = 2\pi\rho U b\left[w_{3/4}(t_0)\phi(t) + \int_{\tau=t_o}^{t} \frac{dw_{3/4}(\tau)}{d\tau}\phi(t-\tau)d\tau\right], \tag{2.59}$$

$$m^{(C)}(t) = -2\pi\rho U b^2 w_{3/4}(t)\frac{1}{2} + \left(a + \frac{1}{2}\right)\ell^{(C)}(t). \tag{2.60}$$

If the Wagner function is assumed in its original form in Equation 2.59, the Duhamel's integral must be numerically solved for each step of time. This evaluation is in fact computational time consuming and an approximation function is acceptable in order to avoid the numerically time integration. The exponential approximation presented by Jones (1946) in Equation 2.54 was adopted. Thus, the Duhamel's integral may be analytically solved as presented in Equation 2.61

and Equation 2.62.

$$\int_{\tau=t_o}^{\tau=t} \frac{dw_{\frac{3}{4}}(\tau)}{d\tau}\phi(t-\tau)d\tau = w_{\frac{3}{4}}(t) - w_{\frac{3}{4}}(t_0) + \int_{t_o}^{t} \frac{dw_{\frac{3}{4}}(\tau)}{d\tau}A_1 e^{b_1 \frac{U}{b}(t-\tau)}d\tau + \int_{t_o}^{t} \frac{dw_{\frac{3}{4}}(\tau)}{d\tau}A_2 e^{b_2 \frac{U}{b}(t-\tau)}d\tau \tag{2.61}$$

$$\int_{\tau=t_o}^{\tau=t} \frac{dw_{\frac{3}{4}}(\tau)}{d\tau}\phi(t-\tau)d\tau = w_{\frac{3}{4}}(t) - w_{\frac{3}{4}}(t_0) + \lambda_1(t) + \lambda_2(t). \tag{2.62}$$

The terms $\lambda_1(t)$ and $\lambda_2(t)$ in Equation 2.62 are the lag state variables, introduced in the Duhamel's integral to calculate the analytical solution. $\lambda_1(t)$ and $\lambda_2(t)$ can be defined by the differential equations in Equation 2.63 and Equation 2.64.

$$\dot{\lambda}_1(t) = a_1 \frac{U}{b}\lambda_1(t) + A_1 \dot{w}_{\frac{3}{4}}(t), \tag{2.63}$$

$$\dot{\lambda}_2(t) = a_2 \frac{U}{b}\lambda_2(t) + A_2 \dot{w}_{\frac{3}{4}}(t). \tag{2.64}$$

Considering a steady condition, the term $w_{\frac{3}{4}}(t_0)$ in Equation 2.62 is zero. So that, the Equation 2.63 and Equation 2.64 can be inserted in Equation 2.62 resulting in the substitution of numerical time integration by ordinary differential equations. That is the mean advantage to approximate Wagner's function by an exponential function (SILVESTRE, 2012). For this reason, the circulatory lift and pitching moment, are given in Equation 2.65 and Equation 2.66.

$$\ell^{(C)}(t) = 2\pi\rho U b[w_{3/4}(t) + \lambda_1(t) + \lambda_2(t)] \tag{2.65}$$

$$m^{(C)}(t) = -2\pi\rho U b^2 w_{3/4}(t)\frac{1}{2} + \left(a + \frac{1}{2}\right)\ell^{(C)}(t) \tag{2.66}$$

Regarding that the right term of the 2nd-order equation of motion (see Equation 2.4) correspond to the generalized forces, which comprehend in the aerodynamic forces acting on the aircraft. The Equation 2.41 is the main equation to calculate de lift forces and has the first term ($\ell^{(NC)}$) corresponding to the non circulatory lift and the second one $\ell^{(C)}$ to the circulatory lift. The non circulatory portion may be calculated by Equation 2.42 and the circulatory portion by the Equation 2.65. These equations were used to calculate the unsteady aerodynamic behavior in lift forces and pitch moment calculations.

Furthermore, two equations are presented considering the fact that the deflection of control surfaces change the lift and pitching moment slope(SILVESTRE, 2012). The influence of this surfaces connected at the wing's trailing edge are represented by empirical equations in function of the ratio of the control surface chord (c_c) and strip chord (c): $E = \frac{c_c}{c}$. The equation for lift and moment coefficients with respect to a deflection of a flap (δ_c) are given by:

$$C_{\ell\delta_c} = \frac{C_{\ell}\alpha}{\pi}\left[\arccos(1-2E) + 2\sqrt{E(1-E)}\right], \tag{2.67}$$

$$C_{m\delta_c} = -\frac{C_{\ell}\alpha}{\pi}(1-E)\sqrt{E(1-E)}, \tag{2.68}$$

where $C_{\ell\delta_c}$ and $C_{m\delta_c}$ are the lift and pitch moment derivatives in relation to a flap deflection with angle δ_c.

Next, the section 2.3 presents the theoretical background necessary to design a pitch damper. The linearized equations of motions in state space representation, the specifications requirements as well as the longitudinal and short period approximations are introduced.

2.3 Flight Control System

This section introduces the theoretical background necessary to design a pitch damper. The aircraft forces, moments and velocities are illustrated in Figure 7. Moreover, the linearized EOM in state-space formulation are discussed. The linearized EOM may be decoupled in longitudinal dynamics and lateral-directional dynamics. The short period motion approximation is derived from the longitudinal dynamics and the feedback loop to augment the pitch rate in relation to elevator control is given. The flight qualities requirements are defined following the military specification for piloted airplanes MIL-F-8785C (1980).

Figure 7: Representation of forces, moments and velocities associated with the aircraft motion.

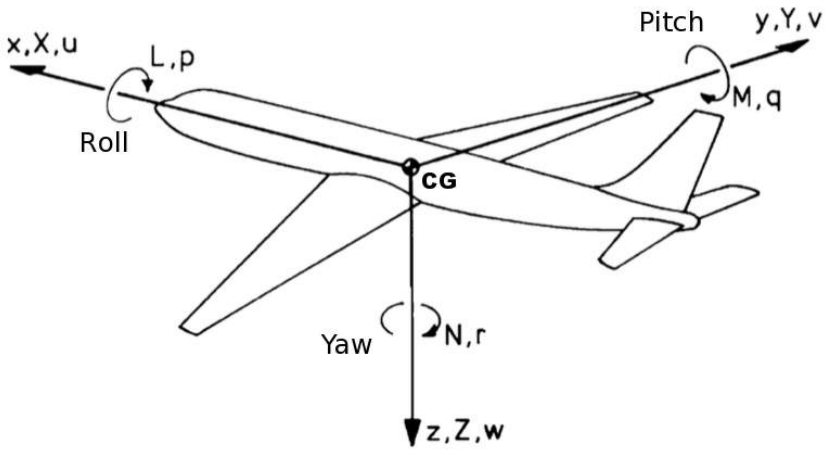

Source: adapted from Brockhaus, Alles e Luckner (2011), pg 9.

2.3.1 Longitudinal Dynamics

The aircraft's EOM describes the behavior of the flight vehicle in terms of its motion as a function of the time. The derivations particularities are given in flight mechanics literatures such as Etkin e Reid (1998), Cook (2012) and Brockhaus, Alles e Luckner (2011). In Figure 7 the roll, pitch and yaw axes as well as aerodynamic forces, momenta and velocities are illustrated. The EOM can be decoupled into longitudinal and lateral motions. The longitudinal motion

comprehends the motion constrained in the longitudinal plane of symmetry. The components included are only the axial force X, the normal force Z and the pitching moment M. For the control deflections, in the longitudinal motion only the elevator η and flaps η_k may influence the aircraft motion. On the other hand, in the lateral equations of motion the variables consider are only the side force Y, the rolling moment L and the yawing moment N (see Figure 7). The controllers that change the longitudinal flight qualities are the rudder ζ and ailerons ξ.

According to Cook (2012), two stability modes are typical in the longitudinal dynamics, the phugoid and the short period motions. The phugoid is a lightly damped low frequency oscillation in aircraft forward speed, which couples pitch attitude θ and height h, while the incidence attack angle remains constant during the motion. The short period mode comprehends a damped oscillation in pitch. If an aircraft has its pitch equilibrium disturbed in some way like a step command in elevator η, this motion is excited varying the attack angle α, pitch rate q and pitch attitude θ with a second order system behavior. During the short period motion, the aircraft forward speed remains constant. The Figure 8 illustrates the effects of the short period into the flight altitude and attack angle. In the following section the state space formulation for the longitudinal motion is presented.

2.3.2 State Space Formulation

The linearized EOM of the aircraft can be written in the state space formulation. The system matrix $\mathbf{A}$ and system's input matrix $\mathbf{B}$, are written as a function of the stability derivatives. The Equation 2.69 and Equation 2.70 give the general formulation of a state space formulation without disturbances (NISE, 20011).

$$\dot{\mathbf{x}} = \mathbf{A}\,\mathbf{x} + \mathbf{B}\,\mathbf{u}, \tag{2.69}$$

$$\mathbf{y} = \mathbf{C}\,\mathbf{x} + \mathbf{D}\,\mathbf{u}. \tag{2.70}$$

Figure 8: Behavior of the short period motion with exaggerated effects on attack angle and altitude deviations, and lower damping.

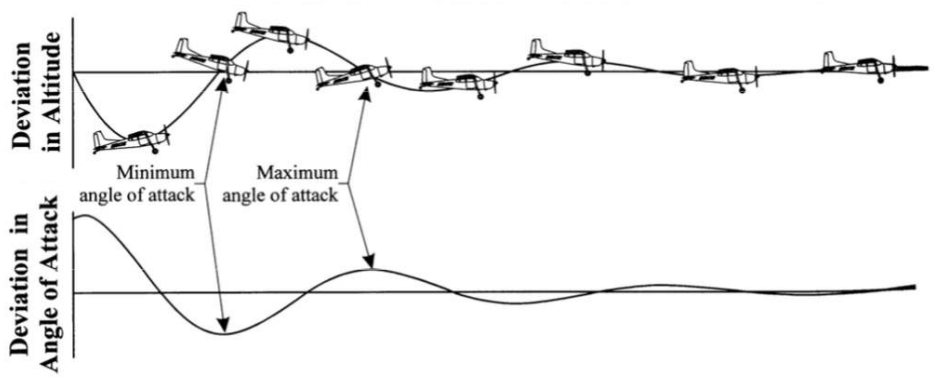

Source: Adapted from Nelson (1998).

For the aircraft system of equations the state vector, $\mathbf{x}$, and the controls vector, $\mathbf{u}$, have respectively the following arrangement:

$$\mathbf{x} = \Big[V \underbrace{\quad \theta \quad q \quad \alpha \quad H \quad}_{\text{Longitudinal Motion}} \underbrace{\beta \quad p \quad \phi \quad r}_{\text{Lateral Motion}}\Big]^T, \tag{2.71}$$

$$\mathbf{u} = \Big[\eta_F \quad \eta_k \quad \xi \quad \eta \quad \zeta\Big]^T. \tag{2.72}$$

In Equation 2.71, the first five terms in state vector correspond to the longitudinal motion and the last four terms to the lateral motion. In the control vector, thrust (η_F) and elevator (η) controls have influence in the longitudinal motion. For the lateral motion, flaps (η_k), rudder (ζ), and aileron (ξ) are considered. Considering the effects of elasticity, the state vector presented in Equation 2.71 is extended to consider the modal amplitudes and the aerodynamic lag states. Thus, the state vector becomes:

$$\mathbf{x}_{flex} = \Big[\mathbf{x} \quad \eta_1 \quad \dot{\eta_1} \quad \eta_2 \quad \dot{\eta_2} \quad \dots \quad \eta_{n_e} \quad \dot{\eta_{n_e}} \quad \lambda_{11} \quad \lambda_{21} \quad \dots \quad \lambda_{1j} \quad \lambda_{2j}\Big]^T. \tag{2.73}$$

In order to develop a pitch damper to decrease the effects of the short period in the aircraft motion, the state space is reduced to take account only to the longitudinal motion. In this case, the flight dynamic equations for the line flight without disturbances into the longitudinal motion in state space formulation read:

$$\begin{bmatrix} \dot{V} \\ \dot{\theta} \\ \dot{q} \\ \dot{\alpha} \\ \dot{H} \end{bmatrix} = \begin{bmatrix} X_V & X_\theta & X_q & X_\alpha & 0 \\ 0 & 0 & 1 & 0 & 0 \\ M_V & M_\theta & M_q & M_\alpha & 0 \\ Z_V & Z_\theta & Z_q & Z_\alpha & 0 \\ 0 & V_0 & 0 & 0 & 0 \end{bmatrix} \begin{bmatrix} V \\ \theta \\ q \\ \alpha \\ H \end{bmatrix} + \begin{bmatrix} X_\eta & X_{\eta_F} \\ 0 & 0 \\ M_\eta & M_{\eta_F} \\ Z_\eta & Z_{\eta_F} \\ 0 & 0 \end{bmatrix} \begin{bmatrix} \eta \\ \eta_F \end{bmatrix} \tag{2.74}$$

The Equation 2.74 gives the first order linearized equations of aircraft's longitudinal motion. As introduced above, the longitudinal motion have two typical rigid body motions: phugoid and short period. Based on the system of Equation 2.74 both motions can be decoupled into reduced state space systems. The terms of velocity V and pitch angle θ in state vector approximate the phugoid motion, while pitch rate q, attack angle α and altitude H give the short period approximation. Since the objective comprehends to design a pitch damper, only the short period approximation is considered. The pitch rate q and alpha angle α are used to formulate the short period state-space system approximation.

In face of the presented, the longitudinal motion system of Equation 2.74 are reduced to the short period motion system of equations given in Equation 2.75.

$$\begin{bmatrix} \dot{q} \\ \dot{\alpha} \end{bmatrix} = \begin{bmatrix} M_q & M_\alpha \\ Z_q & Z_\alpha \end{bmatrix} \begin{bmatrix} q \\ \alpha \end{bmatrix} + \begin{bmatrix} M_\eta \\ Z_\eta \end{bmatrix} \Big[\eta\Big] \tag{2.75}$$

As written in Equation 2.75 the following characteristic equation can be written:

$$\Delta(s) = s^2 - s(M_q + Z_\alpha) + M_q Z_\alpha - M_\alpha = 0. \tag{2.76}$$

According to Equation 2.76, the frequency and damping of the second order system are written in Equation 2.77 and Equation 2.78.

$$w_{SP} \approx \sqrt{Z_\alpha M_q - M_\alpha} \tag{2.77}$$

$$\zeta_{SP} \approx \frac{1}{2}(M_q + Z_\alpha) \tag{2.78}$$

2.3.3 Flying Qualities Requirements

The flying qualities requirements are stated in order to specify the performance criteria necessary to attend the safety and dynamic behavior of the aircraft. For this work the American Military Specifications *MIL-F-8785C (1980)* is adopted. This document present several definitions for aircraft's lateral and longitudinal motions derived according to the aircraft class, flight phase category and level of flight qualities. One important fact is that the requirements are developed based on the dynamics of classical aircraft whose short period is given by a second order function.

The flying qualities requirements are defined based on the aircraft flight phase, level of flight and flight envelope. The aircraft type can be classified in one of the following classes:

- Class I: small light airplanes;
- Class II: medium weight, low to medium maneuverability aircraft;
- Class III: Large, heavy, low to medium maneuverability aircraft;
- Class IV: High maneuverability aircraft;

The aircraft flight phase is defined based on the sequence of piloting tasks. The categories are:

- Category A: Non terminal flight phases that require rapid maneuvering, precision tracking, or precise flight path control.
- Category B: Non-terminal flight phases that require gradual maneuvering, less precise tracking and accurate flight path control.
- Category C: Terminal flight phases that require gradual maneuvering and precision flight path control.

Next, the levels of flying qualities are given. The levels quantify the degree of acceptability of an airplane in terms of its ability to complete the mission for which is designed. The levels that indicate the severity of the pilot workload in the execution of a mission are given:

- Level 1: Flying qualities clearly adequate for the mission flight phase;
- Level 2: Flying qualities adequate to accomplish the mission flight phase, but with an increase in pilot workload and, or, degradation in mission effectiveness;
- Level 3: Degraded flying qualities, but such that the aircraft can be controlled, inadequate mission effectiveness and high, or, limiting, pilot workload;

Table 1: Operational flight envelopes.

Flight Phase Category	Flight Phase
A	Air-to-air combat
	Ground Attack
	Weapon delivery/launch
	Reconnaissance
	In-flight refuel (receiver)
	Terrain following
	Maritime search
	Aerobatics
	Close formation flight
B	Climb
	Cruise
	Loiter
	In-flight refuel (tanker)
	Descent
	Aerial delivery
C	Takeoff
	Approach
	Overshoot
	Landing

Source: MIL-F-8785C (1980).

The following parameter is the operational flight envelope. In this requirement the aircraft must be capable of operate on the limits defined by the flight envelope during the execution of its mission. The Table 1 lists the operational flight envelopes listed by MIL-F-8785C (1980).

With the flying qualities presented, the reference values of damping and frequency are presented only for the short period because the objective is to design a pitch damper controller. The short period requirements are specified in terms of natural frequency and damping. The investigated aircraft need to be classified under a Class, a Category and a Flight Level in order to define the frequency and damping limits according to Table 2.

Table 2: Short period mode damping.

Flying Phase	Level 1		Level 2		Level 3
	$\zeta_{SP,min}$	$\zeta_{SP,max}$	$\zeta_{SP,min}$	$\zeta_{SP,max}$	$\zeta_{SP,min}$
CAT A	0.35	1.30	0.25	2.00	0.10
CAT B	0.30	2.00	0.20	2.00	0.10
CAT C	0.50	1.30	0.35	2.00	0.25

Source: Adapted from MIL-F-8785C (1980).

The Figure 9 shows the frequency limits for the short period motion of an aircraft with flight phase Category B.

Figure 9: Short period frequency requirements for flight phases Category B.

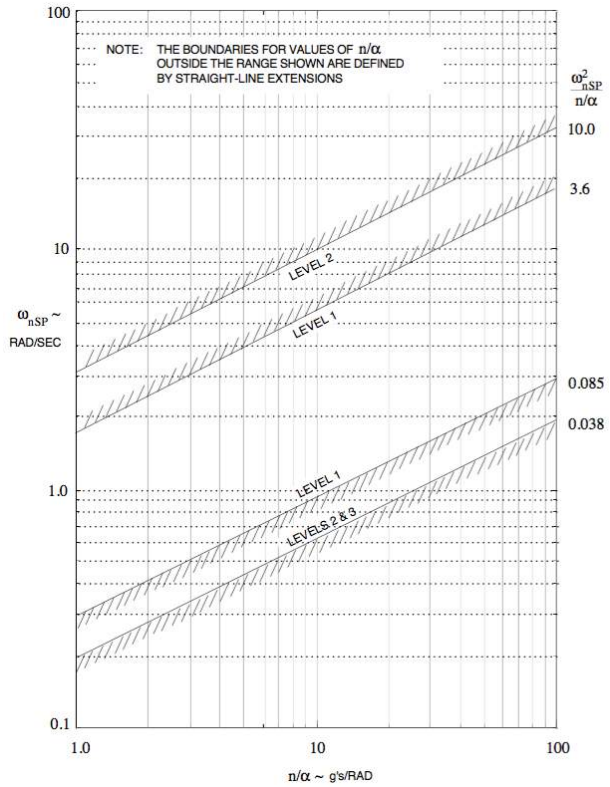

Source: MIL-F-8785C (1980).

The Table 3 lists the damping and frequency ratio limits for an aircraft with flight phase Category B and Level 1.

The term n_α in the frequency specification presented in Figure 9 and Table 3 is the aircraft load-factor response to angle of attack in g's per radian. Due this definition the frequency specifications should be obtained indirectly. The restricted values of damping and frequency represent the domain where the closed loop system may work respecting the flying qualities proposed by the MIL-F-8785C. The next section will present the implementation of the feedback

Table 3: Short period damping and frequency ratio limits for an aircraft with flight phase Category B and Level 1.

Mode	Damping Specification	Frequency Specification
Short-period	$0.30 \leq \zeta_{SP} \leq 2.00$	$0.085 \leq \frac{\omega_{n_{SP}}^2}{(n_\alpha)} \leq 3.60$

Source: Adapted from MIL-F-8785C (1980).

controller pitch damper.

2.3.4 Pitch Damper Implementation

The Figure 10 illustrates the block diagram of the closed loop system. The pitch damper is designed with gain factors $k_{\eta\alpha}$ and $k_{\eta q}$, or in terms of a vector: $\mathbf{k} = [k_{\eta q} \quad k_{\eta\alpha}]$. The aircraft model comprehends in the state-space formulation defined in Equation 2.69 and Equation 2.70 .

Figure 10: Block diagram of the pitch damper feedback with the state space aircraft model and the actuator dynamic block.

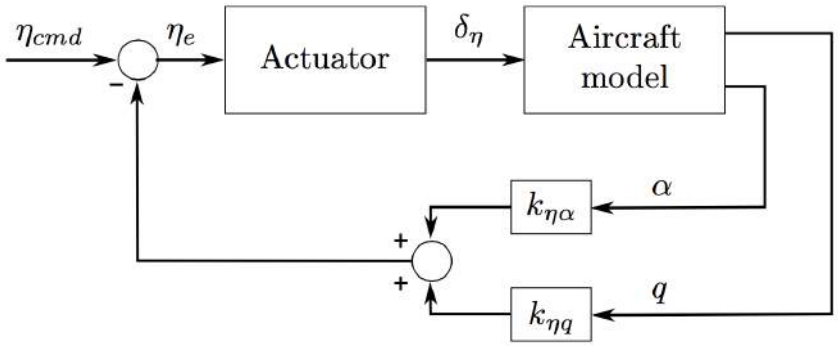

Source: Mila (2013).

Rewriting the state-space formulation for the augmented system, the short-period approximation with damping is given by:

$$\dot{\mathbf{x}} = (\mathbf{A} - \mathbf{B}\,\mathbf{K})\mathbf{x} + \mathbf{B}\,\mathbf{u}, \tag{2.79}$$

$$\dot{\mathbf{x}} = \mathbf{A}_{mod}\,\mathbf{x} + \mathbf{B}\,\mathbf{u}, \tag{2.80}$$

$$\begin{bmatrix} \dot{q} \\ \dot{\alpha} \end{bmatrix} = \left\{ \begin{bmatrix} M_q & M_\alpha \\ Z_q & Z_\alpha \end{bmatrix} - \begin{bmatrix} M_\eta \\ Z_\eta \end{bmatrix} . \begin{bmatrix} k_{\eta q} & k_{\eta\alpha} \end{bmatrix} \right\} \begin{bmatrix} q \\ \alpha \end{bmatrix} + \begin{bmatrix} M_\eta \\ Z_\eta \end{bmatrix} \begin{bmatrix} \eta \end{bmatrix} . \tag{2.81}$$

The characteristic equation of the modified system is given in Equation 2.82.

$$\Delta(s) = |s\mathbf{I} - \mathbf{A}_{mod}| = |s\mathbf{I} + \mathbf{A} + \mathbf{B}\,\mathbf{k}| = \mathbf{0} \tag{2.82}$$

In the Equation 2.82 the the system's closed loop frequency $\omega^*_{n_{SP}}$ and damping ζ^*_{SP} may be calculated, respectively, by respecting the following equations:

$$\omega^*_{n_{SP}} = \sqrt{(M_q - M_\eta k_{\eta q}).(Z_\alpha - Z_\eta k_{\eta\alpha}) - (M_\alpha - M_\eta k_{\eta\alpha})(Z_q - Z_\eta k_{\eta q})}, \tag{2.83}$$

$$\zeta^*_{SP} = \frac{M_\eta k_{\eta q} - Z_\alpha - M_\alpha + Z_\eta k_{\eta\alpha}}{2\omega_{n_{sp}}} \tag{2.84}$$

3 Models

This chapter presents the two aircraft investigated in this work. The first aircraft, also called reference aircraft, is the Stemme S15. The Stemme S15 was investigated by Silvestre (2012) through the implementation of the methodology adopted in this work. Due the new wing structural properties with unmodified geometry, the Stemme S15 was renamed to Ecarys ES15. The second aircraft investigated in this work is the Ecarys ES15 with two configurations, with and without attached pods under the aircraft's wing. The attached pods may be used either as external fuel tanks or to allocate cameras and further equipments necessary to surveillance roles or even sensors in atmospheric research flights. Moreover, the non-linear-high-fidelity flight simulation model developed at TU Berlin is briefly introduced followed by the aeroelastic models. Due the fact that new aircraft's wing geometry remains the same and only the structural properties have been modified, the spanwise aerodynamic properties for incremental aerodynamic modeling remain the same and are not presented here, the reader is than referred to chapter 4 in Silvestre (2012). Therefore, the following topics presented are, respectively, the simulation model, the aeroelastic models of previous wing release and new wing release with and without pods attached under the aircraft's wing. The GVT results are given in subsection 3.3.2 as well as its linear interpolation. Last, the definition of flying qualities requirements are listed.

3.1 Flight Simulation Model

The *Department of Flight Mechanics, Flight Control and Aeroelasticity (FMRA)* at *Technische Universität Berlin (TUB)* developed in recent years a project entitled LAPAZ, where a non-linear high-fidelity flight simulation model was developed in MATLAB® Simulink for the rigid motor glider aircraft analyzed in this work (DALLDORFF R. LUCKNER, 2013). This flight model simulation defines the aircraft as a rigid body, with 6 DGOF equations of motion, considering the earths rotation and the fact that it is an ellipsoid. The model considers the aircraft's flight dynamics, power plant and the necessary sensors used as an input to validate the flight control system design at low level (SILVESTRE, 2012). Regarding to this fact, to considered the aircraft elastic properties in flight simulation model is something desired in order to have a hight fidelity physical interpretation.

3.2 Aircraft

The properties of motor glider aircraft Ecarys (EC) ES15 developed by the German company Stemme and supported by *"Europäischer Fonds für regionale Entwicklung" (EFRE)* are presented. The EC ES15 is a motor glider multi role aircraft designed on the platform of the motor

glider Stemme S15, with the objective to operate as a platform to surveillance, reconnaissance and in flight research. Environmental protection, infrastructure monitoring, lenticular measurements and atmospheric research are some of roles that this aircraft is able to perform. The Figure 11 presents the aircraft in flight with pods attached under the both sides of the wing. Following that in Figure 12 the aircraft's three views is depicted.

Figure 11: EC ES15 in flight with pods attached under the wing.

Source: Ecarys (2014).

Figure 12: Details of the aircraft geometry in three views.

Source: Adapted from Ecarys (2014).

The general design properties of the aircraft are listed in Table 4. The EC ES15 is equipped with a *ROTAX 914 F Turbo* engine, that delivers $115hp$ at maximal takeoff power. The aircraft has two seats, tail with *"T"* configuration and retractile land gears. An upgrade feature of the EC ES15 in relation to the Stemme S15 is higher payload mass due structure optimization. Thus, the mean modification are the aircraft's wing structural properties to decrease the structure mass.

In order to reduce the wing's structural mass the manufacturing and structural properties of the spar flange were improved by means of fiber enforcement techniques. Previous researches

have demonstrated that the aircraft spar could fracture due compression, due this fact the effort focused on developing a test method of the compressive strength of certain materials and manufacturing processes in a partnership with *Frauenhofer Institut PYCO* in Berlin. The *Prepregs* (Pre-impregnated composite fibers) technique was used in the EC ES15 shown that considerable higher compression strengths were achieved. Additionally, more homogeneous fiber distribution as well as fewer and lower air bubbles were achieved between fiber and resin in comparison with the wet process performed by Stemme. Nevertheless the manufacture effort to accomplish such properties were excessively meticulous to be adopted in series production. The decision was then to improve and maintain the wet process (ECARYS, 2014).

Table 4: EC ES15 general properties.

General Properties	Symbol	Unit	Value
mass full filled	m_{total}	1100.00	kg
mass empty	m_{empty}	750.00	kg
payload mass	m_{PL}	350.00	kg
wing span	$2b$	18.00	m
length	L	8.50	m
reference area (wing's area)	S	17.40	m^2
reference length, longitudinal	MAC	1.01	m
CG position (nose), x (GCS)	xCG	-2.60	m
CG position (nose), y (GCS)	yCG	0.00	m
CG position (nose), z (GCS)	zCG	-0.21	m
Service Ceiling	$H_{operational}$	7620	m
operating Speed (true speed, TAS)	V_{TAS}	270.00	km/h

Source: Adapted from Ecarys (2012).

3.3 Aeroelastic Model

As introduced in chapter 1, the aeroelastic model is defined based on a structural and an aerodynamic model. These models are coupled in order to analyze the effects of structural flexibility and the changes in aerodynamic derivatives due such displacements, which consequently influence the aircraft flight dynamical performance. Due this fact, structural dynamic and aerodynamic theories were applied aiming to represent this elastic influence on the vehicle response. In the Figure 13 the basic steps to create a aeroelastic model are presented. The structural model consider ground vibration tests (GVT) and/or a finite element model of the structure. Parallel to this the aerodynamic model defines the aerodynamic theory, wind tunnel test and/or computational fluid dynamics (CFD). Next, the block (SAC) presents the structural-aerodynamic coupling. Following this an analysis of results is performed. If the flight qualities are satisfactory the flight tests are performed and in if not it is necessary to go back and update the models.

Figure 13: Steps to perform an aeroelastic analysis.

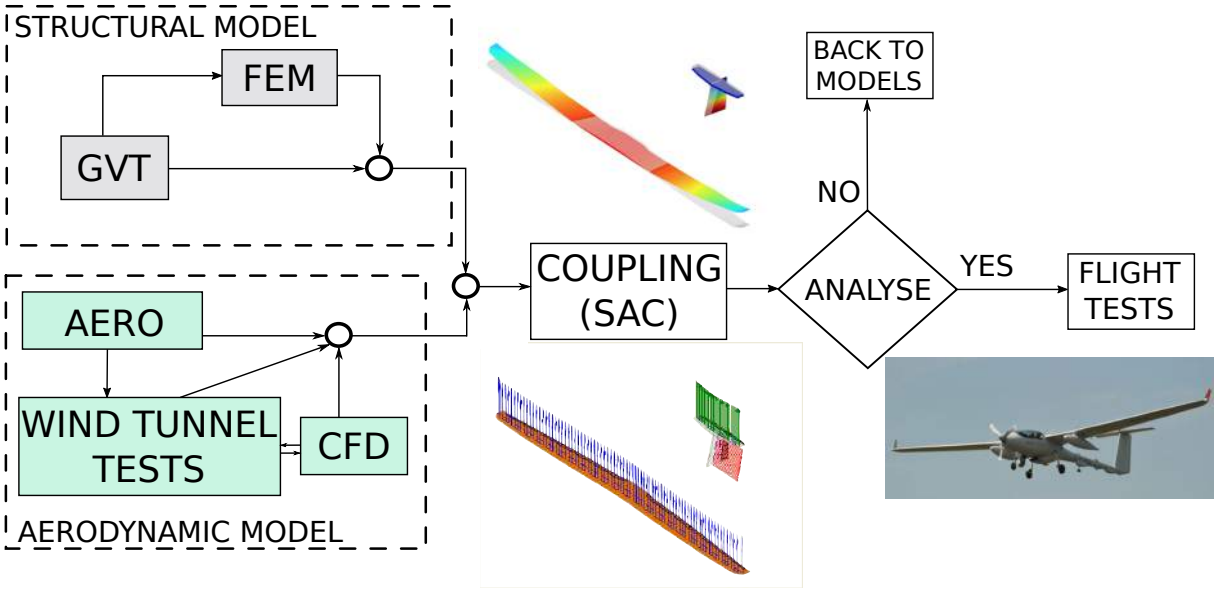

Source: Author.

In order to automate the steps presented by the Figure 13, Silvestre (2012) developed the graphical interface software *FlexSim* in MATLAB®, which was used in this work. *FlexSim* requires a set of input data to simulate the aircraft dynamical response, which are respectively: flight, atmosphere and aircraft general properties (e.g. mass, inertia momenta, CG Position), control surfaces, aerodynamic strips model and aircraft structural properties. The structural properties input comprehend one of the main efforts of this work due to EC ES15 new wing structural properties.

Organizing the steps to define an aeroelastic simulation model with *FlexSim* in a systematic way, the following points are presented:

1. Load aircraft general properties (e.g. mass, inertia momenta, CG Position);
2. Load structure file where aircraft geometry, eigenvalues, eigenvectors and referential values are defined;
3. Create a strip model defining number of strips, elastic line and mean aerodynamic line, aerodynamic properties such as incidence angle, lift slope and pitching moment coefficient at zero attack angle, for each strip, and finally the control surfaces geometry, variables and their aerodynamic properties as well (see Figure 14);
4. Perform the linearization of elastic modes and definition of stripwise equivalent displacement and torsion;
5. Define the flight condition by means of aircraft speed, flight altitude, path and side slip angle;

Figure 14: Aircraft's wing and empennages geometry modeled with strips and lift slopes representation.

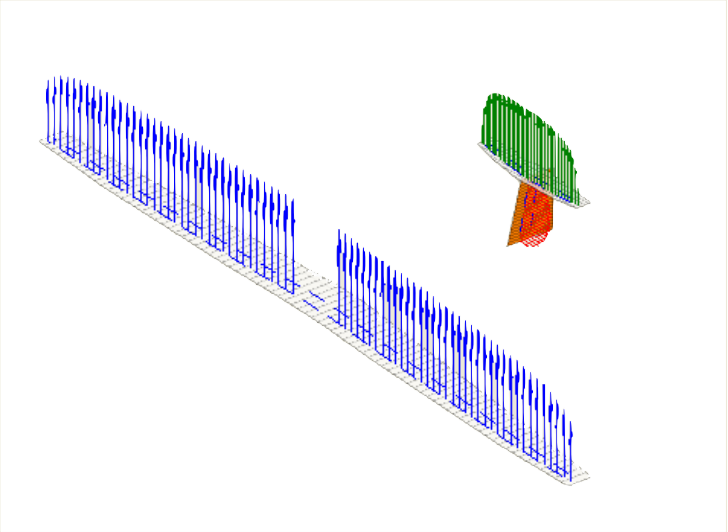

Source: Author.

6. Select the control to trim the aircraft;
7. Linearize the model to obtain the system matrices;
8. Simulate the model as rigid body or elastic with unsteady aerodynamic approach to obtain the aircraft dynamical response.

The three aircraft's structural properties are presented in next section. First the motor glider Stemme S15 investigated by Silvestre in his methodology is briefly presented, next the GVT results give the structural properties of the EC ES15 with pods and without pods.

3.3.1 Structural Properties

In subsection 2.1.2 the equations that describe the aircraft structural dynamics were written in the modal approach. When working with simple models the eigenvalues and eigenvectors matrices can be analytical solved, but as more complex as the structure becomes, harder is to solve them. Thus, numerical or experimental results are a good option to solve the problem. Ground vibration tests (GVT) were performed to identify the aircraft's structural behavior and are presented in subsection 3.3.2. Additionally, with exception to the aircraft Stemme S15, there were no available finite element models (FEM).

The structural properties of the three models, such as frequencies, damping and modal shapes are presented. Regarding that as flexible a structure is, also closer are the rigid body and vibrational frequencies. For this reason, frequencies up to $30Hz$ are investigated in this work. At the EC ES15 the procedure used to interpreter the ground vibration results and adapt them to an input file in readable FlexSim form is demonstrated.

3.3.1.1 Stemme S15

The Table 5 gives the first sixteen structural dynamic modes determined at the GVT realized at the TUHH (Technische Universität Hamburg-Harburg) in 2008.

Table 5: Structural properties of Stemme S15.

k	Denomination	Modal Frequency $\omega_{n_k}\ [Hz]$	Damping $\zeta_{n_k}\ [\%]$	Symmetry
1	1st bending, wings	3.29	0.55	S
2	1st swing, wing and body	4.23	1.24	A
3	1st bending, wings	7.33	1.00	A
4	1st swings, wings	7.39	1.02	S
5	1st torsion, body	8.06	1.75	A
6	1st bending, body	9.01	0.84	S
7	2nd bending, wings	11.55	0.72	S
8	1st swing, horizontal fin	11.72	1.34	A
9	1st bending, horizontal fin	13.34	0.86	A
10	2nd bending, wings	15.37	1.09	A
11	2nd bending, body	19.74	1.74	S
12	2nd swing, wings and body	20.13	0.86	A
13	3rd bending, wings	21.02	2.06	S
14	2nd swing, wings	27.52	1.98	S
15	1st torsion, wings	28.83	1.26	S
16	1st torsion, wings	28.99	3.01	A

Source: Adapted from Silvestre (2012).

3.3.1.2 Ecarys ES15

The EC ES15 is a configuration derived from Stemme S15 with new design and performance features. Aiming to identify the aircraft's structural properties a GVT was realized by the company *Leichtwerk* in May 2015 in Braunschweig, Germany. The Figure 15 presents the aircraft under tests with a set of accelerometers attached at wing, fuselage and empennages. The tests were performed separately with fixed and free controls, the aircraft was supported by big inner tubes that worked as air dampers. Electromechanical exciters ("*shakers*") were attached to the airframe to excite the normal modes. The *shakers* excite with multiple force levels a single mode of vibration according to the phase resonance method (THORBY, 2008). The normal mode excitation approach vanishes the damping in the structure. This method is commonly adopted in aircraft structure measurements not only because of the accuracy to measure normal modes, that can be directly compared with FEM models, but also due the ability to investigate nonlinearities (MAIA; SILVA, 1997).

The GVT was performed with two aircraft configurations, the first one with pods and the second one without pods. The representation of the aircraft with attached pods is illustrated in

Figure 15: Aircraft EC ES15 at GVT tests performed at the company *Leichtwerk* in Braunschweig, Germany.

Source: Leichtwerk (May, 2015).

Figure 16 and Figure 11.

The results of the GVT are disposed in Table 6. The tests identified a total of twenty eight modal shapes but only the first twenty five with frequency up to $30Hz$ are presented. The Table gives also the elastic modes denomination, the modal frequency (ω_n) of each mode and damping (ζ_n). The last column gives the symmetry of the elastic mode, where the letter *A* is used to asymmetric and *S* for symmetric modal shapes. The modal shapes of EC ES15 with pods are presented in Appendix A for the wing, horizontal (HTP) and vertical (VTP) tailplanes.

Figure 16: Motor glider EC ES15 with pods attached under the both sides of the wing.

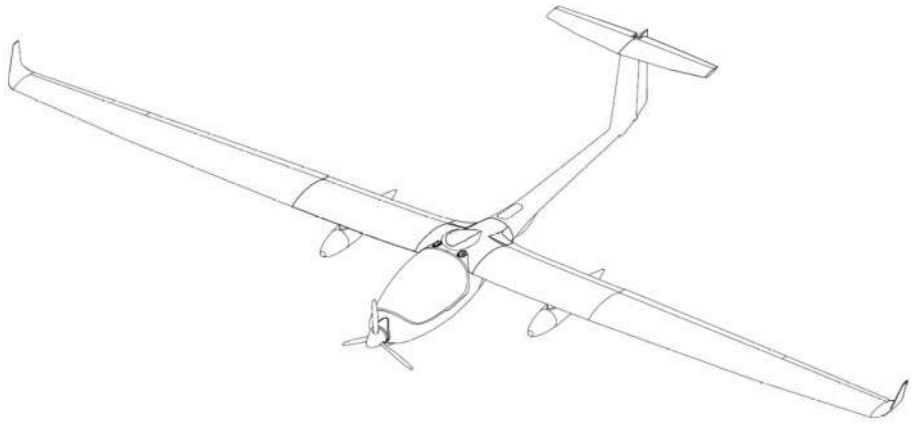

Source: Ecarys (2014), pg 6.

Next, the structural properties of the motor glider without pods are presented. The Figure 17 depicts the aircraft airframe without pods. The GVT test has identified a total of twenty two modal shapes for this case. However, just the first eighteen are of interest. The Table 7 lists the

Table 6: Structural properties of EC ES15 with pods.

k	Denomination	Modal Frequency $\omega_{n_k}\ [Hz]$	Damping $\zeta_{n_k}\ [\%]$	Symmetry
1	1st bending, right pod	3.46	0	A
2	1st bending, wing	3.79	0	S
3	1st swing, tail	4.45	0	A
4	1st bending, left pod	4.75	0	A
5	1st bending, wing	6.67	0	A
6	1st swing, right pod	7.64	0	A
7	1st bending, tail	7.78	0	A
8	1st swing, wing	7.83	0	S
9	1st swing, left pod	8.51	0	A
10	2nd bending, right pod	9.12	0	S
11	1st swing, HTP	11.85	0	A
12	2nd swing, HTP	13.14	0	A
13	2nd bending, wing	13.57	0	S
14	3rd bending, right pod	14.27	0	A
15	2nd bending, left pod	15.33	0	A
16	1st swing, both pods	18.00	0	A
17	2nd swing, wing	18.39	0	A
18	1st bending, HTP	19.13	0	S
19	2nd bending tail	19.51	0	A
20	2st bending, HTP	21.50	0	S
21	2nd swing, left pod	23.71	0	A
22	2nd bending, wing	25.02	0	A
23	3rd bending, wing	25.22	0	S
24	1st torsion, wing	29.74	0	A
25	2nd torsion, wing	29.80	0	S

Source: Author.

mode's denomination, their respective frequencies, damping and symmetry following the same structure presented to the configuration above.

Figure 17: Motor glider EC ES15 without attached pods.

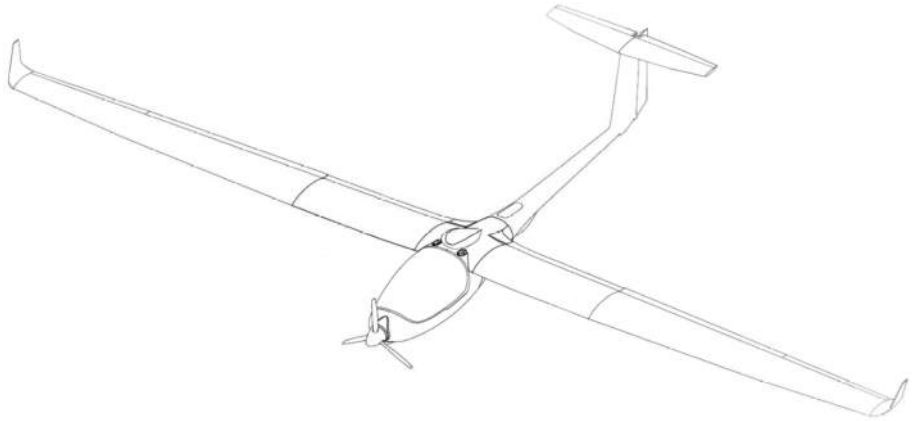

Source: Adapted from Ecarys (2014), pg 6.

The structural properties of three models are based only from ground vibration tests results and no finite element model was available to be compared or updated. Because of that, it was necessary to analyze, interpret and interpolate the GVT results provided by the company that performed the tests in order to arrange the data as an readable input file to *FlexSim*.

Table 7: Structural properties of EC ES15 without pods.

k	Denomination	Modal Frequency $\omega_{n_k}\ [Hz]$	Damping $\zeta_{n_k}\ [\%]$	Symmetry
1	1st bending, wing	3.78	0	S
2	1st bending, tail	4.53	0	A
3	2nd bending, tail	7.77	0	A
4	1st swing, wing	7.97	0	S
5	1st bending, wing	8.14	0	A
6	1st swing, tail	9.35	0	S
7	1st swing, tail	11.89	0	A
8	2nd bengin, wing	12.96	0	S
9	2nd swing, tail	13.34	0	A
10	3rd bending, tail	18.71	0	A
11	1st bending, HTP	19.42	0	S
12	2nd bending, HTP	21.35	0	S
13	1st swing, wing	21.37	0	A
14	3rd bending, wing	25.32	0	A
15	3rd bending, wing	27.87	0	S
16	1st torsion, wing	29.04	0	S
17	1st torsion, wing	29.10	0	A
18	2nd swing, wing	29.78	0	S

Source: Author.

3.3.2 Linear Interpolation of Modal Shapes from Ground Vibration Test

The GVT was performed by the company *Leichtwerk*. The author and the first co-supervisor accompanied the tests during a day in Braunschweig in order to better understand how the steps were developed. To perform the test, a set of accelerometers were attached on wing, fuselage and empennage surfaces. However, only the results measured by the sensors attached on wing and empennages were considered in the analysis. The accelerometers were fixed in a chordwise line pattern for different positions in spanwise. Considering such disposal, two accelerometers were attached per strip and the results were interpolated to a reference point in the three-quarter point of the profile section for every strip of wing and empennages. In doing so, the GVT results were concentrated in in the one-quarter chord point in relation to the leading edge per strip and the displacements being divided in three spatial components: plunging, lagging and pitching. The Figure 18 displays the GVT data results received from *Leichtwerk* disposed through the aircraft's geometry.

Figure 18: Concentrated points containing the ground vibration tests' results interpolated at three-quarter chord for wing and empennages.

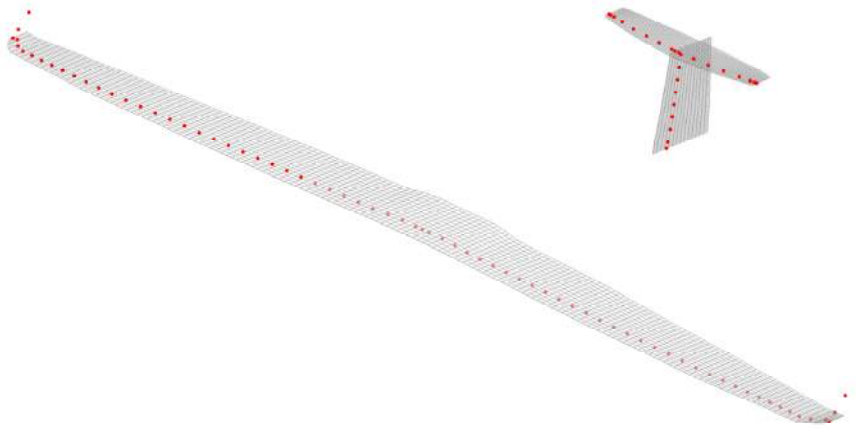

Source: Author.

The Figure 19a depicts the displacement components for the $j-th$ strip in the profile's $3/4\times$chord point. According to Figure 19a the plunging component reads displacement in z axis, lagging the displacements in x axis and pitching the rotation $d\theta$ of a strip. Aiming to extend the displacements over the total aircraft's geometry and have a better representation of its dynamic structural characteristics, interpolations were carried out.

To initialize the interpolation the aircraft's geometry must be known in order to define the interpolation domain. Due the fact that there were no modifications between the geometry of Stemme S15 and EC ES15, the finite element model of the Stemme S15 was taken and verified with the EC ES15 CAD drawings. Once proved that main dimensions remained the same, the aircraft geometry was defined. The leading and trailing edges designated the forward

Figure 19: Interpolation steps performed to represent the structural dynamic over the aircraft geometry.

(a) Representation of data received from GVT

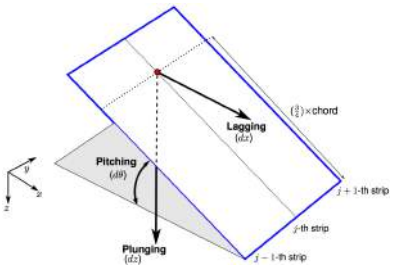

(b) Linear interpolation at strip's spanwise middle point.

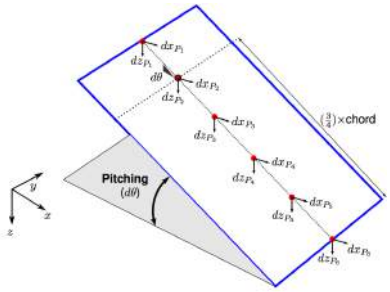

(c) Biharmonic spline interpolation with MATLAB® *griddata* function method *v4* (SANDWELL, 1987).

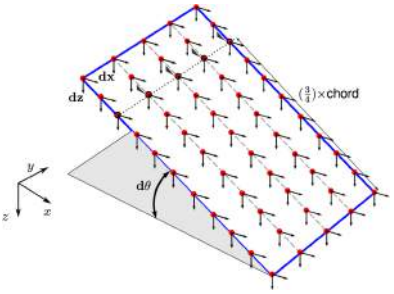

Source: Author.

and backward limits to interpolate the displacements in the wing's chordwise direction and the span width to spanwise direction. Thus, with aircraft's geometry and GVT results, as presented in Figure 19a, the linear interpolation was performed. The goal of such interpolation was to extend the structural displacements from the one-quarter chord point to a set of point through the chordwise direction, as depicted in Figure 19b. The Figure 20 shows the same representation of Figure 19b in two dimensional view. The horizontal profile represent the undeformed structure and the oblique one the deformed structure. The profile is considered rigid, what means no deformations through the chord line. The points P_i and $P_i + dP_i$ can be easily related with trigonometrical equations in order to calculate the displacements in x and z axes and torsion (pitching) for every point through the chordwise. The equations derived to calculate the displacements in z and x directions, read respectively:

$$dz_{P_i+dP_i} = dz + \frac{b}{2}\sin(d\theta), \tag{3.1}$$

$$dx_{P_i+dP_i} = dx + \frac{b}{2}\frac{\sin^2(d\theta)}{\cos(d\theta)}. \tag{3.2}$$

Further, a second interpolation was carried out to achieve a grid of points over the aircraft surface, as displayed in Figure 19c.

The Figure 19c represents the goal of last interpolation and the difference with Figure 19b shall be analyzed. To reach a net of displacement points the MATLAB® function *Griddata* was used. This function has as input the aircraft's geometry data and the displacements through the chord line obtained with Equation 3.1 and Equation 3.2. This interpolation was carried out for all strips in wing and empennages surfaces. The *Griddata* method *"v4"* was adopted, which means biharmonic spline interpolations and was developed based on the work developed by Sandwell (1987). However, the particularities of this interpolation method are not in the scope of

Figure 20: Two dimensional representation of undeformed and deformed wing profile with pitching, plunging and lagging components to perform the linear interpolation of modal shapes.

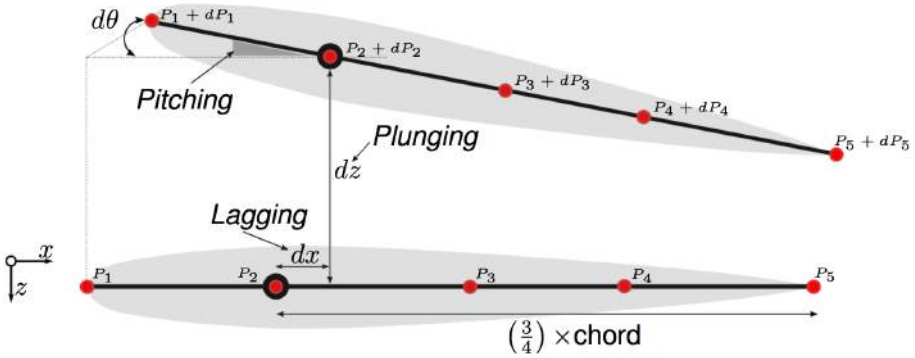

Source: Author.

this work and the reader is referred to Sandwell (1987) and Hunt, Lipsman e Rosenberg (2014) for more details.

The interpolation through the surface's chordwise and surface's spanwise direction to achieve a grid of displacements over the structure fit very well the points determined in the GVT and were used also in other references such as Hamann (2014) and Silvestre (2012). As presented by the last author, for bigger frequency values the modal shapes becomes more complex and consequently the chordwise displacements become higher as well. Nevertheless, as this work focus on frequencies up to $30Hz$ the errors are assumed to be of minor importance.

The algorithms implemented to perform the linear interpolations of the EC ES15 structural properties are given in Appendix C. The main function calls *mfv2StructFlexSimInput.m*, given in section C.1. The sub-functions implemented are *InterpStreifenGVT.m* and *ReadGVTData.m*, presented respectively in subsection C.1.1 and subsection C.1.2.

As a result of the steps performed in this section, the aircraft modal shapes can be plotted. The Figure 21 illustrates the aircraft undeformed structure in gray color and the first wing torsion with colors. In the Appendix A all modal shapes listed in Table 6 and 7 with their respective frequencies are depicted.

3.4 Definition of Flying Qualities Requirements

Based on the flying qualities requirements presented in subsection 2.3.3 the Table 8 gives the definitions whose the aircraft EC ES15 fits.

Figure 21: Representation of the first asymmetric wing torsion of EC ES15 aircraft, with modal frequency equal $29.10Hz$.

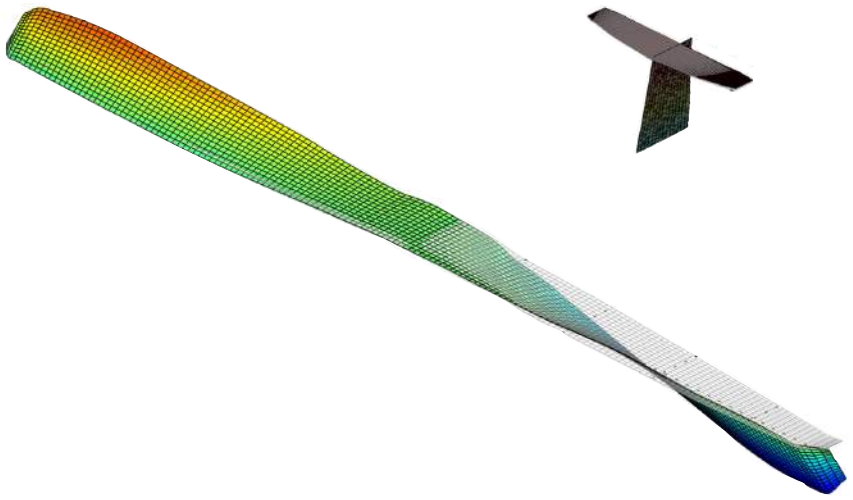

Source: Author.

Table 8: Definition of flying qualities for the utility aircraft EC ES15 following (MIL-F-8785C, 1980).

Flying Quality	Option	Definition
Class	Class I	Small light airplanes;
Flight Phase	Category B	Non-terminal flight phases that require gradual maneuvering, less precise tracking and accurate flight path control
Level of flight	Level 1	Flying qualities clearly adequate for the mission flight phase
Flight Envelope	Category B	Cruise flight (CR)

Source: Author.

4 Results and Discussion

This chapter present the main results achieved in this work. First the effects of structural flexibility are and trim values are introduced, then the simulations of flight dynamics and finally the results of the pitch damper are presented.

4.1 Effects of Structural Flexibility

The definition of the methodology applied in this work implies that the aircraft must be trimmed, what means no rotations about the aircraft's center of gravity (ETKIN; REID, 1998). The trim values were calculated with FlexSim for the two aircrafts and three models considering the reference flight condition presented in Table 9. The aircraft flies a stationary horizontal flight with retracted flaps, $\eta_K = 0^{\text{o}}$.

Table 9: Reference condition to trimmed flight.

Parameter	Value	Unit
Flight speed (TAS)	44	m/s
Flight Altitude	220	m
Path Angle	0	$^{\text{o}}$
Side slip angle	0	$^{\text{o}}$
Flaps	0	$^{\text{o}}$
Aircraft Mass	960	kg

Source: Author.

With the reference flight condition to trimmed flight presented in Table 9, the model of Stemme S15 and two configurations of EC ES15 were investigated. The trim values are given in Table 10, where the first seven parameters of the left column read the flight dynamic angles, thrust, controls, respectively. Following them, the first five modal amplitudes of elastic modes are represented by the Greek-letter η_{n_e} and the index "$_{n_e}$" gives the modal shape number. The modal amplitudes listed in Table 10 for the first wing bending are written in bold style because it has the bigger contribution on the deformed structure in trim flight condition. This fact is well represented when analyzing the EC ES15 with pods configuration, whose first wing bending is not the first, but the second modal shape (see section A.3). The results are presented first for the reference aircraft Stemme S15 and are followed by both EC ES15 configurations.

According to Table 10, the trimmed condition of the rigid aircraft gives very small lateral control deflections, as may be seen with rudder and aileron parameters. Besides that, the elevator has the larger deflection to trim the aircraft. The rigid values for the three models are the same due the fact that the geometry remains unchanged. However when the flexible results are analyzed a

Table 10: Values of trim parameters with reference flight at $44m/s$ and retracted flaps.

Parameter	Symbol	Stemme S15		EC ES15 with pods		EC ES15 without pods		Unit
		Rigid	Flexible	Rigid	Flexible	Rigid	Flexible	
Pitch Angle	θ	3.0055	2.9502	3.0055	3.3554	3.0055	3.3233	º
Attack Angle	α	3.0055	2.9502	3.0055	3.3555	3.0055	3.3234	º
Roll Angle	ϕ	-3.87×10^{-18}	0.0242	-3.87×10^{-18}	-0.4033	-3.87×10^{-18}	-0.3096	º
Thrust	T	763.3767	758.1519	763.3767	801.5507	763.3767	799.4623	N
Aileron	ξ	6.59×10^{-12}	-0.0912	6.59×10^{-12}	1.5327	6.59×10^{-12}	1.173	º
Elevator	η	-1.7346	-1.5476	-1.7346	-2.1832	-1.7346	-2.0203	º
Rudder	ζ	-2.62×10^{-15}	-0.0964	-2.62×10^{-15}	1.4917	-2.62×10^{-15}	1.219	º
Modal amplitudes of first five elastic modes	η_1		$\mathbf{-0.459}$		0.0628		$\mathbf{0.3798}$	-
	η_2		4.33×10^{-4}		$\mathbf{0.3888}$		-0.0069	-
	η_3		0.0024		0.0018		0.0022	-
	η_4		0.0019		0.0165		-0.0156	-
	η_5		-1.95×10^{-4}		0.0047		8.12×10^{-4}	-

Source: Author.

considerable difference can be observed. As can be seen from the flexible trim values for the aircraft EC ES15, the controller to trim the aircraft give an asymmetric flight. This suggests that aileron and rudder deflections are necessary for trim flight condition. Due this fact, the data from ground vibration tests were revised in order to find a possible inconsistence.

Investigating the contributions of each modal shape in trim parameters values it was possible to identify some inconsistent with the GVT results of both EC ES15 configurations. For the configuration without pods, the first symmetric wing bending and the first wing asymmetric torsion were corrected by multiplying the pitching eigenvectors by a factor of zero an 1.5, respectively. It was identified that the first wing bending had at the wing tip a pitching component responsible for the asymmetric trim results. Thus, it indicated that the pitching eigenvectors obtained with the ground vibrations tests for this aircraft configuration had measurement errors, which were corrected by the factors multiplication . The same investigation was carried out for the configuration with pods and five modes were corrected, being them: first symmetric wing bending, first asymmetric right and left pod swing, first symmetric and asymmetric wing torsion. The corrected structural models provide more adequate trim values with low lateral controls deflections and symmetric trimmed flight. The Table 11 lists the corrected trim results for both EC ES15 configurations.

With corrected trim values and modal amplitudes for both EC ES15 aircraft configurations given in Table 11, the stationary deformation at the trimmed flight condition can be determined by the sum of the multiplication of each modal shape eigenvector by its respective modal amplitude, η_n. In Figure 22 the stationary deformation at the trimmed flight condition for the aircraft EC ES15 without pods is illustrated, where the eigenvectors were multiplied by a factor of twenty in order to better represent the structural flexibility. The first symmetric wing bending has the larger influence on the aircraft's deformation, as cited before. Thus, the maximal elastic deflections happen at the wing tip and are no bigger than $4cm$. According to this result, the assumption of slightly flexibility adopted when deriving the structural dynamics is suitable for the aircraft

Table 11: Values of trim parameters with reference flight at $44m/s$ and retracted flaps.

Parameter	Symbol	EC ES15 with pods		EC ES15 without pods		Unit
		Rigid	Flexible	Rigid	Flexible	
Pitch Angle	θ	3.055	2.8596	3.055	3.3465	º
Attack Angle	α	3.055	2.8596	3.055	3.3465	º
Roll Angle	ϕ	-3.87×10^{-18}	0.0052	-3.87×10^{-18}	-0.2148	º
Thrust	T	763.3767	745.5409	763.3767	799.3104	N
Aileron	ξ	6.59×10^{-12}	-0.0179	6.59×10^{-12}	0.08109	º
Elevator	η	-1.7346	-1.579	-1.7346	-2.3056	º
Rudder	ζ	-2.62×10^{-15}	-0.0625	-2.62×10^{-15}	0.09197	º
Modal amplitudes of first five elastic modes	η_1		0.0677		$\mathbf{0.3808}$	-
	η_2		$\mathbf{0.3896}$		-0.0054	-
	η_3		0.0108		0.0014	-
	η_4		0.0149		-0.014	-
	η_5		0.0072		-4.94×10^{4}	-

Source: Author.

under investigation.

Figure 22: Stationary deformation at trimmed flight condition established in Table 9 for aircraft EC ES15, configuration without pods.

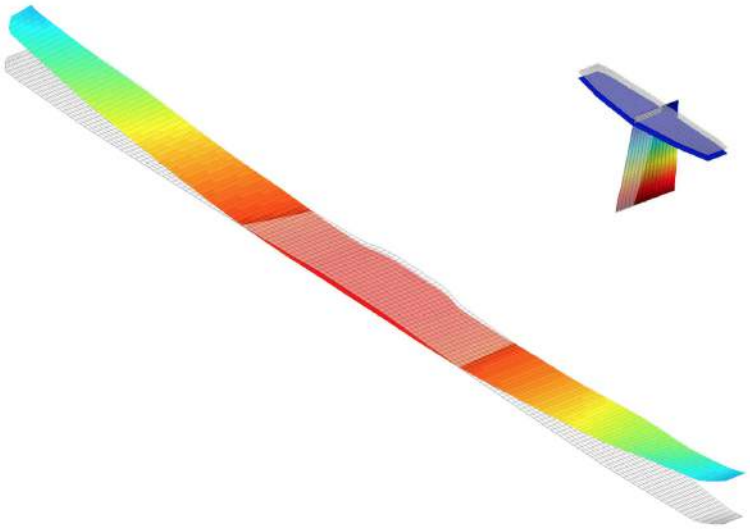

Source: Author.

4.2 Simulation of Aircraft Flight Dynamics

Next, the three aircraft models listed in chapter 3 were simulated with help of software FlexSim and the dynamic response of rigid and flexible aircraft models were compared for two maneuvers, first in longitudinal plane with an elevator command and secondly in lateral plane with a rudder command. In Figure 23 the dynamic response for the reference aircraft Stemme S15 with an elevator step equal 1^{o} at time $1sec$ is presented. The Figure23a displays the flight mechanic angle rates (pitch, roll and yaw in $[^{o}/sec]$) for the rigid and flexible structural models. The dashed lines represent the rigid model, while the full lines the flexible one. As can be seen, the short period pronounces itself by the higher angle rates in pitch, and after approximately $3.5s$ the phugoid motion starts. The differences between rigid and flexible structure models are notable and it is possible to conclude that the flexible model has a higher angle rate. Furthermore, for the rigid model the yaw and roll angle rates are constant to a command in elevator. On the other hand, the yaw and roll angle rates vary for the flexible model. This behavior shows that the modes of vibration have influence on the aircraft's flight dynamic. In addition to that, the effects of structural flexibility can also be seen in Figure 23b, where the variation of altitude is demonstrated.

The next investigation is performed for the lateral motion with 1^{o} rudder command and illustrated in Figure 24. The angle rates and altitude change are presented for rigid and flexible structural models. The higher angle rates are the yaw followed by the roll and pitch. For the

Figure 23: Flight Simulation results for aircraft Stemme S15 with 1° elevator command.

(a) Stemme S15 aircraft, angle rates for 1° elevator command comparing rigid (RB) and flexible (flex) structural models.

(b) Stemme S15 aircraft, altitude change due 1° elevator command for rigid (RB) and flexible (flex) structural models.

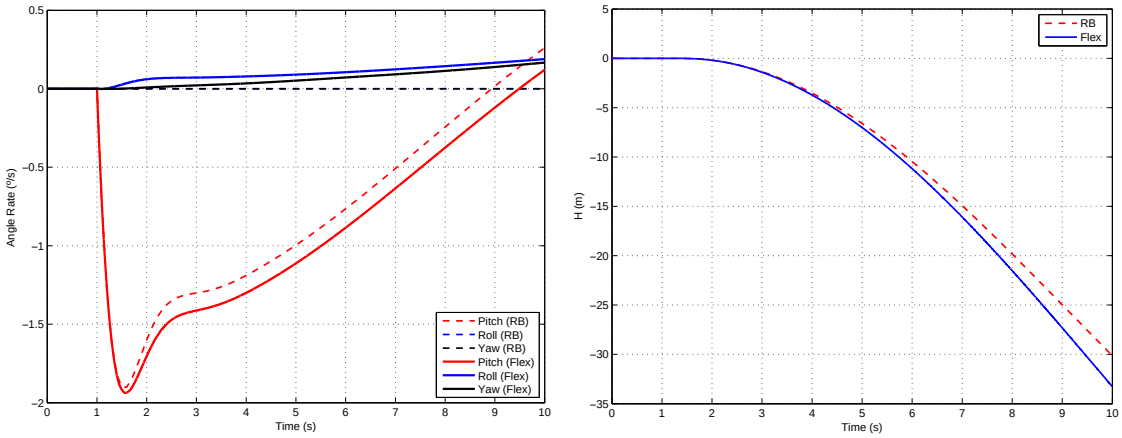

Source: Author.

lateral case the rigid body model has larger angle rate variations than the flexible structural model. The altitude variation with time in Figure 24b presents also a different behavior than the longitudinal motion, in this case the rigid model has higher altitude change.

Figure 24: Flight Simulation results for aircraft Stemme S15 with 1° rudder command.

(a) Stemme S15 aircraft, angle rates for 1° rudder command comparing rigid (RB) and flexible (flex) structural models.

(b) Stemme S15 aircraft, altitude change due 1° elevator command for rigid (RB) and flexible (flex) structural models.

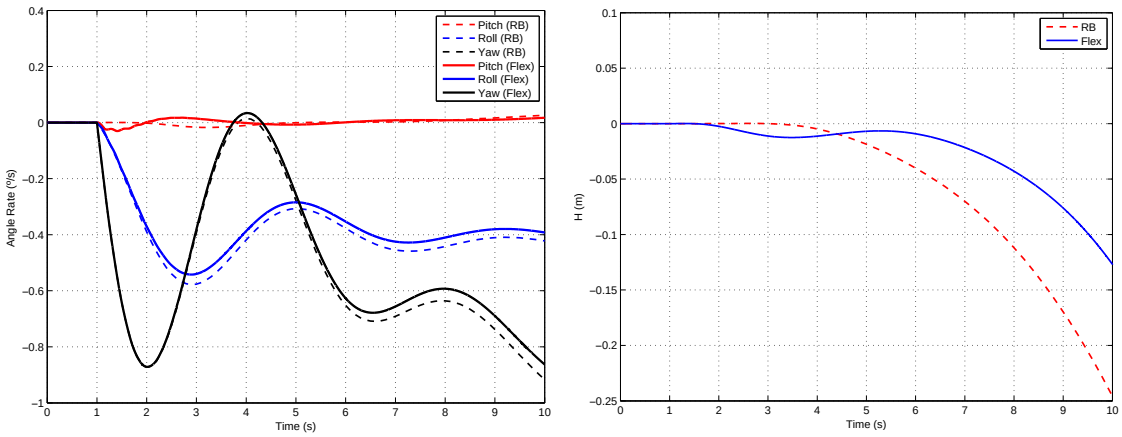

Source: Author.

Further, the first four modal amplitudes for the aircraft Stemme S15 due an elevator and rudder commands are presented, respectively, in Figure 25.

Regarding the denomination of aircraft's modal shapes given in Table 5, the elevator

Figure 25: Modal Amplitudes for the aircraft Stemme S15.

(a) Aircraft Stemme S15, modal amplitudes for 1^o elevator command.

(b) Aircraft Stemme S15, modal amplitudes for 1^o rudder command.

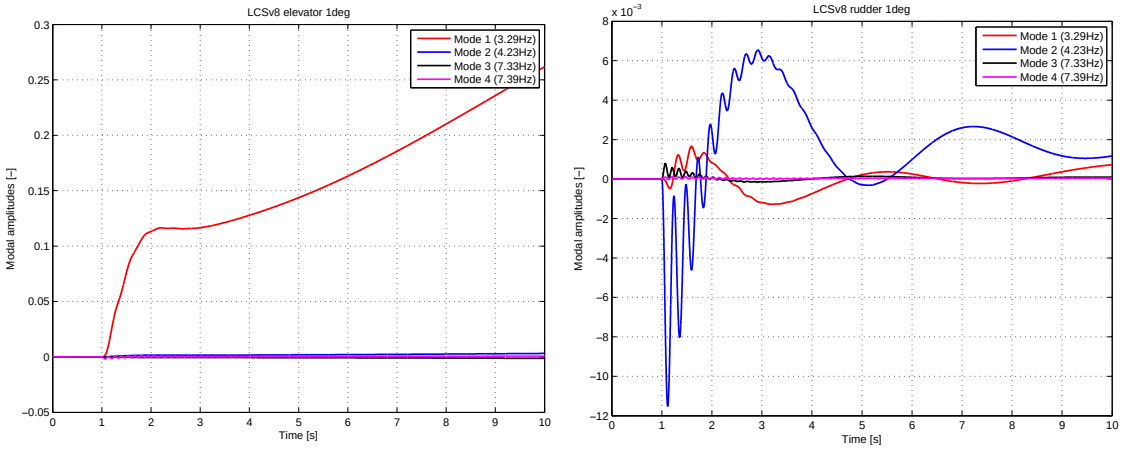

Source: Author.

command acts on the longitudinal flight mechanic plane and excites symmetrical modal shapes. Since first and fourth modal shapes of the aircraft Stemme S15 are symmetric, their modal amplitudes have higher values. In Figure 25b, where the modal amplitudes due a rudder command are depicted, the asymmetric modes should have higher values, as can be seen with the second modal shape.

After having presented the reference aircraft results, the dynamic response of the aircraft EC ES15 without attached pods was investigated. The results are presented following the same logic as the reference model above. The dynamic response due an elevator command is plotted in Figure 26. The Figure 26a illustrates the flight mechanic angle rates to 1^o elevator step. The aircraft EC ES15 has an expected longitudinal dynamic response with the short period and phugoid motions. Nevertheless, the roll and yaw full lines have negative values, contrary to the results presented for the reference aircraft in Figure 23a. Besides that, the pitch motion for flexible structural model has lower change in angle rates than the rigid model. In addition, the larger altitude change for the reference aircraft and EC ES15 without pods are unlike, because the rigid EC ES15 has higher altitude change to an 1^o elevator step.

The Figure 27 gives the dynamic response due an 1^o rudder step at time $1s$. The angle rates in Figure 27a are in agreement with the reference aircraft, with exception that for the lateral motion the flexible model experiences higher angle rates than the rigid structural model. As reported for the longitudinal motion with the EC ES15 without pods, the altitude change displayed in Figure 27b is not similar with the reference aircraft, since the flexible model presents higher altitude change.

Figure 26: Flight Simulation results for aircraft EC ES15 without pods with 1º elevator command.

(a) EC ES15 configuration without pods, angle rate changes due 1º elevator command for rigid (RB) and flexible (flex) structural models.

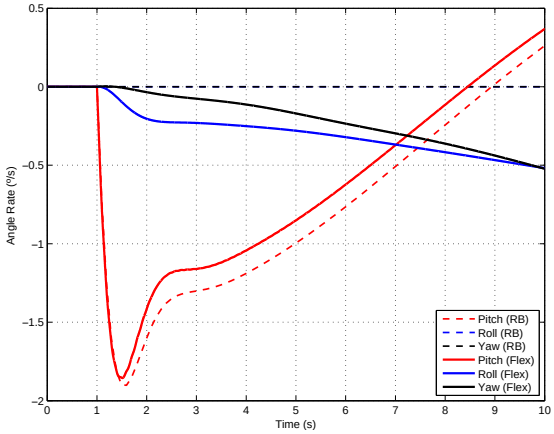

(b) EC ES15 configuration without pods, altitude change due 1º elevator command for rigid (RB) and flexible (flex) structural models.

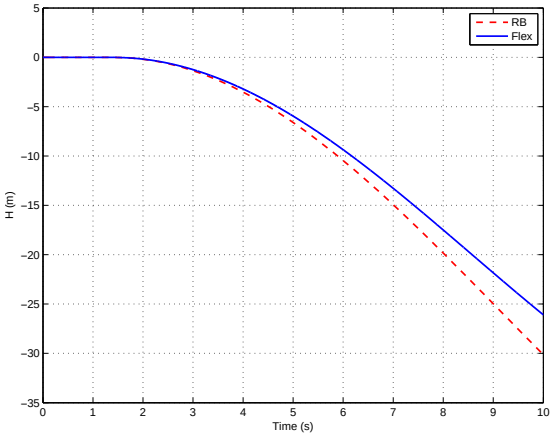

Source: Author.

Figure 27: Flight Simulation results for EC ES15 without pods with rudder command.

(a) EC ES15 configuration without pods, angle rates for 1º command in rudder

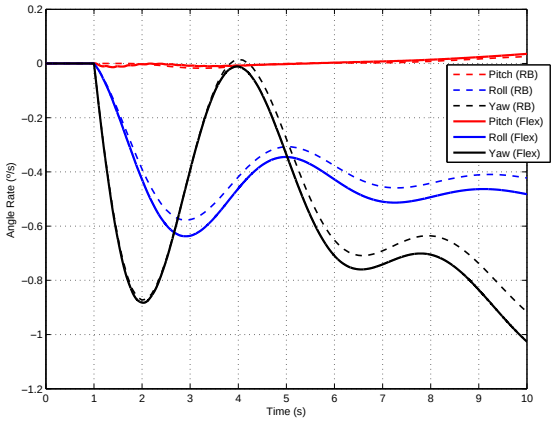

(b) EC ES15 configuration without pods, altitude change due 1º command in rudder for rigid (RB) and flexible (flex) structure.

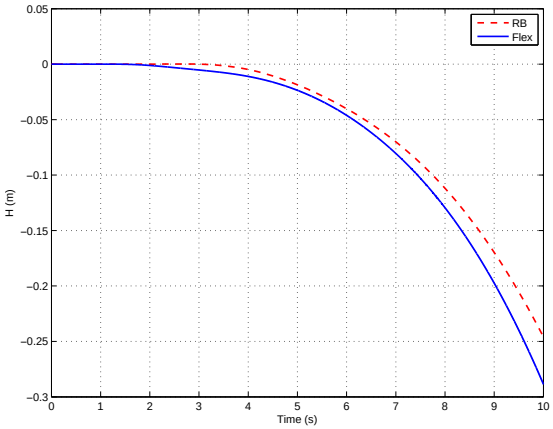

Source: Author.

The Figure 28 shows the first four modal amplitudes for 1º step commands in elevator and rudder. The similar behavior seen with the reference aircraft was observed for the EC ES15 without pods. For the longitudinal motion in Figure 28a the first and fourth modal shapes had the higher modal amplitude values, which represent the symmetric modes of vibration given in Table 7 and illustrated in section A.2. For the rudder step command the asymmetric modal shapes were exited, what means second and third aircraft modes of vibration.

The last dynamic response investigated in this work correspond to the EC ES15 with

Figure 28: Flight Simulation Results for EC ES15 without pods with rudder command.

(a) EC ES15 configuration without podS, modal amplitudes for 1° elevator command.

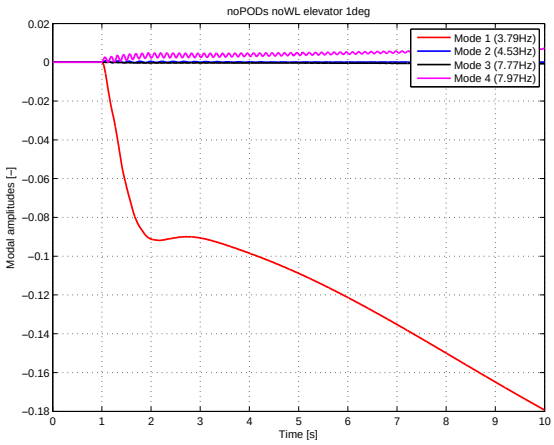

(b) EC ES15 configuration without pods, modal amplitudes for 1° rudder command.

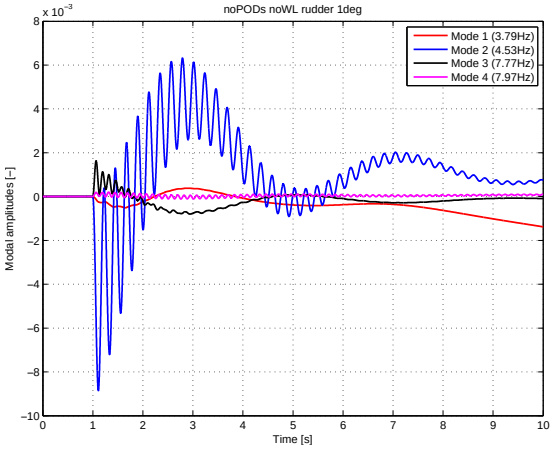

Source: Author.

attached pods. The Figure 29 displays the dynamic response of the aircraft to a step input of 1° in the aileron and rudder commands, respectively. The dashed lines representing the rigid body model and the full lines representing the flexible model show a quite similar behavior with the aircraft without pods. Considering this behavior, the dynamic response of the aircraft with and without pods does not show significant differences based on the results achieved with this work. However, attached pods are generally modeled as concentrated mass points along the wing spanwise direction. Therefore, the mass has influence on the structural dynamic properties, as introduced in subsection 2.1.2. This suggests that additional work is required with the ground vibration test data before the complete understanding of the influence magnitude of pods on the aircraft flight dynamic can be reached.

Figure 29: Flight Simulation results for EC ES15 with pods and rudder step command.

(a) EC ES15 configuration with pods, angle rates for 1° step command in elevator

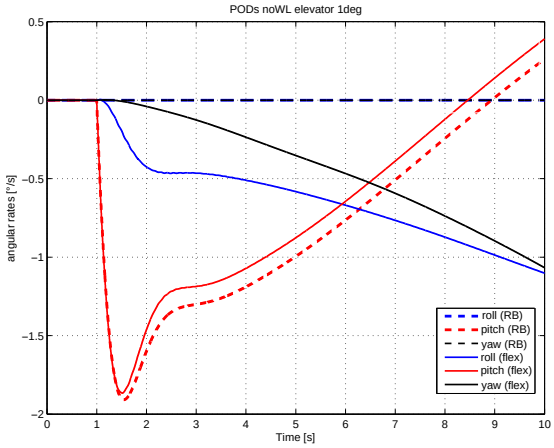

(b) EC ES15 configuration with pods, angle rates for 1° rudder step command.

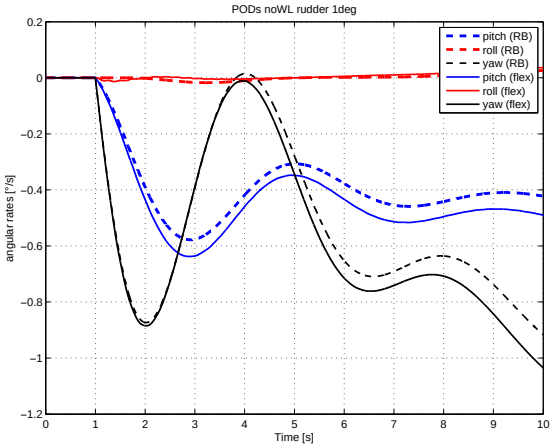

Source: Author.

Figure 30: Flight Simulation Results for EC ES15 without pods with rudder command.

(a) EC ES15 configuration without pods, angle rates for 1° command in rudder

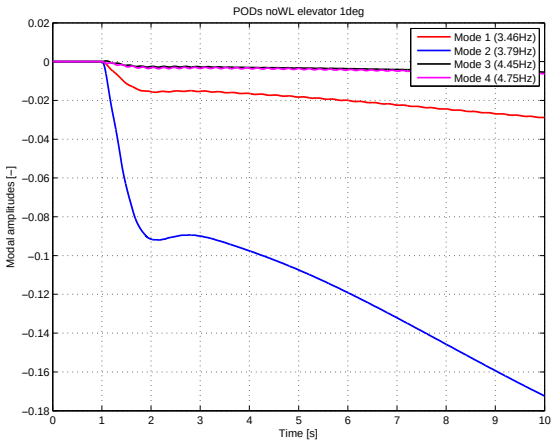

(b) EC ES15 configuration without pods, modal amplitudes for 1° rudder command..

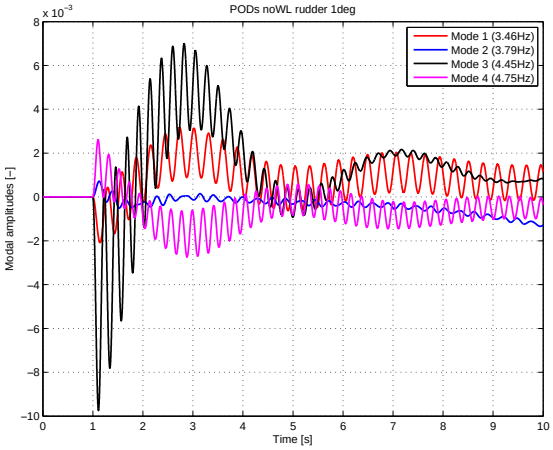

Source: Author.

At last, the modal amplitudes due to step elevator and rudder commands with the aircraft EC ES15 with attached pods are given in Figure 30. The Figure 30a presents the modal amplitudes due the elevator step, as presented in Table 6 and Appendix A.3 between the first four modes of vibration only the second is symmetric, in this way the blue line has the larger value with the time. Further, the Figure 30b shows the modal amplitudes due the rudder step command. It can be then seen that the asymmetric modes of vibrations one, three and four have higher modal amplitude values. The pods attached under the aircraft's wing change the nature of vibration modes, thus, the first symmetric wing bending is not the first modal shape but the second.

4.3 Pitch Damper

The pitch damper theory was firstly introduced in subsection 2.3.4, and has as objective to augment the aircraft pitch rate. In subsection 4.3.1 the assumptions are presented. Next, in subsection 4.3.2 the roots of the longitudinal motion for the aircraft models displayed in chapter 3 are presented. Further, the dynamic response is plotted for the short period approximation, longitudinal reduced system and full aircraft state space system. The MATLAB® Simulink block diagrams as well as the algorithm implemented to design the pitch damper calls *pitch_damper.m* and are given in section C.2.

4.3.1 Assumptions

The design damping and frequency limits are defined following the MIL-F-8785C (1980). Considering Table 8, the aircrafts are defined in Flight Phase Category B, Level Flight 1 and Flight Envelope Category B. Hence, Table 3 summarizes the desirable damping and frequency limit specifications. The damping is considered equal $\zeta_{SP} = 0.707$, according the definition of ideal damping value given by Shinners (1998). Furthermore, according to Table 3, the frequency is indirectly defined. Firstly, the load factor n_α may be defined following the Airworthiness Standards FAA-Part23 (2015). The Part 23 gives the following limits for load factor: $-1.76 < n_\alpha < 3.8$. Hence, adopting arbitrarily a load factor equal $n_\alpha = 2.0$ and frequency equal $\omega_{n_{SP}} = 2.50 rad/s$, the ratio $\frac{\omega^2_{n_{SP}}}{(n_\alpha)}$ defined by MIL-F-8785C (1980) and summarized in Table 3 is equal $\frac{\omega^2_{n_{SP}}}{(n_\alpha)} = 3.125$, respecting the flight qualities requirements.

Furthermore, the pitch damper results are presented for the reference flight condition listed in Table 1. The system linearization performed by the software FlexSim gives the aircraft system matrix $\mathbf{A}$ and input matrix $\mathbf{B}$. Thus, the block diagram to implement the pitch damper and simulate the aircraft dynamic is built with help of MATLAB ® Simulink tool (see Figures 10, 82 and 83. As a result, the system is reduced first into the longitudinal motion approximation and then into the short period approximation. The pole-zero maps as well as the controller factors are calculated and the longitudinal aircraft dynamic response with and without controller is plotted for both rigid and flexible structural models. The pole-zero maps are laid out in the following section for all aircraft models, while the dynamic response with and without controller is presented in the subsequent Section for the aircraft EC ES15 configuration without pods and the other two remaining models are given in Appendix B.

4.3.2 System Roots

The approximated EOM for the short period are adopted to design the pitch damper. Thus, the system has 4×4 order. First, the roots for the reference aircraft Stemme S15 are shown in Table 12. Both rigid and flexible structural models are compared with and without pitch

damper action based on the phugoid roots, short period roots, damping values, and frequency values.

Table 12: Pitch damper results for the reference aircraft Stemme S15.

Stemme S15	Rigid		Flexible	
	Undamped	Damped	Undamped	Damped
		Phugoid		
Roots	$-0.013 \pm j0.215$	$-0.013 \pm j0.167$	$-0.012 + j0.222$	$-0.013 \pm j0.169$
Frequency, $\omega_{n_{PH}}$ [rad/s]	0.215	0.168	0.222	0.170
Damping, ζ_{PH}	0.061	0.079	0.057	0.079
		Short Period		
Roots	$-2.31 \pm j2.69$	$-1.77 \pm j1.78$	$-2.25 \pm j2.74$	$-1.77 \pm j1.78$
Frequency, $\omega_{n_{SP}}$ [rad/s]	3.550	2.510	3.550	2.510
Damping, ζ_{SP}	0.652	0.706	0.634	0.706

Source: Author.

The results listed in Table 12 are also plotted in the complex-plane in Figure 31, where a system root is represented by the term: $\times$. The complex conjugate roots most distant from the origin are the short period motion roots, while the roots near the complex plane read the phugoid motion. The Figure 31a contains all longitudinal motion roots and the Figure 31b focus on the phugoid roots. Since all roots are left from the origin, the aircraft is stable and the damped results match the damping and frequency design with deviation lower than 0.1%. It is also relevant to note, that the roots of rigid and flexible structural models have different values, reinforcing the concern to consider the aircraft flexible effects on the controller design, or in other words, the aeroservoelasticity effects.

Next, following the same arrangement presented to Stemme S15, the system roots for the EC ES15 without and with pods are given. The Table 13 and 14 list, respectively for both models, the short period and phugoid roots for the rigid and flexible structural models with (damped) and without (undamped) the controller action. It is evident that, the rigid models' results have remained unchanged, since the geometry is the same. On the other hand, the flexible models present small but considerable changes that affect the controller gain to set the designed aircraft damping and frequency. Besides that, the major changes in roots place due the pitch damper action occurs for the short period, as expected. In Figure 31b, not only the short period roots but also the phugoid roots are modified, but considerable slightly, what represents the coupling between the longitudinal rigid body motions.

Figure 31: Longitudinal motion approximation for the aircraft Stemme S15. Representation of the short period and phugoid roots for the rigid and flexible models with and without the controller action.

(a) Stemme S15 root loci.

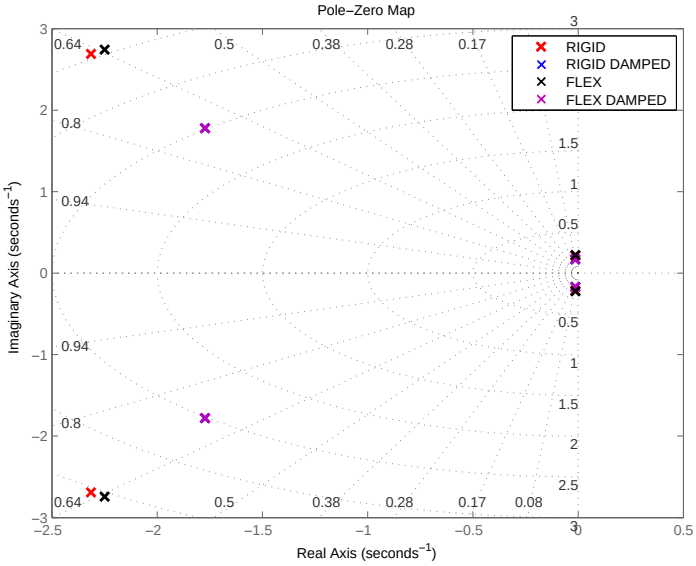

(b) Stemme S15, focus on phugoid roots.

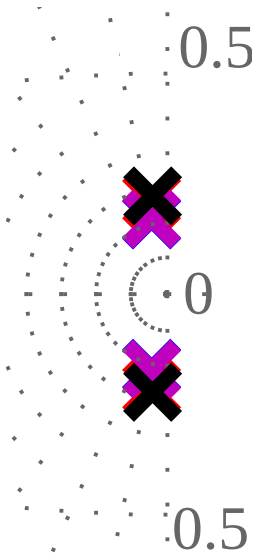

Source: Author.

Table 13: Pitch damper results for the reference aircraft EC ES15 without pods.

EC ES15 without pods	Rigid		Flexible	
	Undamped	Damped	Undamped	Damped
		Phugoid		
Roots	$-0.013 \pm j0.215$	$-0.013 \pm j0.167$	$-0.014 + j0.223$	$-0.015 \pm j0.171$
Frequency, $\omega_{n_{PH}}$ [rad/s]	0.215	0.168	0.223	0.171
Damping, ζ_{PH}	0.061	0.079	0.062	0.088
		Short Period		
Roots	$-2.31 \pm j2.69$	$-1.77 \pm j1.78$	$-2.20 \pm j2.72$	$-1.77 \pm j1.78$
Frequency, $\omega_{n_{SP}}$ [rad/s]	3.550	2.510	3.500	2.510
Damping, ζ_{SP}	0.652	0.706	0.630	0.706

Source: Author.

Figure 32: Longitudinal motion approximation for the aircraft EC ES15 without pods. Representation of the short period and phugoid roots for the rigid and flexible models with and without the controller action.

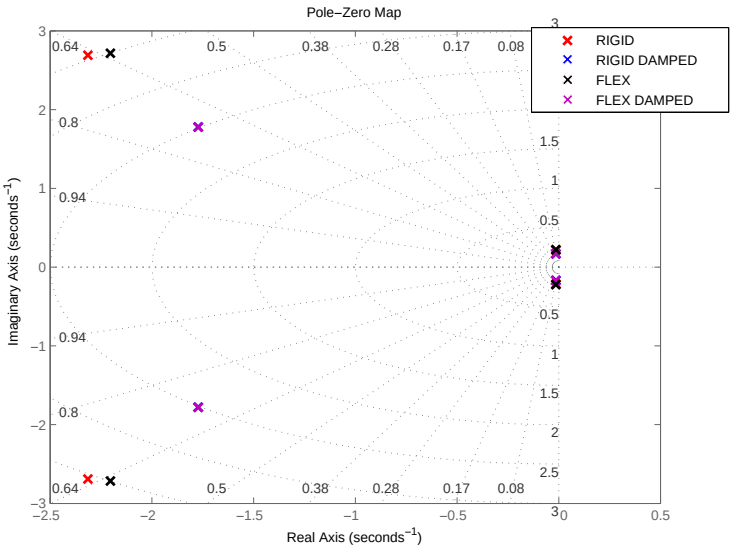

Source: Author.

Table 14: Pitch damper results for the reference aircraft EC ES15 with pods.

EC ES15 with pods	Rigid		Flexible	
	Undamped	Damped	Undamped	Damped
		Phugoid		
Roots	$-0.013 \pm j0.215$	$-0.013 \pm j0.167$	$-0.014 + j0.222$	$-0.015 \pm j0.170$
Frequency, $\omega_{n_{PH}}$ [rad/s]	0.215	0.168	0.222	0.171
Damping, ζ_{PH}	0.061	0.079	0.062	0.089
		Short Period		
Roots	$-2.31 \pm j2.69$	$-1.77 \pm j1.78$	$-2.21 \pm j2.70$	$-1.77 \pm j1.78$
Frequency, $\omega_{n_{SP}}$ [rad/s]	3.550	2.510	3.490	2.510
Damping, ζ_{SP}	0.652	0.706	0.633	0.706

Source: Author.

Figure 33: ECARY ES15 with pods root loci.

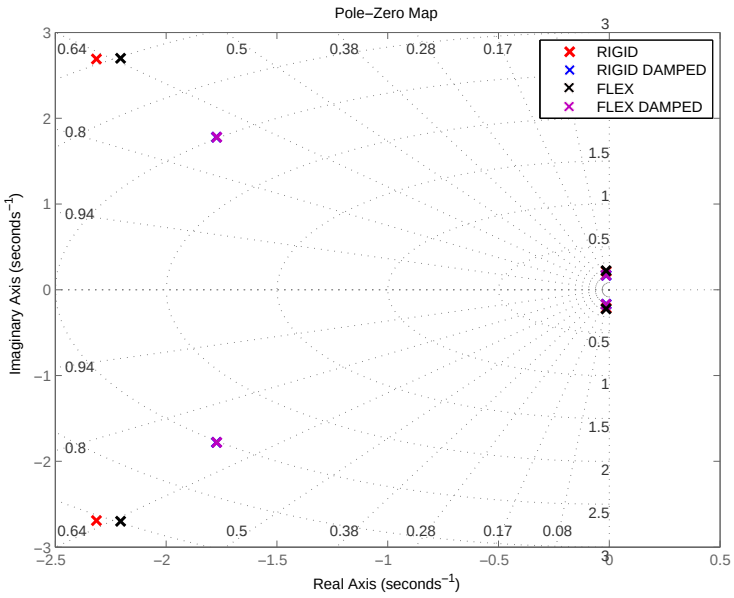

Source: Author.

The Table 15 lists the pitch damper controller gains for the three aircraft models introduced in chapter 3. The results for rigid as well as the flexible structural model are given.

Table 15: Pitch damper controller gains.

Controller gain	Stemme S15		EC ES15 without pods		EC ES15 with pods	
	Rigid	Flex	Rigid	Flex	Rigid	Flex
$k_{\eta q}$	-0.1213	-0.1077	-0.1213	-0.0986	-0.1213	-0.0981
$k_{\eta \alpha}$	-0.4775	-0.5264	-0.4775	-0.5155	-0.4775	-0.5013

Source: Author.

In general, this section presented the aircrafts' longitudinal motion roots in the complex plane. It was shown that the longitudinal motion of all aircraft models are stable and there are no radical changes between the reference aircraft and the EC ES15. The design damping and frequency are defined according the flying qualities of piloted airplanes given in MIL-F-8785C. The results reinforce that the effects of structure flexibility are meaningful when designing an aircraft controller.

4.3.3 Pitch Damper Results

The pitch damper for the aircraft EC ES15 configuration without pods is given in this subsection while the other two aircraft models, Stemme S15 and EC ES15 with pods, are given in Appendix B. All aircraft dynamic responses are presented considering the flight qualities listed in Table 9. The dynamic aircraft response is presented first considering only the short period approximation with a second order system, followed by the longitudinal motion approximation.

The short period approximation transforms the system of EOM into a 2×2 order for the rigid body case. For this case, the control vector $\bar{u}$ has only the elevator η as control surface, and the state vector $\bar{x}$ is equal the pitch rate q and attack angle α. On the other hand, the flexible model includes, besides the rigid body terms, the modal amplitudes ($\eta_1,\ \eta_2,\ \ldots,\ \eta_{n_e}$), and the aerodynamic lag states ($[(\lambda_{11};\lambda_{21}), (\lambda_{12};\lambda_{22}), \ldots, (\lambda_{1j};\lambda_{2j})]$), regarding that jth refers to strip number of the lifting surface. As listed in Table 7, for the EC ES15 without pods only the first eighteen modes of vibration are considered, thus the system order for the flexible model with modal amplitudes and aerodynamic lag states is equal 180×180.

A step input of 1^{o} in the elevator command η_{cmd} and the tracking error signal η_e (difference between the input command and damped feedback signal, see Figure 10) are illustrated in Figure 34. The dashed line displays the input command, while the full line illustrates the tracking error signal η_e, which changes the input command in the elevator based on the feedback signal in order to augment the pitch rate with the required damping and frequency. As illustrated in Figure 82 and 83, the actuator dynamic is not modeled in this work, thus the actuator transfer function is consider equal 1.

Figure 34: Step input of 1^{o} in the elevator command η_{cmd} and the tracking error signal η_e.

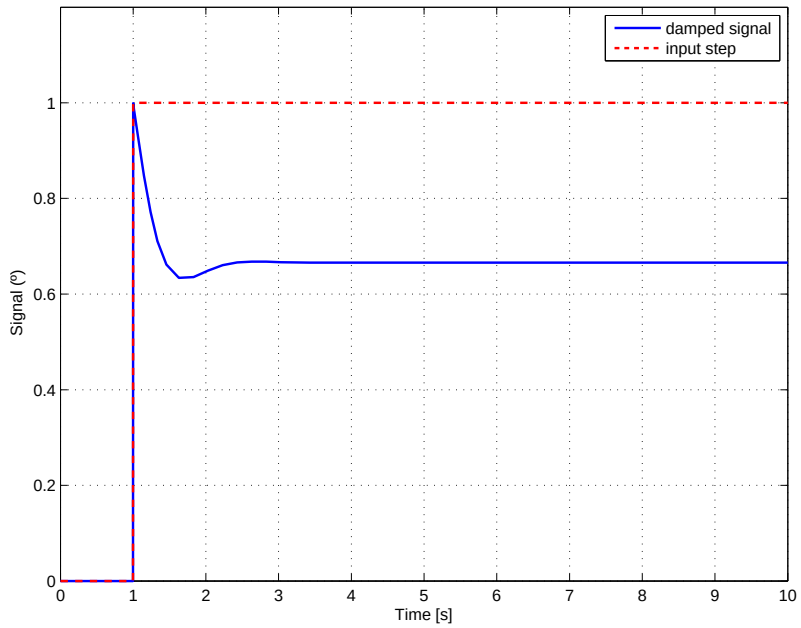

Source: Author.

The aircraft response considering the EOM for the short period approximation are depicted in Figure 35. A step input of 1^{o} in the elevator is given at time $1s$ and the state vectors pitch rate and attack angle are illustrated for the rigid and flexible structural models. The dashed lines illustrate the open loop (OL) system, while the full lines illustrate the closed loop (CL) system.

Since the short period, as the nomenclature suggest, has a immediate and brief effect, the simulation time was chosen equal $5s$, and the steady value is reached at time $2.5s$. The pitch

Figure 35: Short period (SP) approximation. Step input of 1^{o} in elevator command. The pitch rate and attack angle state vectors are illustrated for the rigid and flexible structural models. The dashed lines display the open loop (OL) and the full lines the closed loop (CL) control system.

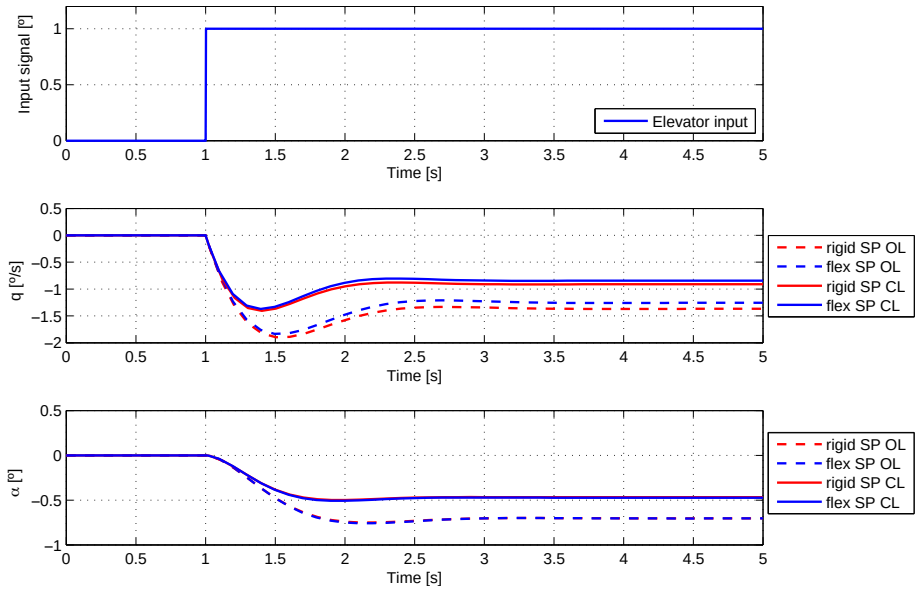

Source: Author.

damper effect is represented by the closed loop system with the reduction in the short period pitch rate values. The maximal pitch rate value for the rigid value is reduced 35.11% at simulation time $1.5s$ while the flexible value is reduced 33.96% at time $1.49s$. Not only for the maximal pitch rates but also for the steady value, the rigid and flexible models present different curves. The reduction in steady value due the pitch damper for the rigid model is equal 33.4% and for the flexible model 32.8%. The attack angle does not shows significant differences between rigid and flexible models, but the pitch damper effect also decreases the steady value into 48.91%.

As can be seen from Figure 35 the structural flexibility has influence on the short period approximation and in the controller design, as asserted in subsection 4.3.2. The differences between the controller gains for rigid and flexible models have been listed in Table 15. The feedback gain $k_{\eta q}$ has decreased 23% and $k_{\eta \alpha}$ increased 7.37% from rigid to flexible models. Besides that, the differences in steady value for the closed loop system between rigid and flexible models are no bigger than $0.1^{o}/s$ for pitch rate. The low differences between the rigid and flexible structural models may be explained because the aircraft structure has slightly flexibility properties. Nevertheless, these differences between both structural models justify the importance of the aeroservoelasticity investigation.

Next, the same investigation presented above considering the EOM for the short period approximation is performed assuming the EOM for the longitudinal motion. In the longitudinal motion there are two rigid body: the phugoid and the short period. In this case, the system of EOM have 5×5 order for the rigid body case. The control vector $\bar{u}$ has the elevator η and thrust η_F, and the state vector $\bar{x}$ has the velocity V, pitch angle θ, pitch rate q, attack angle α and

altitude H. On the other hand, the flexible model has, besides the rigid body terms, the modal amplitudes and aerodynamic lag states. As listed in Table 7, for the EC ES15 without pods only the first eighteen modes of vibration are considered, thus the system order for the flexible model with modal amplitudes and aerodynamic lag states is equal 183×183.

In the Figure 36 the dynamic response considering the EOM for the longitudinal motion are displayed. The short period until simulation time $2.5s$ is seen as illustrated in Figure 35.

Figure 36: Longitudinal Motion (LB) approximation. Step input of 1^{o} in elevator command. The pitch rate and attack angle state vectors are illustrated for the rigid and flexible structural models. The dashed lines display the open loop (OL) and the full lines the closed loop (CL) control system.

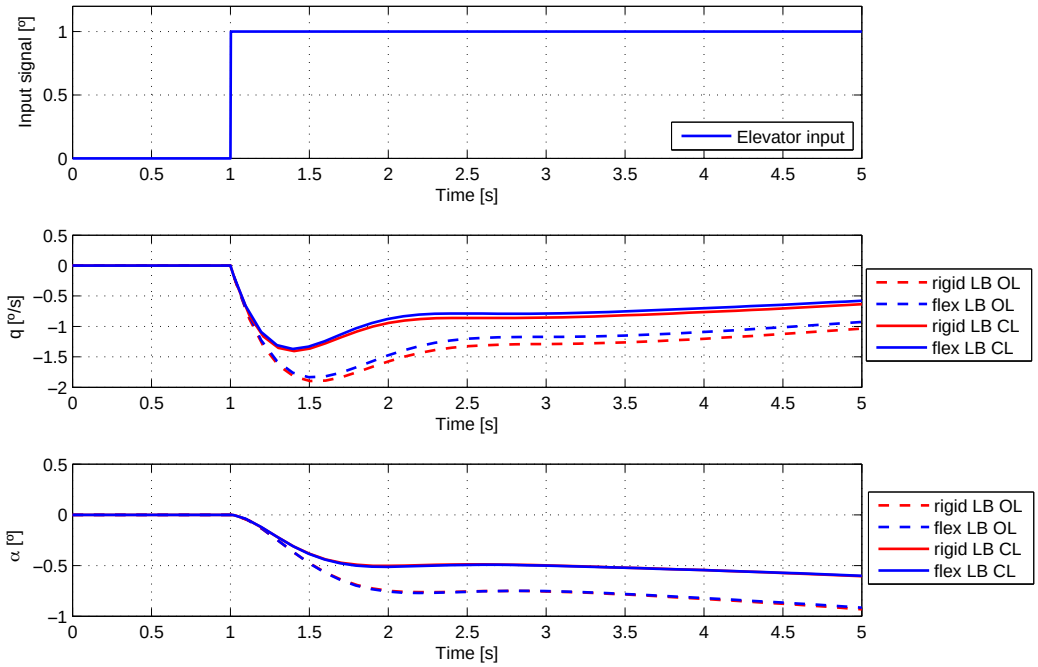

Source: Author.

Even with the short period well represented, the steady value has been modified. After the simulation time $2.5s$ variations in pitch rate and attack angle can be seen. These variations in pitch rate and attack angle represent the first effects of the phugoid motions. Unlike the short period, the phugoid is a slow motion with a large period. For this reason, in order to depict the steady value the simulation time was increased to $400s$ and displayed in Figure 37.

The differences between the period of the short period and phugoid motions are evidenced in Figure 37. While the short period takes $2.5s$ to be pronounced, the phugoid changes the pitch rate and attack angle until the simulation time $300s$. The pitch rate steady value is equal $0^{o}/s$, showing that the motion is stable for both rigid and flexible models. The steady value of attack angle considering the rigid model is equal -1.46^{o} for the open loop system and -0.86^{o} for the closed loop system. Moreover, the flexible model have presented attack angles equal -1.35^{o} for the open loop and -0.79^{o} for the closed loop system.

Figure 37: Longitudinal Motion (LB) approximation. Step input of 1^o in elevator command. The pitch rate and attack angle state vectors are illustrated for the rigid and flexible structural models. The dashed lines display the open loop (OL) and the full lines the closed loop (CL) control system.

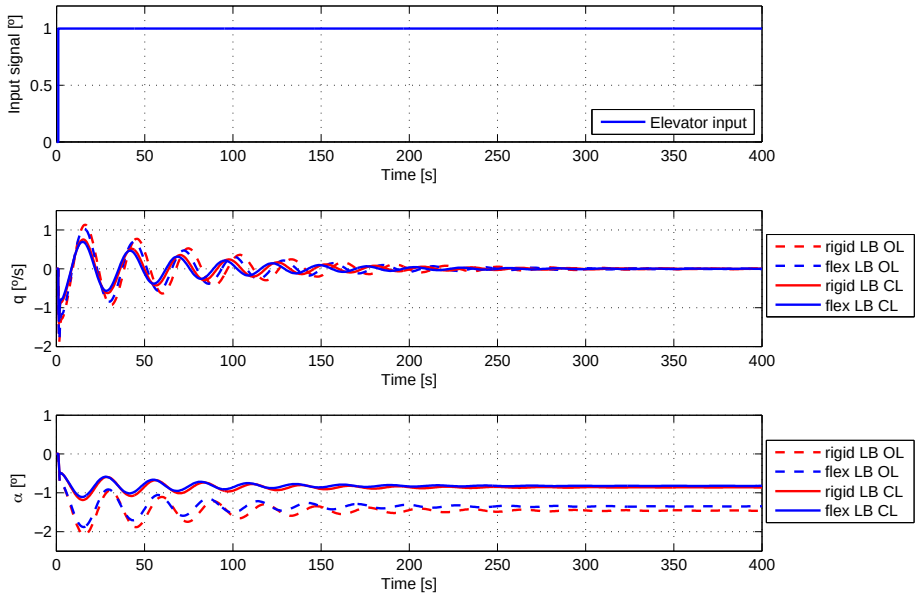

Source: Author.

The results to aircraft Stemme S15 and EC ES15 with pods are presented in Appendix B. Since the geometry of the aircraft remains unchanged, the rigid body values are all the same for the three aircraft models. In Figure 38 the aircraft's flexible dynamic response is compared between themselves and with the rigid body.

Figure 38: Step input of 1^o in elevator command. Pitch rate response of the three aircraft models for open loop (OL) and closed loop (CL) control system. Comparison between rigid model and flexible models.

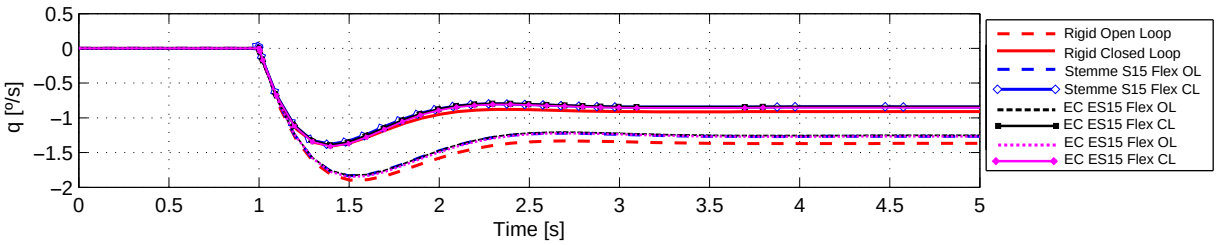

Source: Author.

As illustrated in Figure 38, the open loop and closed loop signals for rigid and flexible models follow the behavior depicted in Figure 35. The flexible models for the closed loop system present major differences between $1.5s$ and $2.5s$. Furthermore, the changes in attack angle for all aircraft models due a step command in elevator are compared in Figure 39.

The curves illustrated in Figure 39 have similar behavior as presented in Figure 35 for the aircraft EC ES15 without pods. No major differences have been evidenced in attack angle

Figure 39: Step input of 1^{o} in elevator command. Attack angle response of the three aircraft models for open loop (OL) and closed loop (CL) control system. Comparison between rigid model and flexible models.

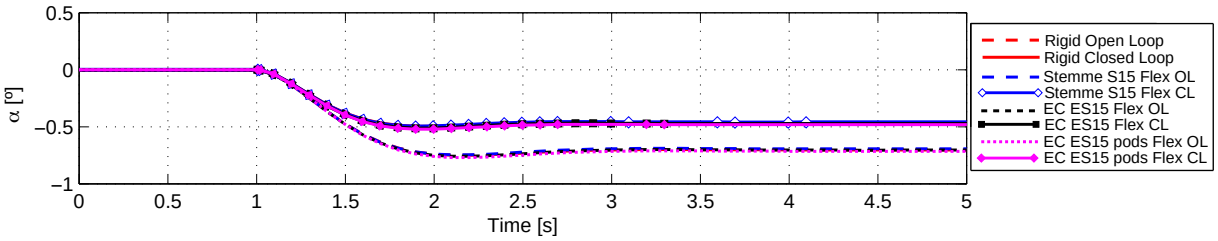

Source: Author.

between the models investigated in this work. Since the steady values illustrated in Figures 38 and 39 are abreast of each other, it is difficult to point out which model gives the largest variations in relation with the rigid body model. Due this fact, the steady values are listed in Table 39 for rigid and flexible models for open loop (OL) and closed loop (CL) systems.

Table 16: Steady values of aircraft models given in Figures 38 and 39.

Aircraft Model	Pitch Rate, q ($^{o}/s$)		Attack Angle, α (^{o})	
	OL	CL	OL	CL
Rigid	-1.368	-0.911	-0.704	-0.468
Stemme S15, flex	$-1,265$	$-0,842$	$-0,694$	$-0,462$
EC ES15, flex	$-1,256$	$-0,845$	$-0,705$	$-0,705$
EC ES15 pods, flex	$-1,269$	$-0,855$	$-0,717$	$-0,483$

Source: Author.

The steady values for the flexible models listed in Table 16 are divided by the rigid model values in order to present the differences in percentage. In doing so, the Table 17 lists the differences percentage for the steady value between the rigid and flexible structural models.

Table 17: Differences between the rigid and flexible structural models in percentage.

Aircraft Model	Variations in pitch rate, Δq (%)		Variations in attack angle, $\Delta\alpha$ (%)	
	OL	CL	OL	CL
Stemme S15	$-8,142\%$	$-8,131\%$	$-1,383\%$	$-1,363\%$
EC ES15	$-8,917\%$	$-7,862\%$	$0,184\%$	$0,170\%$
EC ES15 pods	$-7,801\%$	$-6,488\%$	$1,828\%$	$2,982\%$

Source: Author.

As can be seen from Table 17, excluding the reference aircraft, the EC ES15 without pods has higher differences between the structural models in pitch rate for the open loop system as well as for the closed loop system. On the other hand, the aircraft EC ES15 configuration with pods has higher variations in attack angle either for open loop system or closed loop system.

5 Conclusions and Final Remarks

This work had prior introduced through a briefly bibliography review the efforts to implement integrated models to identify the flight dynamics of airplanes with flexible characteristics. The discipline entitled aeroelasticity, which studies the relationship between aerodynamic, elastic and inertial forces was presented, and among its variations the term aeroservoelasticity was defined in order to account also for control forces. The first historical problems related with aeroelastic phenomena into aircraft design showed that this subject was addressed as a source of problem, triggering uncommon vibrations on aircraft's fuselage, tail and wings. Due the increase of flight speed and the adoption of lighter and strengthen materials, the aeroelastic phenomena became even more evident into the airplane design. The flexible behavior changed also the aerodynamic load distribution and consequently the aircraft's center of gravity and moment of inertia, interfering on the aircraft flight dynamics and feedback control systems.

The literature review has shown the efforts to derive the equations of motion of aeroelastic flight vehicles. The first efforts started considering models with only 3 DGOF. Further, more complex derivations considering 6 DGOF with float reference frames, Lagrangian Mechanics and generalized coordinates were achieved. The methodology applied in this work was proposed by Silvestre (2012), where the derivations to model the dynamics of flexible, high-aspect-ratio aircrafts in the time domain were performed. In subsection 2.1.1 the aircraft was defined in time and space by means of the mean axes reference frames and in subsection 2.1.3 the equations of motion were presented with Lagrangian Mechanics considering linear structural dynamics in modal coordinates introduced in 2.1.2. The incremental aerodynamic theory due to elastic deformations adopted in the methodology adopted in the present work was given in section 2.2. This aerodynamic theory deal with unsteady strip theory formulation in the time domain based on the Wagner function. This methodology was implemented in the in-house software FlexSim at the department of Flight Mechanics, Flight Control and Aeroelasticity (FMRA) at TU Berlin by Silvestre (2012).

In chapter 3 the aircraft models investigated were presented. The first model was the utility aircraft Stemme S15 used by Silvestre (2012) to validate the methodology adopted in this work. The second aircraft investigated was the motor glider EC ES15 with two configurations: with and without attached pods. The aircraft EC ES15 was the result of modifications into the wing spar and shell structural properties of the Stemme S15 (the geometry remained unchanged), so that the Stemme S15 was entitled as reference aircraft. The usage of the methodology given in chapter 2 required the elastic properties of the aircraft, that were defined with ground vibration tests (GVT) performed in partnership with the company Leichtwerk in Braunschweig, Germany. In subsection 3.3.2 the linear interpolation of the eigenvectors was carried out for the EC ES15 models. The elastic displacements of the aircraft under trimmed flight condition as well as the

flight dynamic response and aircraft system matrix necessary to implement the pitch damper were introduced.

In chapter 4 the flight dynamic response and pitch damper implementation results were presented. The aircraft geometry, position of elastic axis, control surfaces and structural and aerodynamic models of the aircraft, the trimmed condition as well as the linearized model and the flight dynamic simulations were obtained working with the software FlexSim. In section 4.1 the trimmed flight condition obtained with the structural model from the modal operational analysis was not satisfactory because the controls aileron and ruder have presented significant non symmetric values. For this reason, the eigenvectors were investigated in order to find a possible inconsistence. The contribution of each modal shape into modal amplitudes and trim parameters was investigated. The first symmetric wing bending and the first asymmetric wing torsion were corrected by multiplying the torsion component per zero and 1.5 factors, respectively, for the configuration without pods. The same investigation was carried out for the configuration with pods and five modal shapes were corrected. After the fixing of eigenvectors the corrected structural properties of both EC ES15 configurations still presented asymmetric trimmed flight due an elevator input but not so critical as previous. With the corrected trimmed values the model was linearized and the system matrix was obtained.

Further, in section 4.2 the flight dynamic response of aircraft models introduced in chapter 3 was carried out. The aircraft models were simulated with classical flight mechanics considering the structure as a rigid-body and also with flexible linear structural dynamics. The response was presented for two distinguish maneuvers, the first comprehended a step input of 1^{o} in the elevator and second a step input of 1^{o} in the rudder. The elevator command was defined to investigate the longitudinal flight dynamic angle rates, specially the pitch rate. On the other hand, the step in rudder was carried out in order to see most the lateral motion angle rates. The differences between the rigid-body and flexible approach could be clearly seen, due the fact that the angle rates are modified due the flexibility effects. The comparison between the two aircraft has showed differences between the Stemme S15 and both EC ES15 configurations. In general, in the longitudinal motion the rigid body model of aircraft EC ES15 has higher angle rates than the flexible model, while the Stemme S15 has presented inverse results. Next, in the lateral motion both EC ES15 configurations have higher yaw rates for the flexible than the rigid body model, and the Stemme S15 presented higher yaw rates for the rigid body. No relevant differences between the configurations of EC ES15 were identified. Besides that, the modal amplitudes of the first four modal shapes with its respective frequencies were plotted. It has been possible to see that the elevator commands had excited mostly the symmetric modes of vibration, while the rudder command the lateral ones. Unlike the Stemme S15 and EC ES15 without pods, the EC configuration with pods had the first wing symmetric bending modal shape as the second mode of vibration instead of the first. This fact has well demonstrated the effects of control inputs on the modal amplitudes excitation.

The linearized EOM in state space arrangement had able to implement the pitch damper. Due simplification the actuator dynamics was not modeled in this work. The design frequency and damping were defined following the military specifications MIL-F-8785C. The longitudinal and short period motion approximation were performed with help of MATLAB® and the open and closed loop block diagrams were created with the Simulink tool. The open and closed loop responses were compared for rigid body and flexible structural model, as well. The feedback loop augmented the damping of the system reducing the effect of the pitch rates variations in the short period motion and improving the flight comfort. The comparison between the Ecarys ES15 models showed that for the configuration without pods higher differences between the rigid and flexible structural models in pitch rates for the open loop system as well as for the closed loop system are seen. On the other hand, the configuration with pods had higher variation in attack angle either for the open loop system or for the closed loop system. Besides that, even with the aircrafts not presenting higher differences between themselves, the effects of structural flexibility had influence on the controller gains as well as on the steady and maximum values.

5.1 Final Remarks

This work applied a methodology to model the dynamics of flexible, high-aspect-ratio aircraft in time domain to identify the dynamic response of the utility aircraft EC ES15 with and without attached pods. The structural dynamic properties of the aircraft were defined by means of eigenvectors from ground vibrations tests. These eigenvectors were linear interpolated over the aircraft geometry and the modes of vibration could be represented. The rigid body as well as the flexible structure dynamics were investigated and its influence on the flight dynamic angle rates were plotted for input steps in elevator and rudder controls. The results obtained with this work showed that they are in good agreement with the reference aircraft Stemme S15. The pitch damper was designed following the military specifications for piloted aircrafts and damping the pitch rate. High differences were not observed between the rigid body and flexible models. Nevertheless, the effects of the aircraft flexibility changed the flight dynamic response and the control gains, proving that for high fidelity feedback systems, to include the flexibility effects of the aircraft structure is a recommended measure.

5.2 Future Works

Although the results presented here have demonstrated not only the effectiveness of the methodology and the pitch damper, but also the relevance of to consider the effects of structural flexibility on the aircraft flight dynamics, the following activities could be developed in future works:

- Since the effect of pods into the flight dynamics was not significantly shown, a detailed

investigation of the pods' effects on the aircraft dynamics would be interesting;

- The consideration of the wing let effects on the aerodynamic and structural models;
- Since the structural properties of the aircraft were obtained based only in GVTs, a FEM could be carried out to compare the results;
- In the pitch damper design, to model the actuator dynamics as a electric servo-motor to identify the dead time and optimize the parameters for the elastic models by using Multi-Objective Parameters Synthesis with the software MOPS (JOOS, 2002), for instance;
- Investigation of different flight phases varying the flight speed in order to identify the flutter speeds with the $k-$method;

Bibliography

ANDERSON, J. D. *Fundamentals of Aerodynamics*. 5. ed. New York, USA: McGraw-Hill, 2010. Cited 2 times at pages 38 and 39.

BARBARINO, S. et al. A review of morphing aircraft. *Journal of Intelligent Material Systems and Structures*, Sage Publications, v. 22, n. 9, p. 823–877, 2011. Available from Internet: <http://dx.doi.org/10.1177/1045389X11414084>. Cited at Page 22.

BISMARCK-NASR, M. N. *Structural dynamics in aeronautical engineering*. 1. ed. São José dos Campos, Brazil: AIAA, 1999. Cited 3 times at pages 30, 35, and 36.

BISPLINGHOFF, R. L.; ASHLEY, H. *Principles of aeroelasticity*. 1. ed. New York, USA: Dover Publication, 2013. Cited 7 times at pages 22, 38, 39, 40, 41, 42, and 43.

BMOP A.G. PARKINSON, J. P. R. Linear analysis of transient vibration. *Journal of Sound and Vibration*, v. 9, n. 2, 1969. Available from Internet: <http://dx.doi.org/10.1016/0022-460X(69)90037-6>. Cited at Page 32.

BROCKHAUS, R.; ALLES, W.; LUCKNER, R. *Flugregelung*. 3. ed. Berlin Heidelberg, Deutschland: Springer-Verlag, 2011. Cited at Page 47.

CAVIN III, R.; DUSTO, A. Hamilton's principle-finite-element methods and flexible body dynamics. *AIAA Journal*, v. 15, n. 12, p. 1684–1690, 1977. Available from Internet: <http://dx.doi.org/10.2514/3.7473>. Cited at Page 23.

CHIOZZOTTO, G. P. A modular implementation of aircraft simplified loads methods for conceptual design and variable fidelity processes. *Proceedings, 62nd Deutsche Luft- und Raumfahrtkongress (DLRK)*, Stuttgart, Germany, 2013. Available from Internet: <http://elib.dlr.de/84431/>. Cited at Page 22.

COLLAR, A. The expanding domain of aeroelasticity. *Journal of the Royal Aeronautical Society*, v. 1, p. 613–636, 1946. Cited at Page 22.

COOK, M. V. *Flight dynamics principles: a linear systems approach to aircraft stability and control*. 3. ed. Waltham, USA: Elsevier, 2012. Cited 3 times at pages 27, 47, and 48.

DALLDORFF R. LUCKNER, R. R. L. A full-authority automatic flight control system for the civil airborne utility platform s15 – lapaz. *CEAS 2nd EuroGNC 2013, Conference in Guidance, Navigation and Control in Aerospace, Delft, Netherlands*, April 10-12 2013. Cited at Page 55.

DOWELL, E. H. *A Modern Course in Aeroelasticity*. 4. ed. Dordrecht, USA: Springer, 2014. Cited at Page 22.

ECARYS. Ecarys' brochure - efficient airborne platform. *Strausberg, Brandenburg, Deutschland*, p. 13, 2012. Available from Internet: <http://assets.stemme.de/ECARYS/ecarys.html>. Cited at Page 57.

ECARYS. Strukturtechnologien für innovative arbeitsflugzeuge. *Report - Interne Referenz. Strausberg, Brandenburg, Deutschland*, 2014. Available from Internet: <http://www.ecarys-.com/app/download/9543071721/ECARYS+summary+report.pdf?t=1402902668>. Cited 4 times at pages 56, 57, 61, and 63.

ETKIN, B.; REID, L. D. *Dynamics of Flight: Stability and Control*. 3. ed. New York, USA: John Wiley & Sons, 1998. Cited 4 times at pages 23, 27, 47, and 68.

FAA-PART23. Part 23 - airworthiness standards: Normal, utility, acrobatic, and commuter category airplanes. Federal Aviation Administration (FAA), USA, 2015. Cited at Page 77.

FÖRSCHING, H. W. *Grundlagen der aeroelastik*. 1. ed. Berlin-Heidelberg, Deutschland: Springer-Verlag, 2013. Cited at Page 44.

FOX, R. W.; MCDONALD, A. T.; PRITCHARD, P. J. *Introduction to fluid mechanics*. 7. ed. New York, USA: John Wiley & Sons, 1985. Cited at Page 38.

FUNG, Y.-c. *An introduction to the theory of aeroelasticity*. 1. ed. Mineola, New York, USA: Dover Publications, 2002. Cited 6 times at pages 22, 38, 40, 41, 42, and 43.

HAMANN, A. Development of a model of a flexible aircraft for investigations of longitudinal flight mechanics. *10th Pegasus-AIAA Student Conference*, 2014. Cited 4 times at pages 37, 44, 45, and 66.

HEINZE, S. *Aeroelastic Concepts for Flexible Aircraft Structures*. Thesis (PhD), Stockholm, Sweden, 2007. Available from Internet: <https://www.diva-portal.org/smash/get/diva2:8047-/FULLTEXT01.pdf>. Cited at Page 38.

HULL, D. G. *Fundamentals of airplane flight mechanics*. Austin, Texas, USA: Springer, 2007. Cited at Page 27.

HUNT, B. R.; LIPSMAN, R. L.; ROSENBERG, J. M. *A guide to MATLAB: for beginners and experienced users*. 3. ed. New York, USA: Cambridge University Press, 2014. Cited at Page 66.

INMAN, D. J.; SINGH, R. C. *Engineering vibration*. 4. ed. Virginia, USA: Prentice Hall Englewood Cliffs, NJ, 2013. Cited at Page 37.

JONES, W. P. *The calculation of aerodynamic derivative coefficients for wings of any plan form in non-uniform motion.* [S.l.]: HM Stationery Office, 1946. Cited 3 times at pages 41, 43, and 45.

JOOS, H.-D. A multiobjective optimisation-based software environment for control systems design. *Computer Aided Control System Design, 2002. Proceedings. 2002 IEEE International Symposium on*, IEEE, Glasgow, Scotland, UK, p. 7–14, 2002. Available from Internet: <http://www.dlr.de/rm/Portaldata/52/Resources/dokumente/m_t/joos_cacsd02.pdf>. Cited at Page 90.

KADEN B. BOCHE, R. L. A. Hardware-in-the-loop flight simulator – an essential part in the development process for the automatic flight control system of a utility aircraft. In: ____. *Advances in Aerospace Guidance, Navigation and Control*. [s.n.], 2013. p. 585–602. Available from Internet: <http://dx.doi.org/10.1007/978-3-642-38253-6>. Cited at Page 24.

KÜSSNER, H. G. Zusammenfassender bericht über den instationären auftrieb von flügeln. *Luftfahrtforschung*, v. 13, n. 12, p. 410–424, 1936. Cited 2 times at pages 41 and 43.

LIVNE, E. Future of airplane aeroelasticity. *Journal of Aircraft*, v. 40, n. 6, p. 1066–1092, 2003. Available from Internet: <http://dx.doi.org/10.2514/2.7218>. Cited at Page 22.

LOOYE, G. H. N. *An Integrated Approach to Aircraft Modeling and Flight Control Law Design*. Thesis (PhD), 2008. Available from Internet: <http://repository.tudelft.nl/assets-/uuid:3c921dd4-c9f5-439e-a412-afd0856ba689/looye_20080116.pdf>. Cited 3 times at pages 23, 24, and 33.

MAIA, N. M. M.; SILVA, J. M. M. e. *Theoretical and experimental modal analysis*. 1. ed. Tauton, Somerset, England: Research Studies Press Taunton, 1997. Cited at Page 60.

MIL-F-8785C. U.s. department of defense military specification: Flying qualities of piloted airplanes. Department of Defense, USA, 1980. Cited 9 times at pages 12, 25, 47, 50, 51, 52, 53, 67, and 77.

MILA, J. S. *Autonomous Flight Control Design for Longitudinal Motion of a Forward Swept Wing Aircraft*. Dissertation (Master) — Technische Universitaet Berlin - Fachgebiet Flugmechanik, Flugregelung und Aeroelastizitaet, 2013. Cited 2 times at pages 24 and 53.

MILNE, R. Some remarks on the dynamics of deformable bodies. *AIAA Journal*, v. 6, n. 3, p. 556–558, 1968. Available from Internet: <http://dx.doi.org/10.2514/3.4541>. Cited at Page 23.

NELSON, R. C. *Flight stability and automatic control*. 2. ed. New York, USA: WCB/McGraw Hill, 1998. Cited 2 times at pages 23 and 48.

NISE, N. S. *Control Systems Engineering*. 6. ed. Danvers, MA, USA: John Wiley & Sons, 20011. Cited at Page 48.

RAO, S. S. *Mechanical Vibrations*. 5. ed. New York, USA: Pearson, 2011. Cited 3 times at pages 30, 31, and 36.

SANDWELL, D. T. Biharmonic spline interpolation of geos-3 and seasat altimeter data. *Geophysical Research Letters*, v. 14, n. 2, p. 139–142, 1987. ISSN 1944-8007. Available from Internet: <http://dx.doi.org/10.1029/GL014i002p00139>. Cited 2 times at pages 65 and 66.

SEARS, W. R. On the reaction of an elastic wing to vertical gusts. *Journal of the Aeronautical Sciences (Institute of the Aeronautical Sciences)*, n. 230, p. 95–111, 1941. Cited at Page 43.

SHINNERS, S. M. *Modern control system theory and design*. 2. ed. New York, USA: John Wiley & Sons, 1998. Cited at Page 77.

SILLER, H. R. E. *Non-linear modal analysis methods for engineering structures*. Thesis (PhD) — University of London, 2004. Cited at Page 31.

SILVESTRE, F. J. *Methodology for Modelling the Dynamics of Flexible, High-Aspect-Ratio Aircraft in the Time Domain for Aeroservoelastic Investigations*. [S.l.]: mbvberlin, 2012. Cited 19 times at pages 22, 24, 27, 28, 29, 30, 32, 33, 34, 37, 38, 39, 42, 43, 46, 55, 58, 60, and 66.

SILVESTRE, F. J. Aeroservoelastic investigation of a high-aspect-ratio experimental aircraft. In: ____. *Advances in Aerospace Guidance, Navigation and Control*. [S.l.]: Springer Verlag, 2013. cap. Atmospheric Applications, p. 639–658. ISBN 978-3-642-38252-9. Cited at Page 24.

SILVESTRE, F. J.; PAGLIOLE, P. Method for evaluating the structural dynamics influence on the flight mechanics of a flexible aircraft. *19th International Congress of Mechanical Engineering. Brasilia - DF, Brazil*, 2007. Cited 3 times at pages 22, 24, and 27.

SILVESTRE, F. J.; PAGLIONE, P. *Dynamics and control of a flexible aircraft*. Thesis (PhD), 2008. Cited at Page 33.

THEODORSEN, T. General theory of aerodynamic instability and the mechanism of flutter. *NACA Report Number 496*, 1934. Cited 4 times at pages 39, 40, 41, and 42.

THORBY, D. *Structural dynamics and vibration in practice: an engineering handbook*. 1. ed. Waltham, USA: ELSEVIER, 2008. Cited 3 times at pages 29, 32, and 60.

WAGNER, H. Über die entstehung des dynamischen auftriebes von tragflügeln. *ZAMM - Journal of Applied Mathematics and Mechanics / Zeitschrift für Angewandte Mathematik und Mechanik*, WILEY-VCH Verlag, Berlin, Deutschland, v. 5, n. 1, p. 17–35, 1925. ISSN 1521-4001. Available from Internet: <http://dx.doi.org/10.1002/zamm.19250050103>. Cited 3 times at pages 41, 42, and 43.

WASZAK, M. R.; DAVIDSON, J. B.; SCHMIDT, D. K. A simulation study of the flight dynamics of elastic aircraft. volume 1: Experiment, results and analysis. NASA Contractor Report 4102, 1987. Cited 2 times at pages 23 and 32.

WASZAK, M. R.; DAVIDSON, J. B.; SCHMIDT, D. K. A simulation study of the flight dynamics of elastic aircraft. volume 2: Data. NASA Contractor Report 4102, 1987. Cited 2 times at pages 23 and 32.

WASZAK, M. R.; SCHMIDT, D. K. Flight dynamics of aeroelastic vehicles. *Journal of Aircraft*, v. 25, n. 6, p. 563–571, 1988. Available from Internet: <http://dx.doi.org/10.2514/3.45623>. Cited 7 times at pages 23, 24, 27, 28, 29, 32, and 33.

WRIGHT, J. R.; COOPER, J. E. *Introduction to Aircraft Aeroelasticity and Loads*. 2. ed. New York, USA: John Wiley & Sons, 2015. Cited 2 times at pages 22 and 23.

YOUNG, H. D.; FREEDMAN, R. A. *Sears and Zemansky's university physics*. 13. ed. [S.l.]: Addison-Wesley, 2011. Cited at Page 30.

Appendix

APPENDIX A – Modal Shapes of Models

A.1 Stemme S15

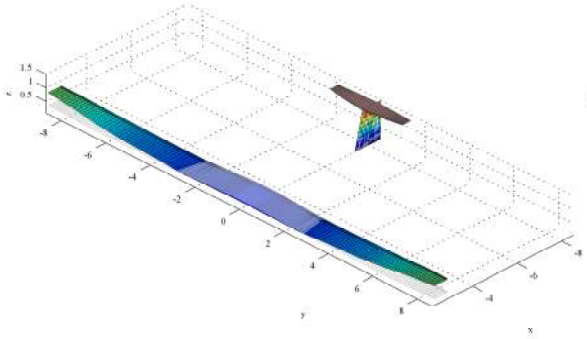

Mode Number: 1. Frequency= 3.29Hz

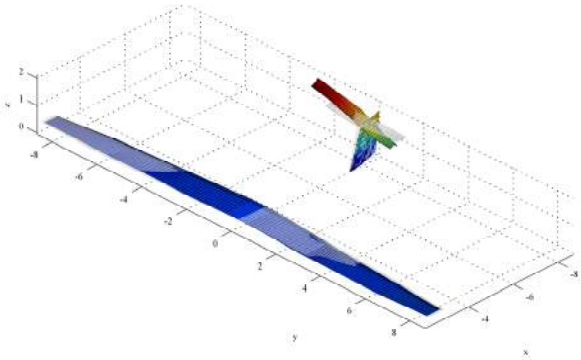

Mode Number: 2. Frequency= 4.24Hz

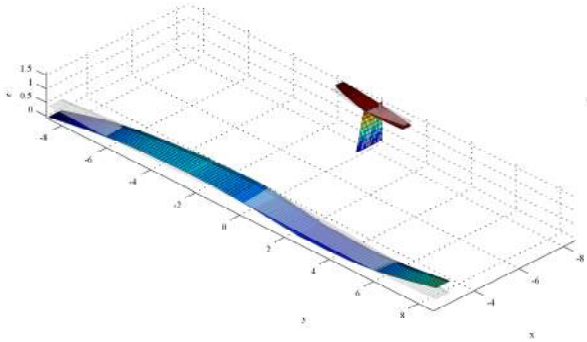

Mode Number: 3. Frequency= 7.34Hz

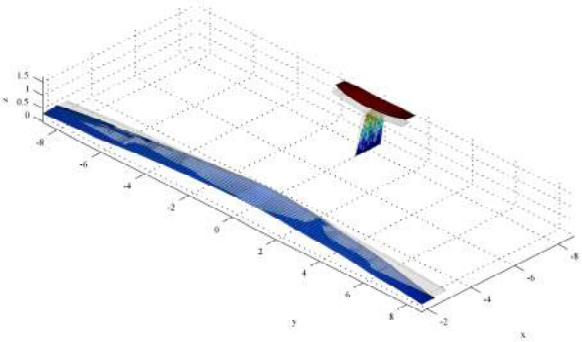

Mode Number: 4. Frequency= 7.39Hz

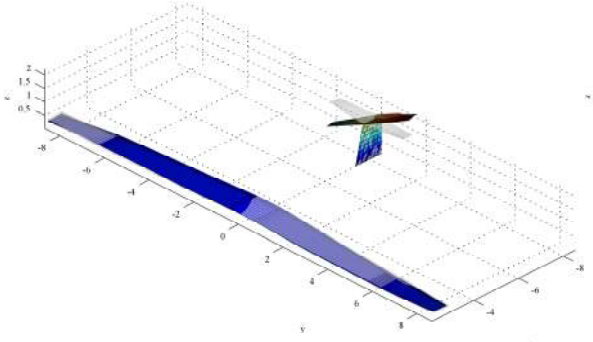

Mode Number: 5. Frequency= 8.07Hz

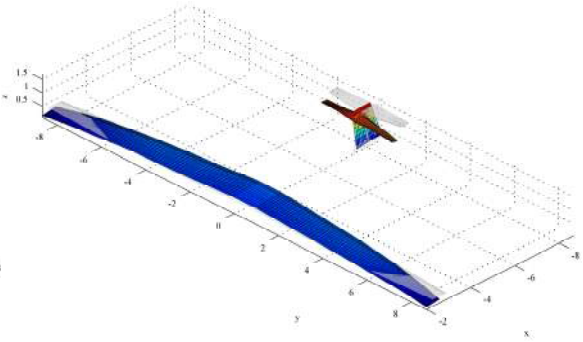

Mode Number: 6. Frequency= 9.02Hz

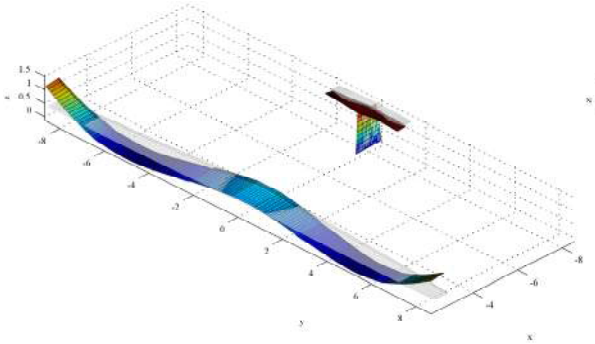

Mode Number: 7. Frequency= 11.55Hz

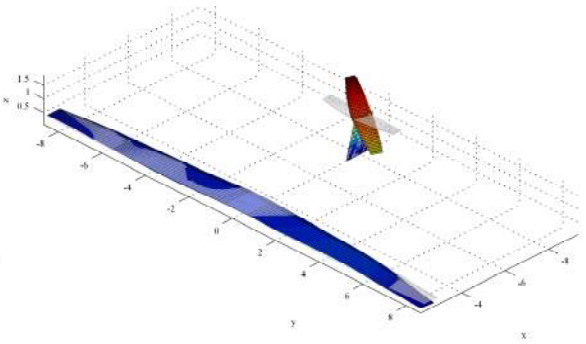

Mode Number: 8. Frequency= 11.72Hz

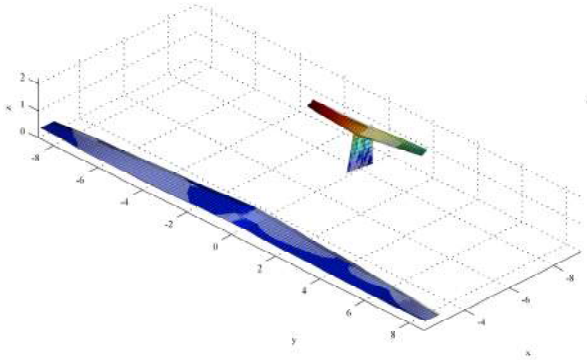

Mode Number: 9. Frequency= 13.35Hz

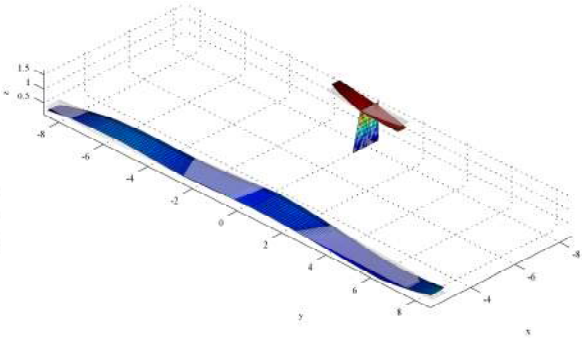

Mode Number: 10. Frequency= 15.37Hz

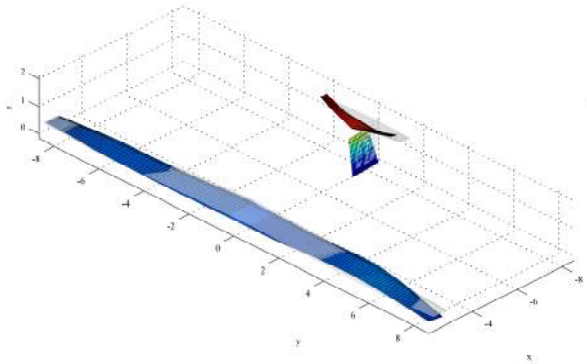

Mode Number: 11. Frequency= 19.74Hz

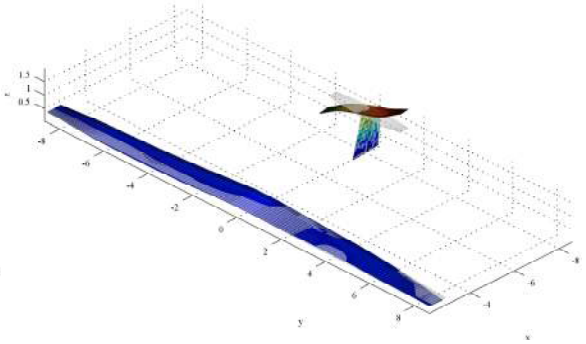

Mode Number: 12. Frequency= 20.13Hz

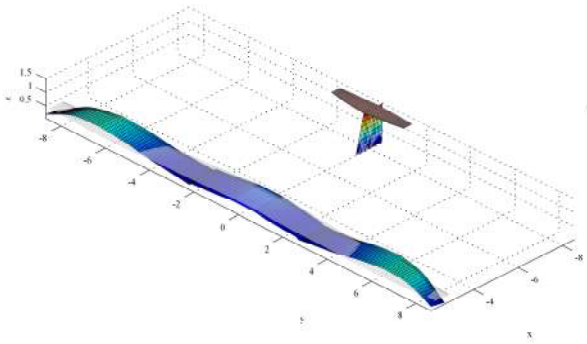

Mode Number: 13. Frequency= 21.024Hz

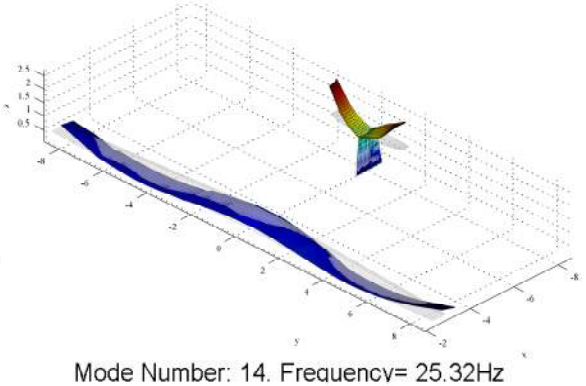

Mode Number: 14. Frequency= 25.32Hz

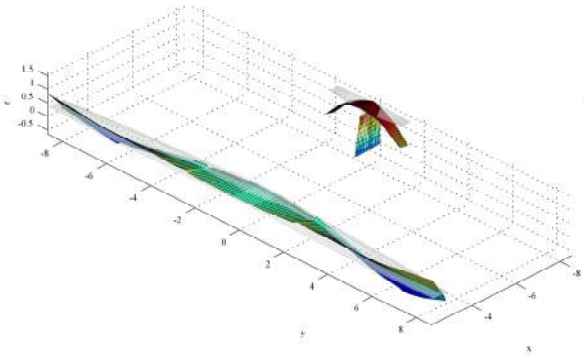

Mode Number: 15. Frequency= 27.873Hz

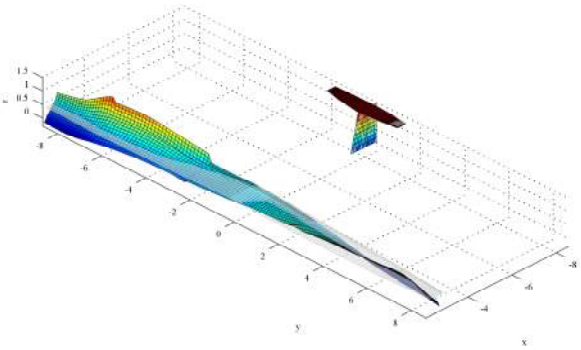

Mode Number: 16. Frequency= 28.99Hz

A.2 Ecarys ES15 without PODs

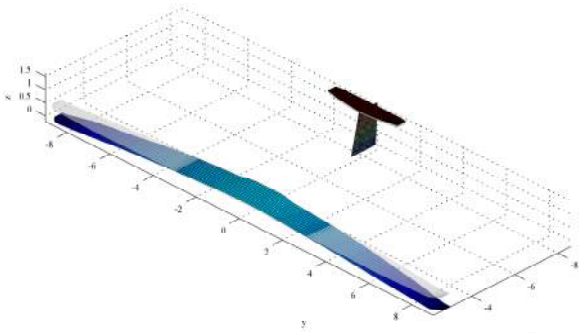

Mode Number: 1. Frequency= 3.785Hz

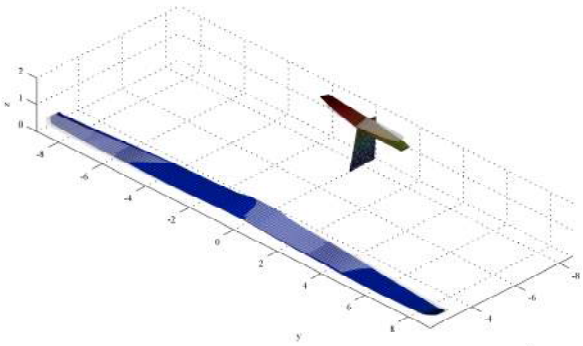

Mode Number: 2. Frequency= 4.525Hz

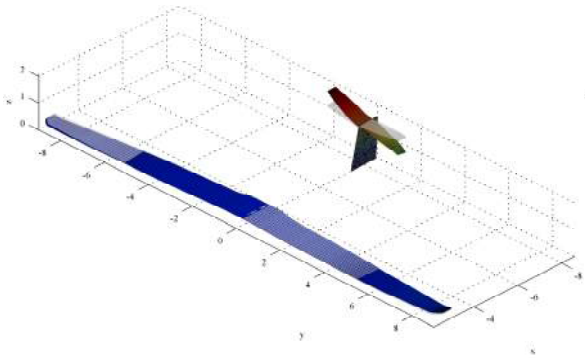

Mode Number: 3. Frequency= 7.772Hz

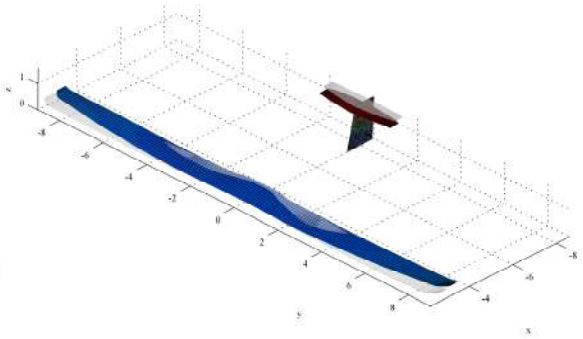

Mode Number: 4. Frequency= 7.974Hz

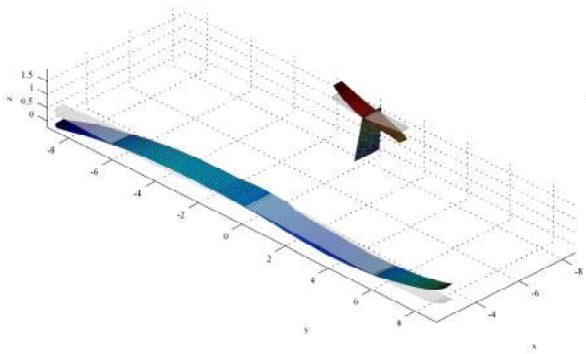

Mode Number: 5. Frequency= 8.143Hz

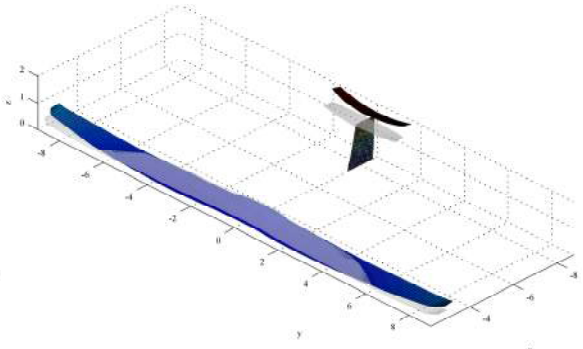

Mode Number: 6. Frequency= 9.352Hz

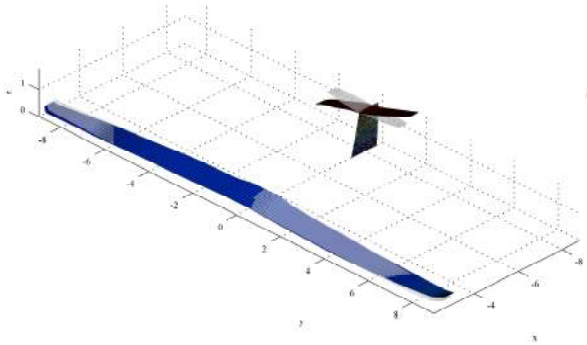

Mode Number: 7. Frequency= 11.892Hz

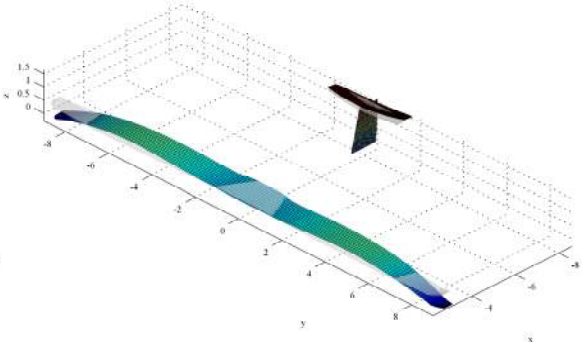

Mode Number: 8. Frequency= 12.959Hz

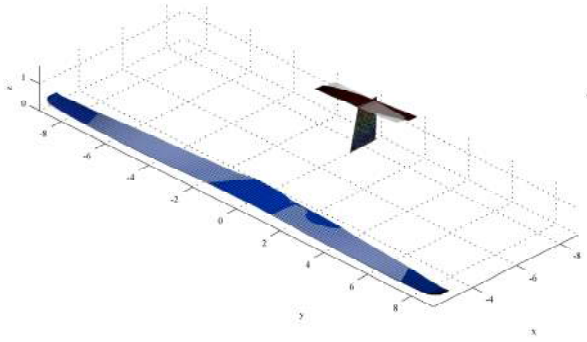

Mode Number: 9. Frequency= 13.34Hz

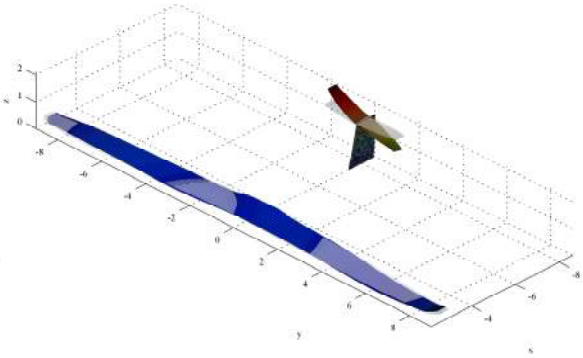

Mode Number: 10. Frequency= 18.709Hz

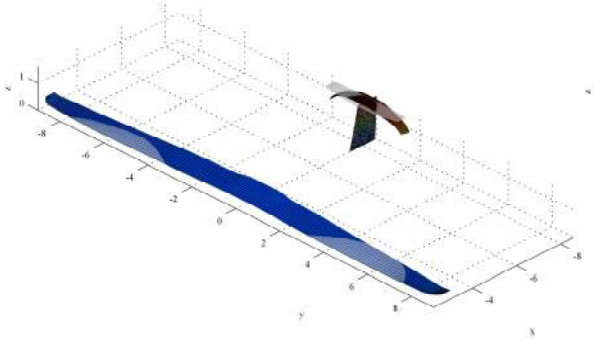

Mode Number: 11. Frequency= 19.423Hz

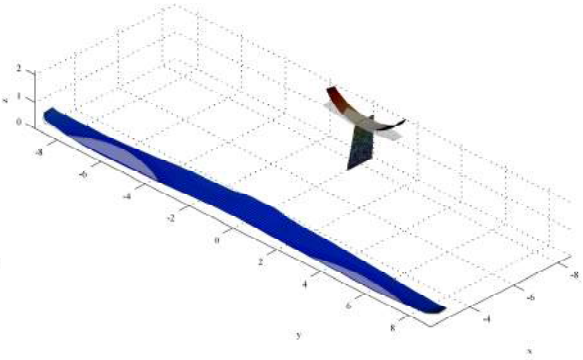

Mode Number: 12. Frequency= 21.353Hz

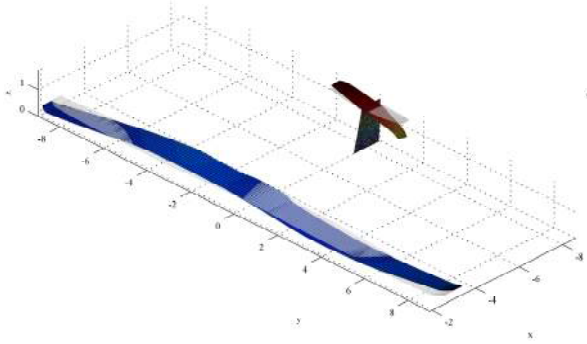

Mode Number: 13. Frequency= 21.368Hz

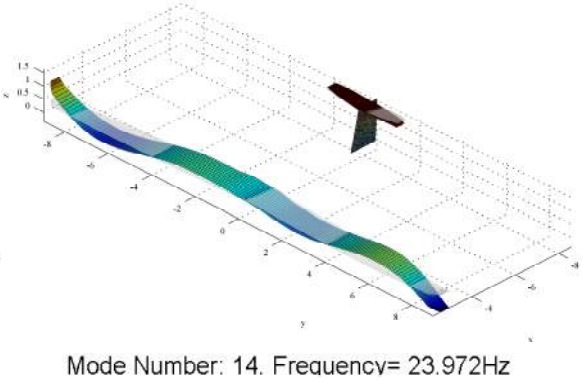

Mode Number: 14. Frequency= 23.972Hz

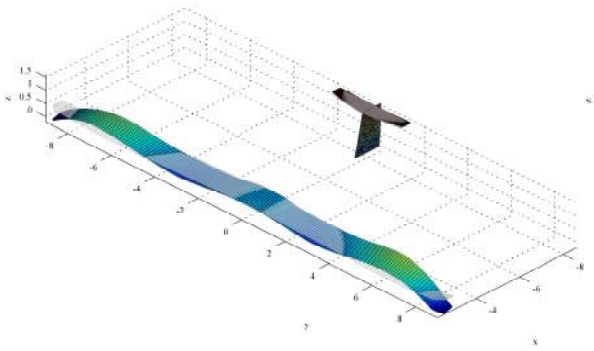

Mode Number: 15. Frequency= 27.616Hz

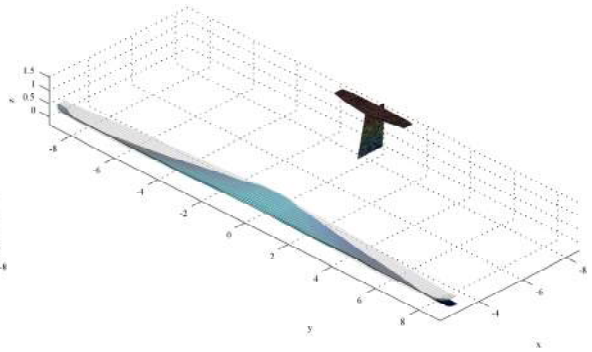

Mode Number: 16. Frequency= 29.039Hz

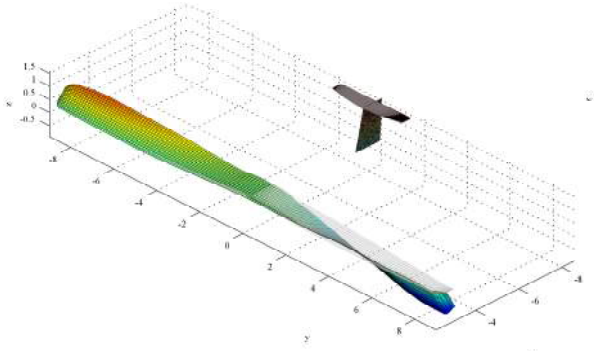

Mode Number: 17. Frequency= 29.098Hz

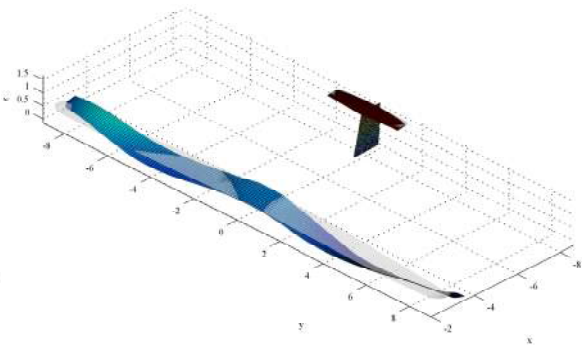

Mode Number: 18. Frequency= 29.78Hz

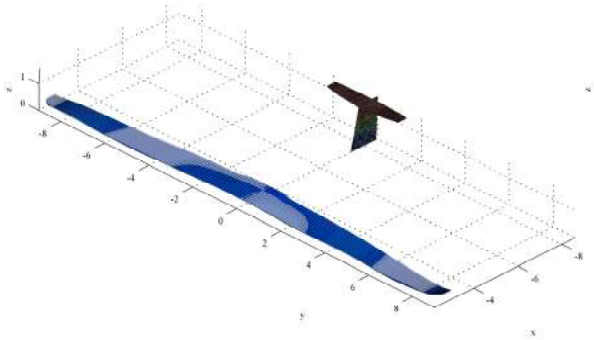

Mode Number: 19. Frequency= 41.008Hz

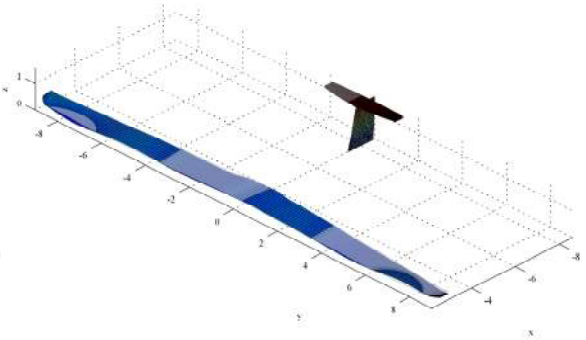

Mode Number: 20. Frequency= 43.86Hz

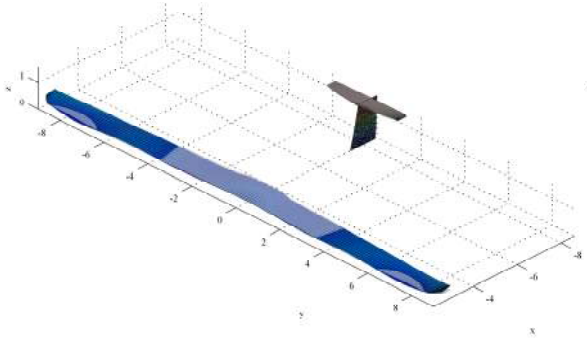

Mode Number: 21. Frequency= 44.942Hz

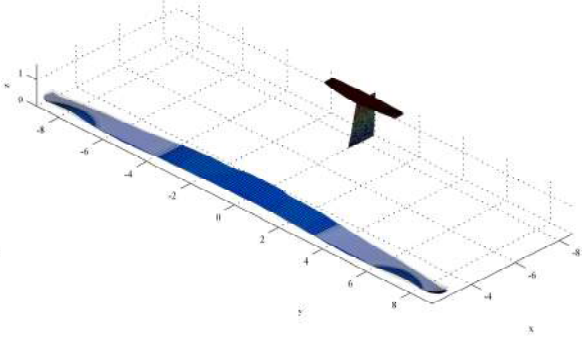

Mode Number: 22. Frequency= 45.292Hz

A.3 Ecarys ES15 with PODs

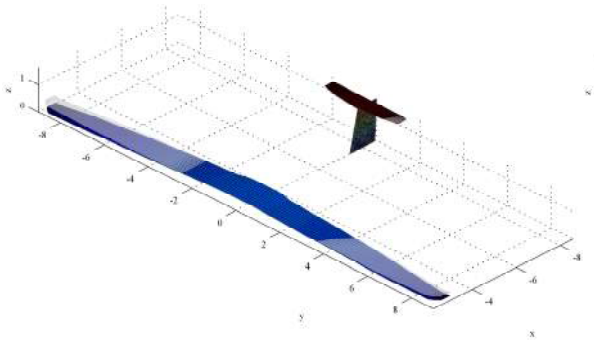

Mode Number: 1. Frequency= 3.458Hz

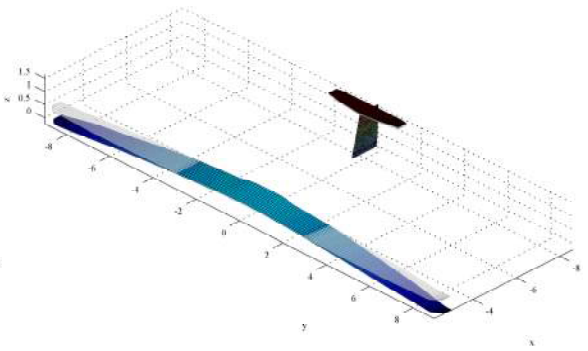

Mode Number: 2. Frequency= 3.79Hz

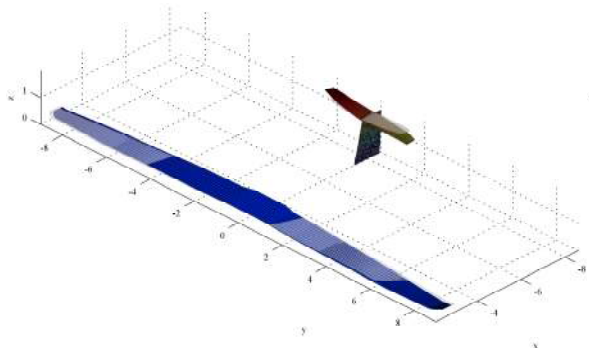

Mode Number: 3. Frequency= 4.452Hz

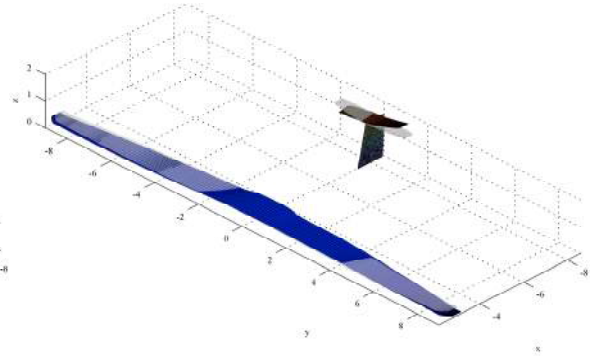

Mode Number: 4. Frequency= 4.746Hz

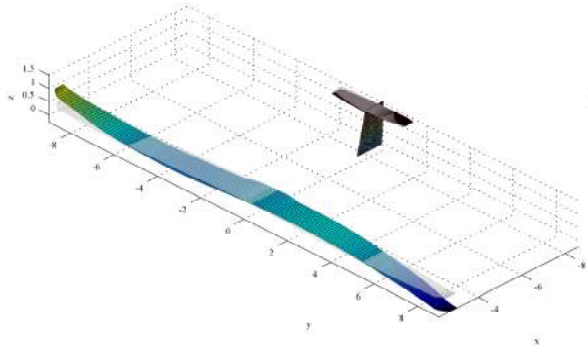

Mode Number: 5. Frequency= 6.675Hz

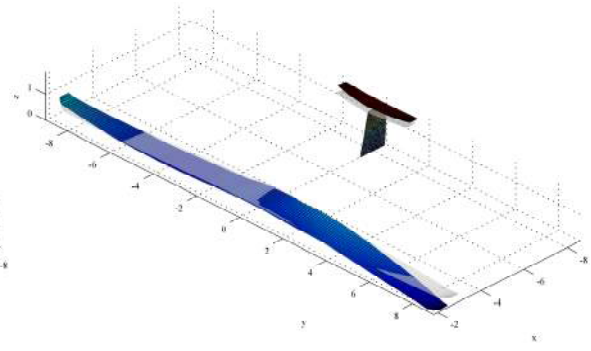

Mode Number: 6. Frequency= 7.639Hz

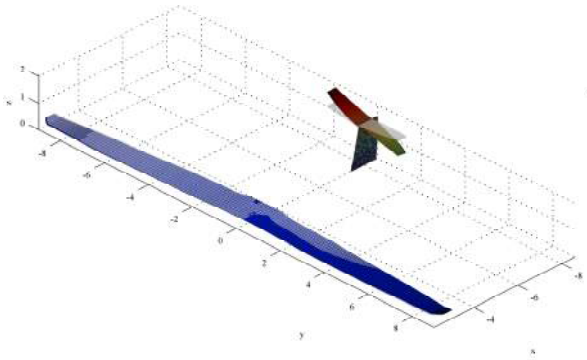

Mode Number: 7. Frequency= 7.781Hz

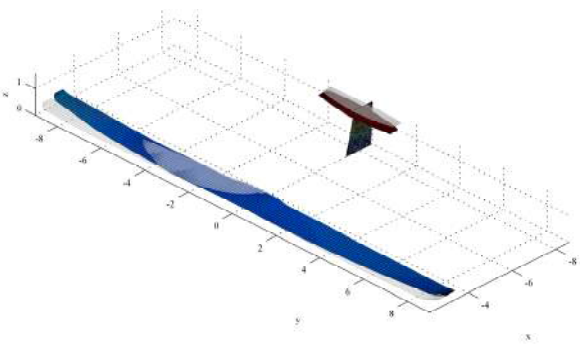

Mode Number: 8. Frequency= 7.83Hz

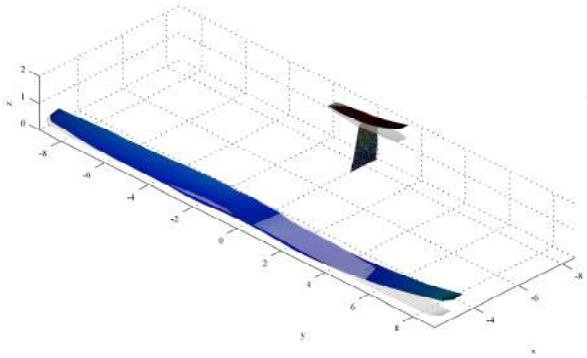

Mode Number: 9. Frequency= 8.515Hz

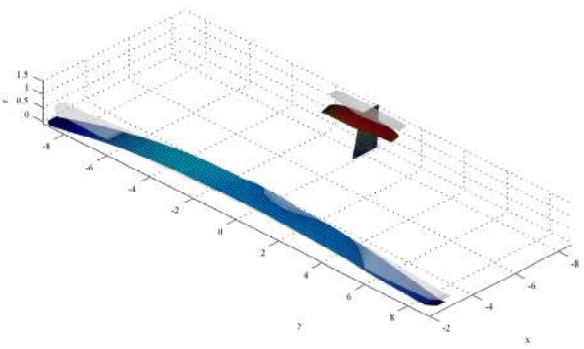

Mode Number: 10. Frequency= 9.118Hz

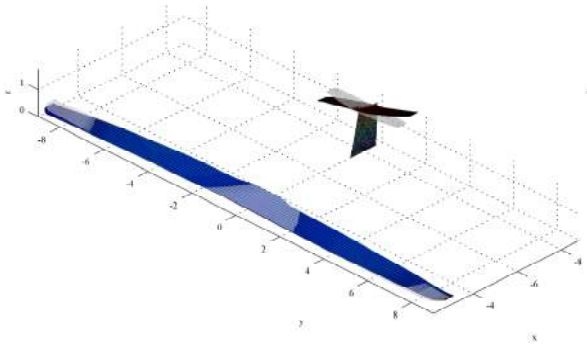

Mode Number: 11. Frequency= 11.851Hz

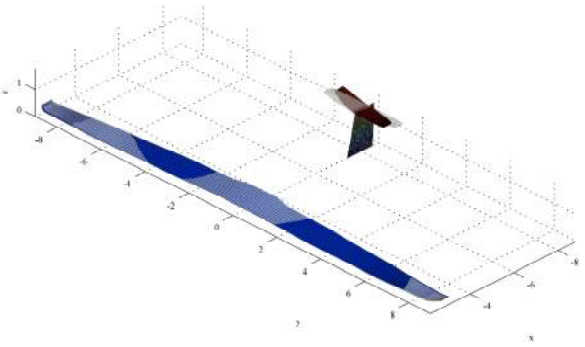

Mode Number: 12. Frequency= 13.137Hz

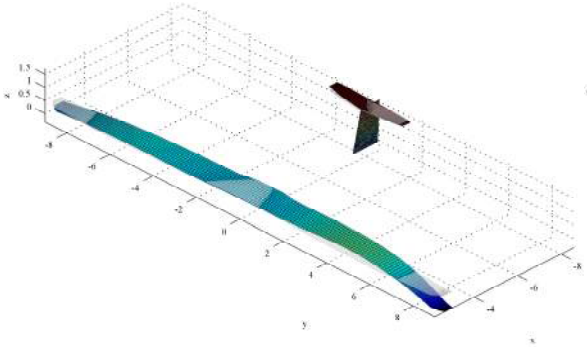

Mode Number: 13. Frequency= 13.57Hz

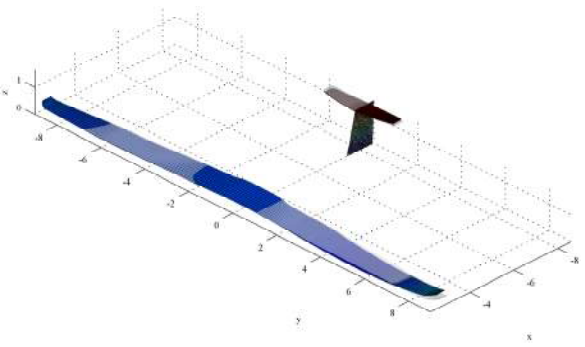

Mode Number: 14. Frequency= 14.271Hz

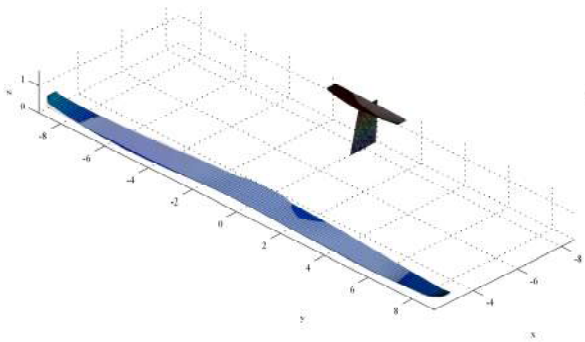

Mode Number: 15. Frequency= 15.329Hz

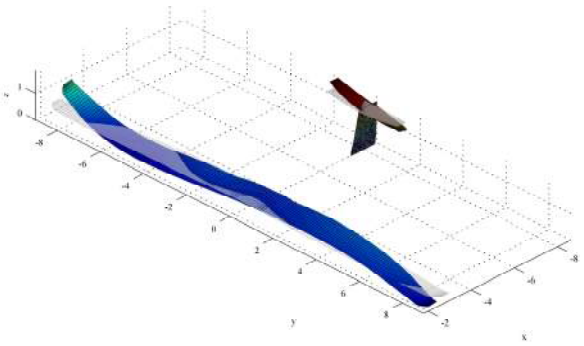

Mode Number: 16. Frequency= 18.001Hz

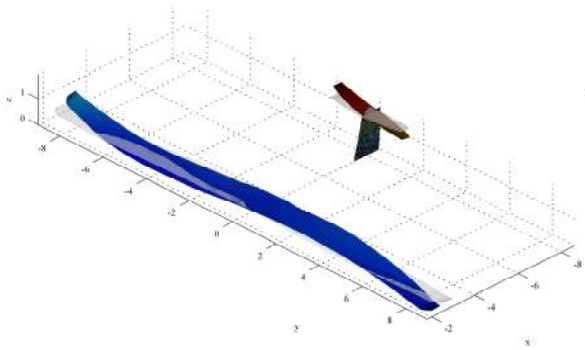

Mode Number: 17. Frequency= 18.399Hz

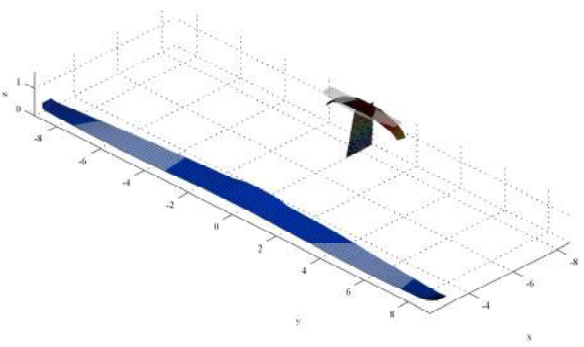

Mode Number: 18. Frequency= 19.132Hz

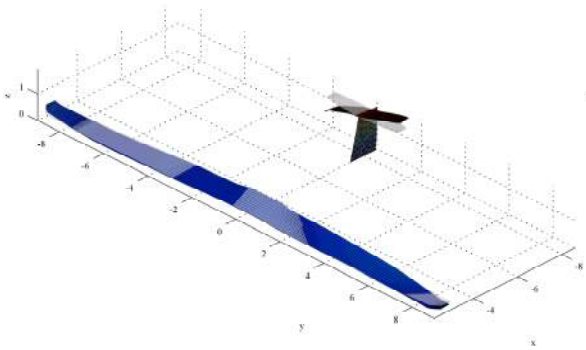

Mode Number: 19. Frequency= 19.513Hz

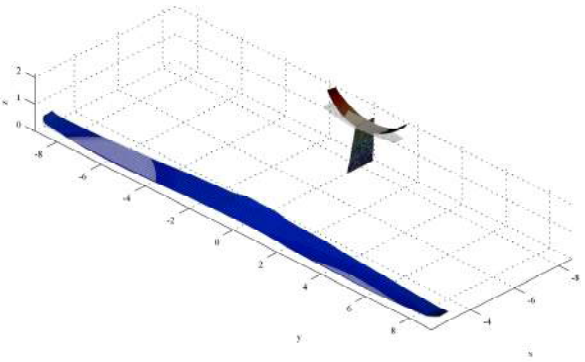

Mode Number: 20. Frequency= 21.503Hz

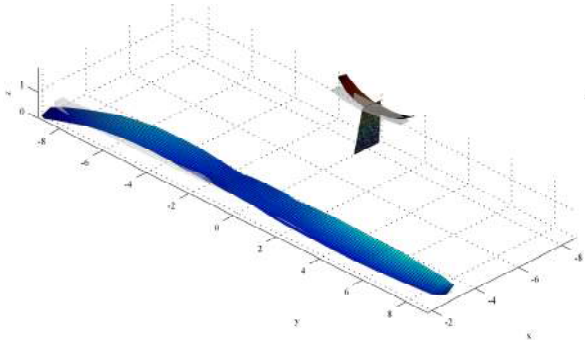

Mode Number: 21. Frequency= 23.714Hz

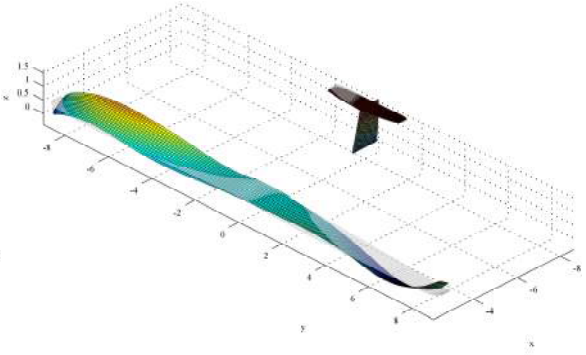

Mode Number: 22. Frequency= 25.028Hz

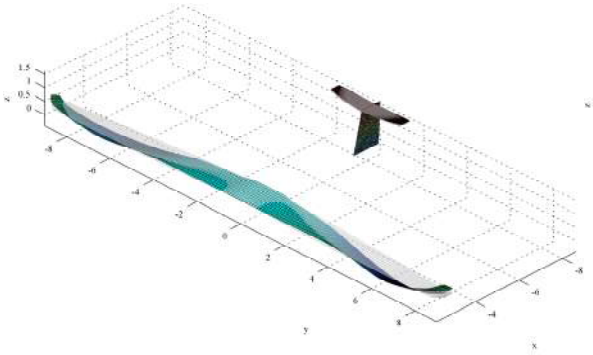

Mode Number: 23. Frequency= 25.217Hz

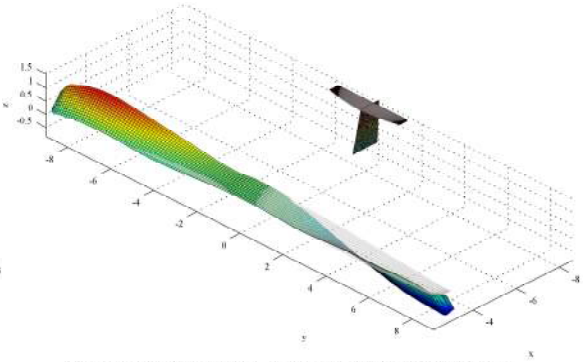

Mode Number: 24. Frequency= 29.738Hz

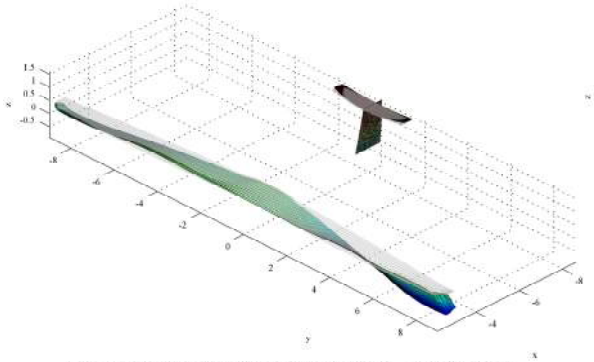

Mode Number: 25. Frequency= 29.802Hz

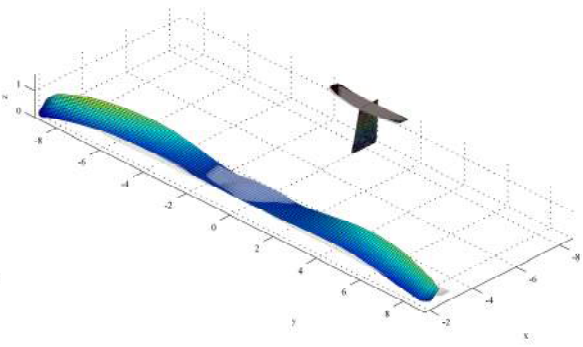

Mode Number: 26. Frequency= 32.017Hz

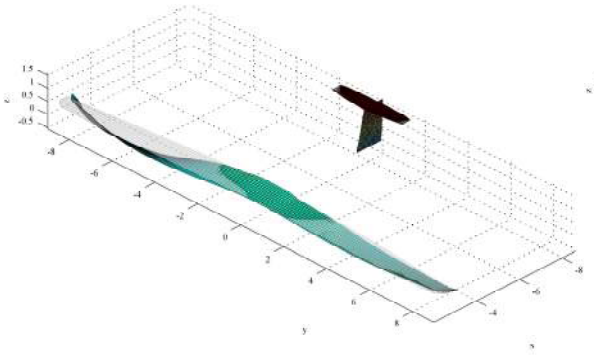

Mode Number: 27. Frequency= 34.522Hz

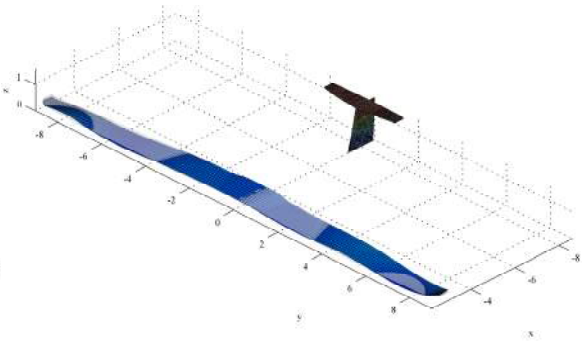

Mode Number: 28. Frequency= 43.534Hz

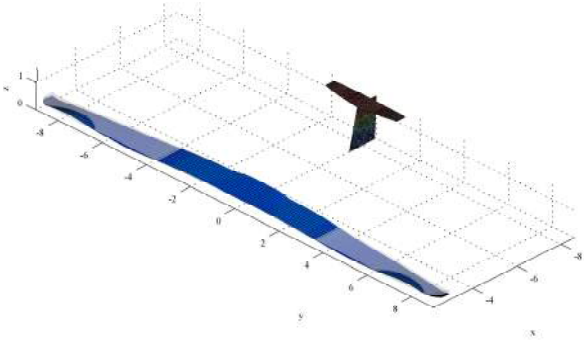

Mode Number: 29. Frequency= 43.827Hz

APPENDIX B – Pitch Damper Results

B.1 Stemme S15

Figure 74: Short period (SP) approximation. Step input of 1^{o} in elevator command. Pitch rate and attack angle variations for rigid and flexible structural models. The dashed lines display the open loop (OL) and the full lines the closed loop (CL) control system. Simulation time $5s$.

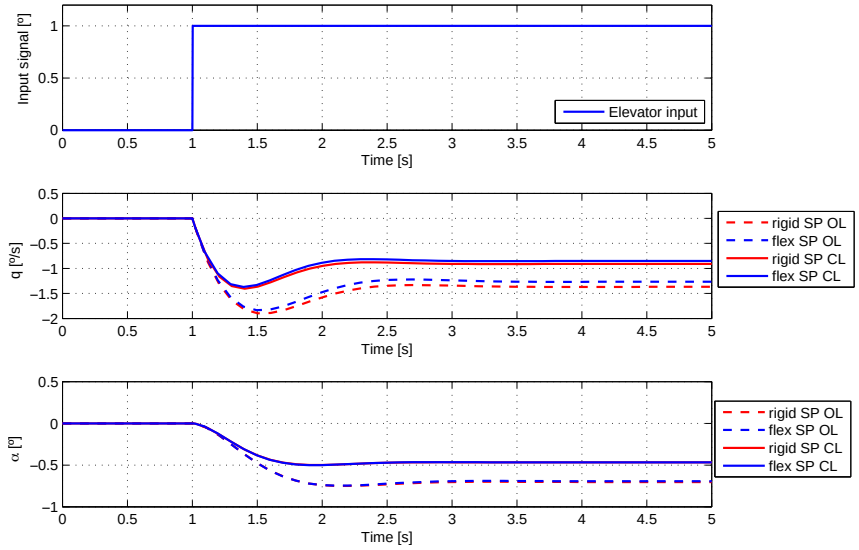

Source: Author.

Figure 75: Longitudinal Motion (LB) approximation. Step input of 1^o in elevator command. Pitch rate and attack angle variations for rigid and flexible structural models. The dashed lines display the open loop (OL) and the full lines the closed loop (CL) control system. Simulation time $5s$.

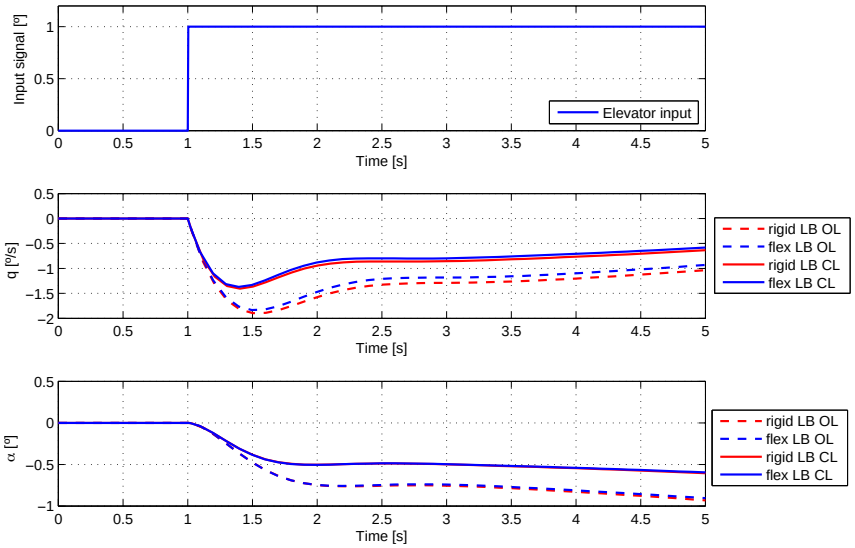

Source: Author.

Figure 76: Longitudinal Motion (LB) approximation. Step input of 1^o in elevator command. Pitch rate and attack angle variations for rigid and flexible structural models. The dashed lines display the open loop (OL) and the full lines the closed loop (CL) control system. Simulation time $20s$.

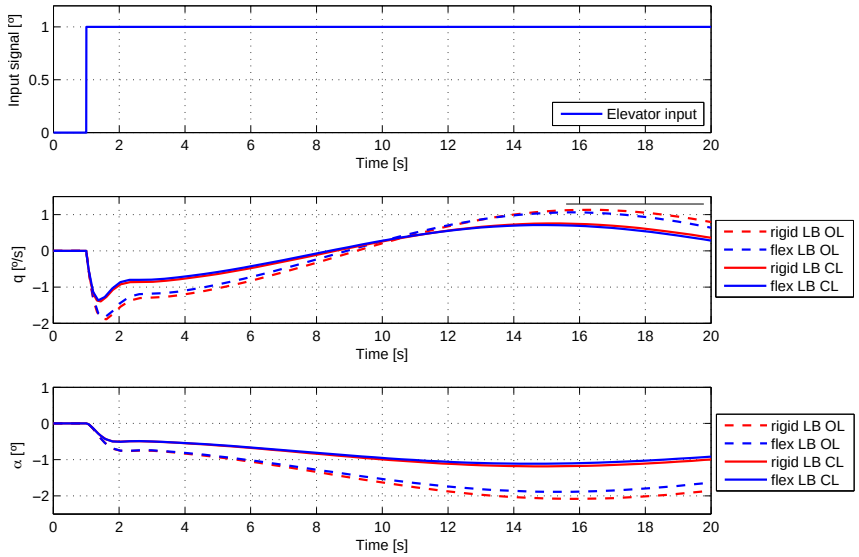

Source: Author.

Figure 77: Longitudinal Motion (LB) approximation. Step input of 1^o in elevator command. Pitch rate and attack angle variations for rigid and flexible structural models. The dashed lines display the open loop (OL) and the full lines the closed loop (CL) control system. Simulation time $400s$.

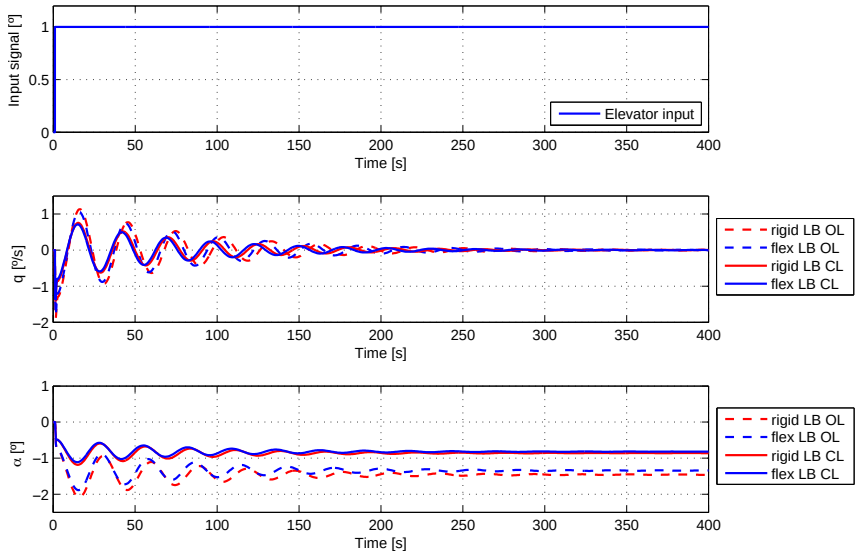

Source: Author.

B.2 Ecarys ES15 with pods

Figure 78: Short period (SP) approximation. Step input of 1^o in elevator command. Pitch rate and attack angle variations for rigid and flexible structural models. The dashed lines display the open loop (OL) and the full lines the closed loop (CL) control system. Simulation time $5s$.

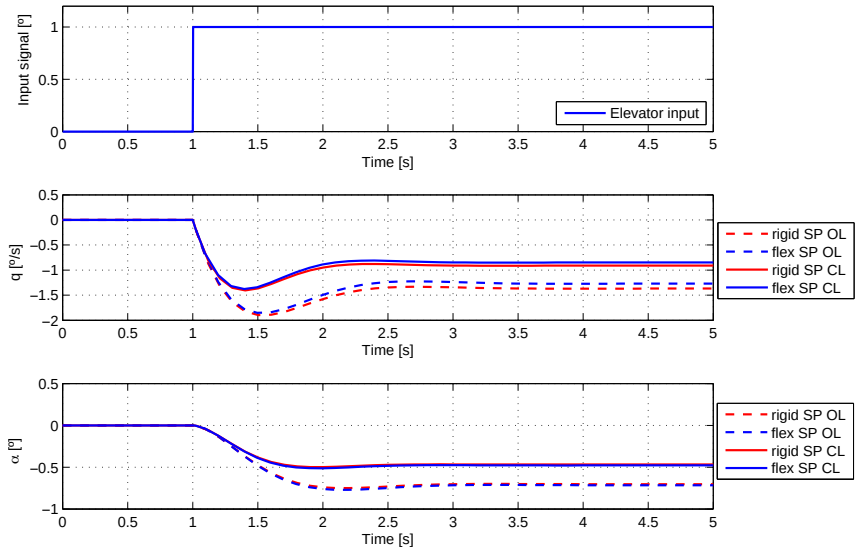

Source: Author.

Figure 79: Longitudinal Motion (LB) approximation. Step input of 1^o in elevator command. Pitch rate and attack angle variations for rigid and flexible structural models. The dashed lines display the open loop (OL) and the full lines the closed loop (CL) control system. Simulation time $5s$.

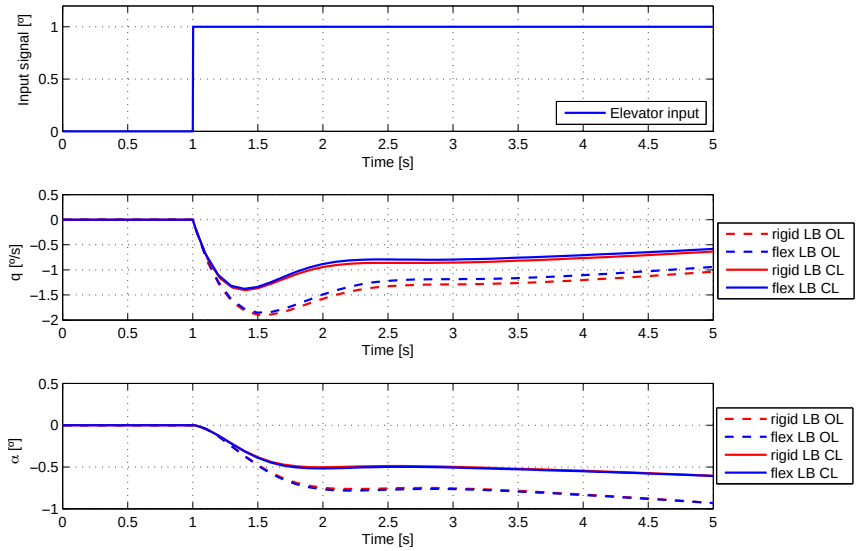

Source: Author.

Figure 80: Longitudinal Motion (LB) approximation. Step input of 1^o in elevator command. Pitch rate and attack angle variations for rigid and flexible structural models. The dashed lines display the open loop (OL) and the full lines the closed loop (CL) control system. Simulation time $20s$.

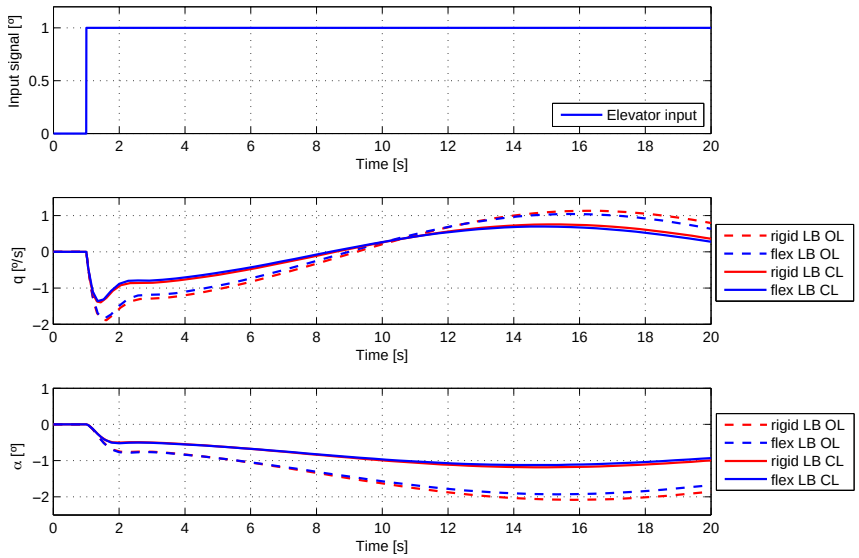

Source: Author.

Figure 81: Longitudinal Motion (LB) approximation. Step input of 1^{o} in elevator command. Pitch rate and attack angle variations for rigid and flexible structural models. The dashed lines display the open loop (OL) and the full lines the closed loop (CL) control system. Simulation time $400s$.

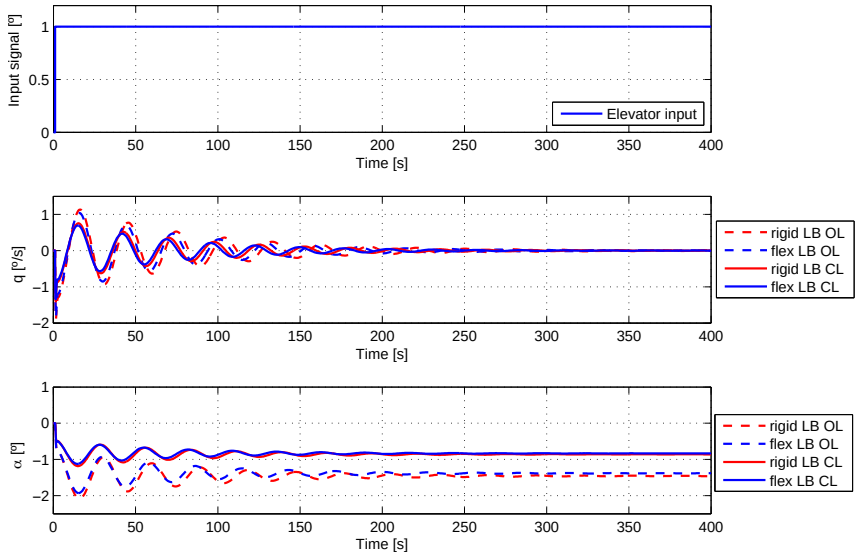

Source: Author.

APPENDIX C – Implemented Algorithms

C.1 mfv2StructFlexSimInput.m

Listing C.1: mfv2StrucFlexSimInput.m

```
close all; clear all; clc;
%% Choose the Configuration
% PODs= 0; % without PODs
PODs= 1; % with PODs
WL=0; % without winglet
% WL=1; % with winglet
%% Import Data from Functions
[GeoTemp,Streifen,GVTRefPoint]=InterpStreifenGVT(); %Geometry and Grids
[Shapes,Modal_damp,Modal_freq,Modal_freq_Hz,Modal_names,Symmetry,Modal_mass,Geo]=
    ...
    ReadGVTData(PODs,GeoTemp,Streifen,GVTRefPoint,WL); % Shapes
%% Define Inputs to FlexSim
LocalEuler.wing = 0;
LocalEuler.HE = 0;
LocalEuler.VE = -90;
LocalPos.wing = [0;0;0];
LocalPos.HE = [0;0;0];
LocalPos.VE = [0;0;0];
R_coord_VE = [0;0;0];
RefPoint = [0;0;0];
RefStructPoint = [0;0;0];
Scale = linspace(20,20,length(Shapes));
Scale = Scale';
for count1=1:length(Shapes)
    Modal_names{count1,2} =char(64+count1);
    Modal_names{count1,3} =char(96+count1);
end
%% Save Structure File according to the configuration selected
if PODs==0 && WL==0
% figname= '150724_Structures_noPODs_noWL.mat';
    figname= 'Structures_GVTVIInoPODSnoWL.mat';
    save(['<input your directory>',figname], ...
```

```
32          'Geo','LocalEuler','LocalPos','Modal_damp','Modal_freq_Hz',...
33          'Modal_freq','Modal_mass','R_coord_VE','RefPoint','Shapes', ...
34          'Scale','RefStructPoint','Modal_names','Symmetry'); % ShapesGVT, GeoGVT
35      disp(['Structure saved: configuration without PODs, "',figname,'"'])
36  elseif PODs==0 && WL==1
37      figname= 'Structures_GVTVIInoPODSWL.mat';
38      save(['<input your directory>',figname], ...
39          'Geo','LocalEuler','LocalPos','Modal_damp','Modal_freq_Hz', ...
40          'Modal_freq','Modal_mass','R_coord_VE','RefPoint','Shapes', ...
41          'Scale','RefStructPoint','Modal_names','Symmetry'); % ShapesGVT, GeoGVT
42      disp(['Structure saved: configuration without PODs, "',figname,'"'])
43  elseif PODs==1 && WL==0
44      figname= 'Structures_GVTVIIPODSnoWL.mat';
45      save(['<input your directory>',figname], ...
46          'Geo','LocalEuler','LocalPos','Modal_damp','Modal_freq_Hz', ...
47          'Modal_freq','Modal_mass','R_coord_VE','RefPoint','Shapes', ...
48          'Scale','RefStructPoint','Modal_names','Symmetry'); % ShapesGVT, GeoGVT
49      disp(['Structure saved: configuration without PODs, "',figname,'"'])
50  elseif PODs==1 && WL==1
51      figname= 'Structures_GVTVIIPODSWL.mat';
52      save(['<input your directory>',figname], ...
53          'Geo','LocalEuler','LocalPos','Modal_damp','Modal_freq_Hz', ...
54          'Modal_freq','Modal_mass','R_coord_VE','RefPoint','Shapes', ...
55          'Scale','RefStructPoint','Modal_names','Symmetry'); % ShapesGVT, GeoGVT
56      disp(['Structure saved: configuration without PODs, "',figname,'"'])
57  end
```

C.1.1 InterpStreifenGVT.m

Listing C.2: InterpStreifenGVT.m

```
1  function [GeoTemp,Streifen,GVTRefPoint]=InterpStreifenGVT()
2  %% Load Data
3  % Streifen Data aus GVT
4  Streifen.wing = xlsread('GeoStreifenTest.xlsx',1); Streifen.wing(:,3:end)=
       Streifen.wing(:,3:end)/100;
5  Streifen.HE = xlsread('GeoStreifenTest.xlsx',2); Streifen.HE(:,3:end)=
       Streifen.HE(:,3:end)/100;
6  Streifen.VE = xlsread('GeoStreifenTest.xlsx',3); Streifen.VE(:,3:end)=
       Streifen.VE(:,3:end)/100;
7  Streifen.WL = xlsread('GeoStreifenTest.xlsx',4); Streifen.WL(:,3:end)=
       Streifen.WL(:,3:end)/100;
```

```
8  % Geometry aus FEM: 'Structures_S6T_FEM.mat'
9  load 'Geo.mat'
10 %% Feinheit der Streifen
11 WingFeinheit = 5;
12 WLFeinheit = WingFeinheit;
13 HEFeinheit = WingFeinheit;
14 VEFeinheit = WingFeinheit;
15 %
16 %% Fluegel
17 % Vorderkante und Hinterkante Vektoren
18 Vorderkante = max(Geo(1,1).wing); Vorderkante= Vorderkante(1,81:end); Vorderkante=
       [-2.3650 Vorderkante -2.7710];
19 Hinterkante = min(Geo(1,1).wing); Hinterkante= Hinterkante(1,81:end); Hinterkante=
       [-3.5093 Hinterkante -2.9160];
20 YKoord = Geo(1,2).wing(1,:); YKoord = YKoord(1,81:end); YKoord = [ 0 YKoord 8.9940];
21 i=length(Vorderkante); ZKoord(1:i) = -0.3160; % Z Dimension is defined in the file/drawn
       "Geometrie_S6_20110120_03.pdf"
22
23 % Streifen: fuer den Fluegel sind 65
24 % Streifen.wing(:,3) = Grenze
25 % Streifen.wing(:,4) = Abschnittsbreite
26 % Streifen.wing(:,5) = Abschinittsmitte
27 % Streifen.wing(:,6) = halbe Flaechentiefe
28 YKoordStreifen = Streifen.wing(33:end,5)';
29 VorderkanteStreifen = interp1(YKoord,Vorderkante,YKoordStreifen);
30 ZKoordStreifen = interp1(YKoord,ZKoord,YKoordStreifen);
31
32 %%%%%%%%%%%%%%%%%%%%
33 % halbe Flaechentiefe= c
34 %%%%%%%%%%%%%%%%%%%%
35 for count1=1:length(VorderkanteStreifen)
36     HinterkanteStreifen(count1) = -2*Streifen.wing(32+count1,6)' +
           VorderkanteStreifen(count1);
37     halbeFlachenTiefe(count1) = -1*Streifen.wing(32+count1,6)' +
           VorderkanteStreifen(count1);
38 end
39
40 for count1=1:length(YKoordStreifen)
41     TiefeStreifen = ...
42         linspace(VorderkanteStreifen(count1),HinterkanteStreifen(count1), ...
43         length(YKoordStreifen));
44     TffStreifen(count1,:) = ...
```

```
45          linspace(TiefeStreifen(1),TiefeStreifen(end),WingFeinheit);
46  end
47
48  Geo_grid(1,1).wing1 = [flipdim(TffStreifen',2) TffStreifen']; % x values
49  Geo_grid(1,2).wing1=zeros(WingFeinheit,length(Geo_grid(1,1).wing1)); % pre-alocate
50  Geo_grid(1,3).wing1=zeros(WingFeinheit,length(Geo_grid(1,1).wing1)); % pre-alocate
51
52  for count1=1:WingFeinheit
53      Geo_grid(1,2).wing1(count1,:) = [flipdim(-YKoordStreifen,2) YKoordStreifen]; % y values
54      Geo_grid(1,3).wing1(count1,:) = [flipdim(ZKoordStreifen,2) ZKoordStreifen]; % z values
55  end
56
57  %%%%%%
58  %GRIDs
59  %%%%%%
60  YKoordGrid = Streifen.wing(33:end,3)'; % Grid benutzt YKoord von der Grenze
61  ygrid = linspace(min(YKoordGrid),max(YKoordGrid),80);
62  xvor = interp1(YKoordGrid,VorderkanteStreifen,ygrid);
63  xhin = interp1(YKoordGrid,HinterkanteStreifen,ygrid); %HinterkanteStreifen2
64  zgrid = interp1(YKoordGrid,ZKoordStreifen,ygrid);
65
66  for count1=1:length(ygrid)
67      tiefe = linspace(xvor(count1),xhin(count1),length(ygrid));
68      tff(count1,:) = linspace(tiefe(1),tiefe(end),15);
69  end
70
71  % Organize in structures with all wing's geometrical data
72  Grid(1,1).wing = [flipdim(tff',2) tff']; % x values
73  Grid(1,2).wing=zeros(15,length(Grid(1,1).wing)); % pre-alocate
74  Grid(1,3).wing=zeros(15,length(Grid(1,1).wing)); % pre-alocate
75
76  for count1=1:15
77      Grid(1,2).wing(count1,:) = [flipdim(-ygrid,2) ygrid]; % y values
78      Grid(1,3).wing(count1,:) = [flipdim(zgrid,2) zgrid]; % z values
79  end
80
81
82  %% Wing let(s)
83  % Vorderkante und Hinterkante Vektoren
84  VorderkanteWL = -1*[2.562 2.807 3.047];
85  HinterkanteWL = -1*[2.949 3.147 3.293];
86
```

```
87  ZKoordWL = [8.994 8.994 8.994]; % in y Richtung
88  YKoordWL = −1∗[0.3160 0.5325 0.749]; % in z Richtung
89
90  % Streifen: fuer den Fluegel sind 65
91  % Streifen.wing(:,3) = Grenze
92  % Streifen.wing(:,4) = Abschnittsbreite
93  % Streifen.wing(:,5) = Abschinittsmitte
94  % Streifen.wing(:,6) = halbe Flaechentiefe
95  YKoordStreifenWL = Streifen.WL(:,5)'; YKoordStreifenWL = −1∗(YKoordStreifenWL+0.316);
96  VorderkanteStreifenWL = interp1(YKoordWL,VorderkanteWL,YKoordStreifenWL);
97  HinterkanteStreifen2WL = interp1(YKoordWL,HinterkanteWL,YKoordStreifenWL);
98  ZKoordStreifenWL = interp1(YKoordWL,ZKoordWL,YKoordStreifenWL);
99
100 % Save Geometry
101 for count1=1:length(YKoordStreifenWL)
102     TiefeStreifenWL = ...
103         linspace(VorderkanteStreifenWL(count1),HinterkanteStreifen2WL(count1), ...
104         length(YKoordStreifenWL));
105     TffStreifenWL(count1,:) = ...
106         linspace(TiefeStreifenWL(1),TiefeStreifenWL(end),WLFeinheit);
107 end
108
109 Geo_grid(1,1).WL1 = [flipdim(TffStreifenWL',2) TffStreifenWL']; % x values
110 for count1=1:WLFeinheit
111     % y values (that in fact are z)
112     Geo_grid(1,2).WL1(count1,:) = [flipdim(−YKoordStreifenWL,2) −YKoordStreifenWL];
113      % z values (that in fact are y)
114     Geo_grid(1,3).WL1(count1,:) = [flipdim(ZKoordStreifenWL,2) −ZKoordStreifenWL];
115 end
116
117 %%%%%%
118 %GRIDs
119 %%%%%%
120 YKoordGrid = Streifen.WL(:,3)'; YKoordGrid = −1∗(YKoordGrid+0.316); % Grid benutzt
        YKoord von der Grenze
121 ygrid = linspace(max(YKoordGrid),min(YKoordGrid),20);
122 xvor = interp1(YKoordGrid,VorderkanteStreifenWL,ygrid);
123 xhin = interp1(YKoordGrid,HinterkanteStreifen2WL,ygrid); %HinterkanteStreifen2
124 zgrid = interp1(YKoordGrid,ZKoordStreifenWL,ygrid);
125
126 clear 'tiefe'; clear 'tff';
127 for count1=1:length(ygrid)
```

```
128     tiefe = linspace(xvor(count1),xhin(count1),length(ygrid));
129     tff(count1,:) = linspace(tiefe(1),tiefe(end),15);
130 end
131
132 % Organize in structures with all wing's geometrical data
133 Grid(1,1).WL = [flipdim(tff',2) tff']; % x values
134 Grid(1,2).WL =zeros(15,length(Grid(1,1).WL)); % pre-alocate
135 Grid(1,3).WL =zeros(15,length(Grid(1,1).WL)); % pre-alocate
136
137 for count1=1:15
138     Grid(1,2).WL(count1,:) = [flipdim(-ygrid,2) -ygrid]; % y values
139     Grid(1,3).WL(count1,:) = [flipdim(zgrid,2) -zgrid]; % z values
140 end
141
142 %% Hoehenleitwerk
143
144 % Vorderkante und Hinterkante Vektoren
145 VorderkanteHE = max(Geo(1,1).HE); VorderkanteHE= VorderkanteHE(1,41:end);
        VorderkanteHE= ...
146     [-7.6990 VorderkanteHE -7.932]; % -7.923 ist ein extrapolierten Punkt
147 HinterkanteHE = min(Geo(1,1).HE); HinterkanteHE= HinterkanteHE(1,41:end);
        HinterkanteHE= ...
148     [-8.3290 HinterkanteHE -8.2562];
149 YKoordHE = Geo(1,2).HE(1,:); YKoordHE = [ 0 YKoordHE(1,41:end) 1.6231];
150 i=length(YKoordHE); ZKoordHE(1:i)= -1.564; % The value of z coordinate is
151 %the same for horizontal empennage. Following the project drawings the value of 1.564 is
        defined.
152
153 % Streifen fuer das Hoehenleitwerk sind 17
154 % Streifen.HE(:,3) = Grenze
155 % Streifen.HE(:,4) = Abschnittsbreite
156 % Streifen.HE(:,5) = Abschinittsmitte
157 % Streifen.HE(:,6) = halbe Flaechentiefe
158 YKoordStreifenHE = Streifen.HE(9:end,3)';
159 VorderkanteStreifenHE = interp1(YKoordHE,VorderkanteHE,YKoordStreifenHE);
160 ZKoordStreifenHE = interp1(YKoordHE,ZKoordHE,YKoordStreifenHE);
161
162 %%%%%%%%%%%%%%%%%%%%
163 % halbe Fl?chentiefe= c
164 %%%%%%%%%%%%%%%%%%%%
165 for count1=1:length(VorderkanteStreifenHE)
```

```
166     HinterkanteStreifenHE(count1)= -2*Streifen.HE(8+count1,6)' +
            VorderkanteStreifenHE(count1);
167     halbeFlachenTiefeHE(count1) = -Streifen.HE(8+count1,6)' +
            VorderkanteStreifenHE(count1);
168     % Differenz zwischen Hinterkante durch Interpolation oder mit der halbe Flaechentiefe
169 % diffHE(count1)= (HinterkanteStreifen2HE(count1)/HinterkanteStreifenHE(count1)-1)*100;
        % Werte in Prozent
170 end
171
172 for count1=1:length(YKoordStreifenHE)
173     TiefeStreifenHE = ...
174         linspace(VorderkanteStreifenHE(count1),HinterkanteStreifenHE(count1), ...
175         length(YKoordStreifenHE));
176     TffStreifenHE(count1,:) = ...
177         linspace(TiefeStreifenHE(1),TiefeStreifenHE(end),HEFeinheit);
178 end
179
180 Geo_grid(1,1).HE1 = [flipdim(TffStreifenHE',2) TffStreifenHE']; % x values
181 Geo_grid(1,2).HE1=zeros(HEFeinheit,length(Geo_grid(1,1).HE1)); % pre-alocate
182 Geo_grid(1,3).HE1=zeros(HEFeinheit,length(Geo_grid(1,1).HE1)); % pre-alocate
183 for count1=1:HEFeinheit
184     Geo_grid(1,2).HE1(count1,:) = [flipdim(-YKoordStreifenHE,2) YKoordStreifenHE]; % y
            values
185     Geo_grid(1,3).HE1(count1,:) = [flipdim(ZKoordStreifenHE,2) ZKoordStreifenHE]; % z
            values
186 end
187
188 %%%%%%
189 %GRIDs
190 %%%%%%
191 YKoordGrid = Streifen.HE(9:end,3)'; % Grid benutzt YKoord von der Grenze
192 ygridHE = linspace(min(YKoordGrid),max(YKoordGrid),40);
193 xvorHE = interp1(YKoordGrid,VorderkanteStreifenHE,ygridHE);
194 xhinHE = interp1(YKoordGrid,HinterkanteStreifenHE,ygridHE); % HinterkanteStreifen2HE
195 zgridHE = interp1(YKoordGrid,ZKoordStreifenHE,ygridHE);
196
197 clear 'tiefe'; clear 'tff';
198 for count1=1:length(ygridHE)
199     tiefe = linspace(xvorHE(count1),xhinHE(count1),length(ygridHE));
200     tff(count1,:) = linspace(tiefe(1),tiefe(end),15);
201 end
202
```

```
% Organize in structures with all HE's geometrical data
Grid(1,1).HE = [flipdim(tff',2) tff']; % x values
Grid(1,2).HE=zeros(15,length(Grid(1,1).HE)); % pre-alocate
Grid(1,3).HE=zeros(15,length(Grid(1,1).HE)); % pre-alocate

for count1=1:15
    Grid(1,2).HE(count1,:) = [flipdim(-ygridHE,2) ygridHE]; % y values
    Grid(1,3).HE(count1,:) = [flipdim(zgridHE,2) zgridHE]; % z values
end

%% Seitenleitwerk

% Vorderkante und Hinterkante Vektoren
VorderkanteVE = max(Geo(1,1).VE); % in x Richtung
HinterkanteVE = min(Geo(1,1).VE); % in x Richtung

YKoordVE = Geo(1,2).VE(1,:); % in z Richtung
i= length(YKoordVE); ZKoordVE(1:i) = 0; % in y Richtung

% Streifen: fuer den Fluegel sind 65
% Streifen.wing(:,3) = Grenze
% Streifen.wing(:,4) = Abschnittsbreite
% Streifen.wing(:,5) = Abschinittsmitte
% Streifen.wing(:,6) = halbe Flaechentiefe
YKoordStreifenVE = Streifen.VE(:,5)';
VorderkanteStreifenVE = interp1(YKoordVE,VorderkanteVE,YKoordStreifenVE);
ZKoordStreifenVE = interp1(YKoordVE,ZKoordVE,YKoordStreifenVE);

%%%%%%%%%%%%%%%%%%%%
% halbe Flaechentiefe= c
%%%%%%%%%%%%%%%%%%%%
for count1=1:length(VorderkanteStreifenVE)
    HinterkanteStreifenVE(count1)= -2*Streifen.VE(count1,6)' +
        VorderkanteStreifenVE(count1);
    halbeFlachenTiefeVE(count1) = -Streifen.VE(count1,6)' +
        VorderkanteStreifenVE(count1);
    % Differenz zwischen Hinterkante durch Interpolation oder mit der halbe Flaechentiefe
% diffHE(count1)= (HinterkanteStreifen2HE(count1)/HinterkanteStreifenHE(count1)-1)*100;
    % Werte in Prozent
end

for count1=1:length(YKoordStreifenVE)
```

```
242     TiefeStreifenVE = ...
243         linspace(VorderkanteStreifenVE(count1),HinterkanteStreifenVE(count1), ...
244         length(YKoordStreifenVE));
245     TffStreifenVE(count1,:) = ...
246         linspace(TiefeStreifenVE(1),TiefeStreifenVE(end),VEFeinheit);
247 end
248
249 Geo_grid(1,1).VE1 = [TffStreifenVE']; % x values
250 for count1=1:VEFeinheit
251     Geo_grid(1,2).VE1(count1,:) = YKoordStreifenVE; % y values (that in fact are z)
252     Geo_grid(1,3).VE1(count1,:) = ZKoordStreifenVE; % z values (that in fact are y)
253 end
254
255 %%%%%%%
256 % GRIDs
257 %%%%%%%
258 YKoordGrid = Streifen.VE(:,3)'; % Grid benutzt YKoord von der Grenze
259 ygridVE = linspace(min(YKoordGrid),max(YKoordGrid),80);
260 xvorVE = interp1(YKoordGrid,VorderkanteStreifenVE,ygridVE);
261 xhinVE = interp1(YKoordGrid,HinterkanteStreifenVE,ygridVE); % HinterkanteStreifen2VE
262 zgridVE = interp1(YKoordGrid,ZKoordStreifenVE,ygridVE);
263
264 clear 'tiefe'; clear 'tff';
265 for count1=1:length(ygridVE)
266     tiefe = linspace(xvorVE(count1),xhinVE(count1),length(ygridVE));
267     tff(count1,:) = linspace(tiefe(1),tiefe(end),15);
268 end
269
270 % Organize in structures with all VE's geometrical data
271 Grid(1,1).VE = tff'; % x values
272 Grid(1,2).VE=zeros(15,length(Grid(1,1).VE)); % pre-alocate
273 Grid(1,3).VE=zeros(15,length(Grid(1,1).VE)); % pre-alocate
274
275 for count1=1:15
276     Grid(1,2).VE(count1,:) = ygridVE; % y values
277     Grid(1,3).VE(count1,:) = zgridVE; % z values
278 end
279
280 %% Elastische Achse: EA 1/4*chord from leading edge point
281 % wing
282 for count1=1:length(VorderkanteStreifen) % Werte abspeichern
```

```
283     GVTRefPoint(1,1).wing(count1,:)= VorderkanteStreifen(count1) −
            (1/2)∗Streifen.wing(32+count1,6)';
284     GVTRefPoint(1,2).wing(count1,:)= YKoordStreifen(count1);
285 end
286 GVTRefPoint(1,3).wing = ZKoordStreifen;
287 %%% Ganze Fluegel organizieren
288 GVTRefPoint(1,1).wing= [flipdim(GVTRefPoint(1,1).wing',2)
        GVTRefPoint(1,1).wing(2:end,1)']; % x values
289 GVTRefPoint(1,2).wing= [flipdim(−GVTRefPoint(1,2).wing',2)
        GVTRefPoint(1,2).wing(2:end,1)']; % y values
290 GVTRefPoint(1,3).wing= [GVTRefPoint(1,3).wing GVTRefPoint(1,3).wing(1,2:end) ]; % z
        values
291
292 % Hoehenleitwerk
293 for count1=1:length(VorderkanteStreifenHE) % Werte abspeichern
294     GVTRefPoint(1,1).HE(count1,:)= VorderkanteStreifenHE(count1) −
            (1/2)∗Streifen.HE(8+count1,6)';
295     GVTRefPoint(1,2).HE(count1,:)= YKoordStreifenHE(count1);
296 end
297 GVTRefPoint(1,3).HE = ZKoordStreifenHE;
298 %%% Ganze Hoehenleitwerk organizieren
299 GVTRefPoint(1,1).HE= [flipdim(GVTRefPoint(1,1).HE',2) GVTRefPoint(1,1).HE(2:end,1)']; %
        x values
300 GVTRefPoint(1,2).HE= [flipdim(−GVTRefPoint(1,2).HE',2) GVTRefPoint(1,2).HE(2:end,1)'];
        % y values
301 GVTRefPoint(1,3).HE= [GVTRefPoint(1,3).HE GVTRefPoint(1,3).HE(1,2:end) ]; % z values
302
303 % WingLet
304 for count1=1:length(VorderkanteStreifenWL) % Werte abspeichern
305     GVTRefPoint(1,1).WL(count1,:)= VorderkanteStreifenWL(count1) −
            (1/2)∗Streifen.WL(count1,6)';
306     GVTRefPoint(1,2).WL(count1,:)= YKoordStreifenWL(count1);
307 end
308 GVTRefPoint(1,3).WL = ZKoordStreifenWL;
309 %%% Ganze WingLet organizieren
310 GVTRefPoint(1,1).WL= [flipdim(GVTRefPoint(1,1).WL',2) GVTRefPoint(1,1).WL']; % x values
311 GVTRefPoint(1,2).WL= [flipdim(GVTRefPoint(1,2).WL',2) GVTRefPoint(1,2).WL']; % z values
312 GVTRefPoint(1,3).WL= [GVTRefPoint(1,3).WL GVTRefPoint(1,3).WL]; % y values
313
314 % Seitenleitwerk
315 for count1=1:length(VorderkanteStreifenVE) % Werte abspeichern
```

```
316     GVTRefPoint(1,1).VE(count1,:)= VorderkanteStreifenVE(count1) −
            (1/2)∗Streifen.VE(count1,6)';
317     GVTRefPoint(1,2).VE(count1,:)= YKoordStreifenVE(count1);
318 end
319 GVTRefPoint(1,1).VE=GVTRefPoint(1,1).VE'; GVTRefPoint(1,2).VE=GVTRefPoint(1,2).VE;
320 GVTRefPoint(1,3).VE = ZKoordStreifenVE;
321
322 %% Output Definitions
323 %!!!!!!!!!!!!!!!!!!!!!!!!!!!!!!!!!!!!!!!!!!!!!!!!!!!!!!!!!!!!!!!!!!!!!!!!!!!
324 % Based on the comparison done with this routine the following consideration will be adopted:
325 %!!!!
326 % The geometry data that will be used to define the leading edge values is
327 % based on the middle point of every strip defined by the experimental
328 % procedure, GVT. It means that the x coordinates of the leading edge are equal
329 % the value of the trailing edge plus two times c.
330 %!!!!!!!!!!!!!!!!!!!!!!!!!!!!!!!!!!!!!!!!!!!!!!!!!!!!!!!!!!!!!!!!!!!!!!!!!!!
331
332 % STREIFEN
333 % wing
334 Streifen(1,1).wing = Geo_grid(1,1).wing1; Streifen(1,1).wing(:,33)=[];
335 Streifen(1,2).wing = Geo_grid(1,2).wing1; Streifen(1,2).wing(:,33)=[];
336 Streifen(1,3).wing = Geo_grid(1,3).wing1; Streifen(1,3).wing(:,33)=[];
337 % wing lets
338 Streifen(1,1).WL = Geo_grid(1,1).WL1;
339 Streifen(1,2).WL = −Geo_grid(1,2).WL1;
340 Streifen(1,3).WL = Geo_grid(1,3).WL1;
341 % right
342 Streifen(1,1).WL = flipdim(Geo_grid(1,1).WL1,2);
343 Streifen(1,2).WL = flipdim(−Geo_grid(1,2).WL1,2);
344 Streifen(1,3).WL = flipdim(Geo_grid(1,3).WL1,2);
345 % Horizontal empennage
346 Streifen(1,1).HE = Geo_grid(1,1).HE1; Streifen(1,1).HE(:,9) = [];
347 Streifen(1,2).HE = Geo_grid(1,2).HE1; Streifen(1,2).HE(:,9) = [];
348 Streifen(1,3).HE = Geo_grid(1,3).HE1; Streifen(1,3).HE(:,9) = [];
349 % Vertical empennage
350 Streifen(1,1).VE = Geo_grid(1,1).VE1;
351 Streifen(1,2).VE = −Geo_grid(1,2).VE1;
352 Streifen(1,3).VE = Geo_grid(1,3).VE1;
353
354 % GEOMETRY Geo in form of GRIDs
355 % wing
356 GeoTemp(1,1).wing = Grid(1,1).wing;
```

```
GeoTemp(1,2).wing = Grid(1,2).wing;
GeoTemp(1,3).wing = Grid(1,3).wing;
% wing lets
% left
GeoTemp(1,1).WL = Grid(1,1).WL;
GeoTemp(1,2).WL = -1*Grid(1,2).WL;
GeoTemp(1,3).WL = -1*Grid(1,3).WL;
% right
GeoTemp(1,1).WL(:,1:length(Grid(1,1).WL)/2) = Grid(1,1).WL(:,1:length(Grid(1,1).WL)/2);
GeoTemp(1,2).WL(:,1:length(Grid(1,1).WL)/2) = -Grid(1,2).WL(:,1:length(Grid(1,1).WL)/2);
GeoTemp(1,3).WL(:,1:length(Grid(1,1).WL)/2) =
    -1*flipdim(Grid(1,3).WL(:,1:length(Grid(1,1).WL)/2),2);
% Horizontal empennage
GeoTemp(1,1).HE = Grid(1,1).HE;
GeoTemp(1,2).HE = Grid(1,2).HE;
GeoTemp(1,3).HE = Grid(1,3).HE;
% Vertical empennage
GeoTemp(1,1).VE = Grid(1,1).VE;
GeoTemp(1,2).VE = -Grid(1,2).VE;
GeoTemp(1,3).VE = Grid(1,3).VE;

% % Correction Winglet: add a tiny displacement in z coordinates because if
% % wing let and wing have 90deg between each other the interpolation in
% % STRIPS DEFINITION doesn't work
dywl=0.01;%m
for count1=1:20
    GeoTemp(1,3).WL(:,20+count1) = GeoTemp(1,3).WL(:,20+count1)+(dywl/100)*count1;
end
GeoTemp(1,3).WL(:,1:20) = -flipdim(GeoTemp(1,3).WL(:,21:end),2);
end
```

C.1.2 ReadGVTData.m

Listing C.3: ReadGVTData.m

```
function
    [Shapes,Modal_damp,Modal_freq,Modal_freq_Hz,Modal_names,Symmetry,Modal_mass,Geo]=
    ...
    ReadGVTData(PODs,GeoTemp,Streifen,GVTRefPoint,WL)
if PODs==1
    % with PODs
    cd('<input your directory>');
```

```
elseif PODs==0
    % without PODs
    cd('<input your directory>');
end
%% Read the GVT Data
Names= dir; Names= Names(3:end);
for count1=1:length(Names)
    FileName(count1,:)= {Names(count1).name};
end
FileName= cell2mat(FileName);

Data= [];
for count1=1:length(FileName)
    fileToRead1= FileName(count1,:);

    DELIMITER = ' ';
    HEADERLINES = 103;

    % Import the file
    rawData1 = importdata(fileToRead1, DELIMITER, HEADERLINES);

    [~,name] = fileparts(fileToRead1);
    newData1.(genvarname(name)) = rawData1;

    % Create new variables in the base workspace from those fields.
    vars = fieldnames(newData1);
    for i = 1:length(vars)
        assignin('base', vars{i}, newData1.(vars{i}));
    end

    Data= [Data newData1.(vars{i})];
end
%% Sort out GVT Data
% Data= Data(6:end-1,:); % save only the displacements and rotations. With characteres
    the function cell2mat doesn't work
% Data= cell2mat(Data); % converts to mat variable
for count1=1:length(FileName)
    Modes(count1,1).name = Data{2,count1}(1:6);
    Modes(count1,1).GenMass = str2num(Data{2,count1}(10:19));
    Modes(count1,1).Freq = str2num(Data{2,count1}(30:38));
    Modes(count1,1).Damping = str2num(Data{2,count1}(20:29));
    i=0;
```

```
47      for count2=6:(length(Data)-1) % The first 6 lines have the mode names, frequency and
            gen. mass.
48          i=i+1;
49          Modes(count1,1).Data(i,1) = str2num(Data{count2,count1}(1:2));
50          Modes(count1,1).Data(i,2) = str2num(Data{count2,count1}(4:5));
51          Modes(count1,1).Data(i,3) = str2num(Data{count2,count1}(11:18));
52          Modes(count1,1).Data(i,4) = str2num(Data{count2,count1}(21:28));
53          Modes(count1,1).Data(i,5) = str2num(Data{count2,count1}(31:38));
54          Modes(count1,1).Data(i,6) = str2num(Data{count2,count1}(41:48));
55      end
56  end
57  % Sort values based on the frequency
58  Frequency = [Modes.Freq]; % create a vector with Frequency
59  [Value,Pos] = unique(Frequency); % sort the values and their position
60  Frequency = Value'; % Frequency vector
61  Modal_freq_Hz = Frequency; % Flexsim input name
62  Modal_freq = Modal_freq_Hz*2*pi;
63  Modal_damp = [Modes.Damping]'; % Modal damping
64  Modes(:,1) = Modes(Pos,1); % Sort the structure: Modes
65  FileName = FileName(Pos,:);
66  Modal_names = cellstr(FileName); % Variable Modal_names
67
68  for count1=1:length(FileName)
69      Modal_mass(count1,:) = Modes(count1).GenMass*1e-4; % Generalized Mass*1e-4:
            cm^2 to m^2
70      % Wing
71      ShapesStreifen1(count1,1).wing= Modes(count1,1).Data(1:65,3);% plunging
72      ShapesStreifen1(count1,2).wing= Modes(count1,1).Data(1:65,4);% pitching
73      ShapesStreifen1(count1,3).wing= Modes(count1,1).Data(1:65,5);% ---
74      ShapesStreifen1(count1,4).wing= Modes(count1,1).Data(1:65,6);% lagging
75      ShapesStreifen1(count1,5).wing= Modes(count1,1).name; % mode name
76      % Horizontal empennage
77      ShapesStreifen1(count1,1).HE = Modes(count1,1).Data(66:82,3);
78      ShapesStreifen1(count1,2).HE = Modes(count1,1).Data(66:82,4);
79      ShapesStreifen1(count1,3).HE = Modes(count1,1).Data(66:82,5);
80      ShapesStreifen1(count1,4).HE = Modes(count1,1).Data(66:82,6);
81      ShapesStreifen1(count1,5).HE= Modes(count1,1).name;
82      % Vertical empennage
83      ShapesStreifen1(count1,1).VE = Modes(count1,1).Data(83:91,3);
84      ShapesStreifen1(count1,2).VE = Modes(count1,1).Data(83:91,4);
85      ShapesStreifen1(count1,3).VE = Modes(count1,1).Data(83:91,5);
86      ShapesStreifen1(count1,4).VE = Modes(count1,1).Data(83:91,6);
```

```
87      ShapesStreifen1(count1,5).VE= Modes(count1,1).name;
88      % Wing let: 92 until 94 Winglet right and 95 until 97 wing let left
89      % Corrections in Position
90      ShapesStreifen1(count1,1).WL(1:3,:) =-flipdim(Modes(count1,1).Data(95:97,3),1); % left
91      ShapesStreifen1(count1,1).WL(4:6,:) =-flipdim(Modes(count1,1).Data(92:94,3),1); %
            right
92
93      ShapesStreifen1(count1,2).WL(1:3,:) = flipdim(Modes(count1,1).Data(95:97,4),1);
94      ShapesStreifen1(count1,2).WL(4:6,:) = flipdim(Modes(count1,1).Data(92:94,4),1);
95
96      ShapesStreifen1(count1,3).WL(1:3,:) = flipdim(Modes(count1,1).Data(95:97,5),1);
97      ShapesStreifen1(count1,3).WL(4:6,:) = flipdim(Modes(count1,1).Data(92:94,5),1);
98
99      ShapesStreifen1(count1,4).WL(1:3,:) = flipdim(Modes(count1,1).Data(95:97,6),1);
100     ShapesStreifen1(count1,4).WL(4:6,:) = flipdim(Modes(count1,1).Data(92:94,6),1);
101 end
102 %
103 %% DIMENSIONS: DISPLACEMENTS/VERSCHIEBUNG
104 % FaktConvert= 0.001; % mm to m
105 FaktConvert= 0.01; % cm to m
106 % FaktConvert= 0.1; % dc to m
107 for ne=1:length(FileName)
108     ShapesStreifen1(ne,1).wing=FaktConvert*ShapesStreifen1(ne,1).wing;
109     ShapesStreifen1(ne,4).wing=FaktConvert*ShapesStreifen1(ne,4).wing;
110     % PITCHING ANGLE THETA:
111 % ShapesStreifen1(ne,2).wing=0.1*ShapesStreifen1(ne,2).wing;
112     %
113     ShapesStreifen1(ne,1).HE=FaktConvert*ShapesStreifen1(ne,1).HE;
114     ShapesStreifen1(ne,4).HE=FaktConvert*ShapesStreifen1(ne,4).HE;
115     % PITCHING ANGLE THETA:
116 % ShapesStreifen1(ne,2).HE=0.1*ShapesStreifen1(ne,2).HE;
117     %
118     ShapesStreifen1(ne,1).VE=FaktConvert*ShapesStreifen1(ne,1).VE;
119     ShapesStreifen1(ne,4).VE=FaktConvert*ShapesStreifen1(ne,4).VE;
120     % PITCHING ANGLE THETA:
121 % ShapesStreifen1(ne,2).VE=0.1*ShapesStreifen1(ne,2).VE;
122     %
123     ShapesStreifen1(ne,1).WL=FaktConvert*ShapesStreifen1(ne,1).WL;
124     ShapesStreifen1(ne,4).WL=FaktConvert*ShapesStreifen1(ne,4).WL;
125     % PITCHING ANGLE THETA:
126 % ShapesStreifen1(ne,2).WL=0.1*ShapesStreifen1(ne,2).WL;
127 end
```

```
128 %% 2. INTERPOLATION (DREIECK) - DISPLACEMENTS FROM THE POINT TO THE
        STRIP LINE
129 %%% Inputs %%%
130     % StreifenPunkt = Floating Point throught the Strip;
131     % Theta angle - Verdreheung = ShapesStreifen1(1,2).XXX
132     % Measured point = GVTRefPoint.XXX
133     % dx_EA,dy_EA,dz_EA = ShapesStreifen1(1,1).XXX, ShapesStreifen1(1,2).XXX,
            ShapesStreifen1(1,3).XXX
134 % ShapesStreifen1(~,1).XXXX = PLUNGING
135 % ShapesStreifen1(~,2).XXXX = PITCHING
136 % ShapesStreifen1(~,3).XXXX = NO VALUES
137 % ShapesStreifen1(~,4).XXXX = LAGGING
138 [lineStreifenWing,~] = size(Streifen(1,1).wing);
139 for modeNum=1:length(ShapesStreifen1) % mode number
140     for stripNum=1:length(GVTRefPoint(1,1).wing) % strip number
141         % Wing
142         for pointNum=1:lineStreifenWing % Points through the chord at each strip
143             % SCALENE TRIANGLE
144             % [SILVESTRE,2012 - Methodology..., Page 57] "Observe that just
145             % the modal shape?s component perpendicular to the lifting surface,
146             % thus the only component considered in the incremental aerodynamic model, is
                    displayed."
147             StreifenPunkt= Streifen(1,1).wing(pointNum,stripNum);
148             % HIPOTENUSA. side of triangle = length of the elastic axe in x direction
149             c= StreifenPunkt-GVTRefPoint(1,1).wing(1,stripNum);
150             % displacement in z direction = height of the scalene triangle.
151             dzp1d = c*sin(ShapesStreifen1(modeNum,2).wing(stripNum,1));
152             %
153             % Allocate the displacements at each strip point for each modal form
154             ShapesStreifen2(modeNum,1).wing(pointNum,stripNum)= ...
155                 ShapesStreifen1(modeNum,4).wing(stripNum,1); %+ dxp1d; % point
                        displacement + gvt displacement
156             ShapesStreifen2(modeNum,2).wing(pointNum,stripNum)= ...
157                 0; % there's no displacement in y direction
158             ShapesStreifen2(modeNum,3).wing(pointNum,stripNum)= ...
159                 ShapesStreifen1(modeNum,1).wing(stripNum,1) + dzp1d; % point
                        displacement + gvt displacement
160         end
161     end
162         % HE
163     [lineStreifenHE,~] = size(Streifen(1,1).HE);
164     for stripNum=1:length(GVTRefPoint(1,1).HE) % number of strips
```

```
165         for pointNum=1:lineStreifenHE;
166             % SCALENE TRIANGLE
167             StreifenPunkt= Streifen(1,1).HE(pointNum,stripNum);
168             % side of triangle = length of the elastic axe in x direction
169             c= StreifenPunkt−GVTRefPoint(1,1).HE(1,stripNum);
170             % displacement in z direction = height of the scalene triangle.
171             dzp1d = c∗sin(ShapesStreifen1(modeNum,2).HE(stripNum,1));
172 % dxp1d = dzp1d∗tan(ShapesStreifen1(modeNum,2).HE(stripNum,1)); % displacement in x
      direction
173             % saving the displacements at each strip point for each modal form
174             ShapesStreifen2(modeNum,1).HE(pointNum,stripNum)= ...
175                 ShapesStreifen1(modeNum,4).HE(stripNum,1);% + dxp1d; % point
                        displacement + gvt displacement
176             ShapesStreifen2(modeNum,2).HE(pointNum,stripNum)= ...
177                 0; % there's no displacement in y direction
178             ShapesStreifen2(modeNum,3).HE(pointNum,stripNum)= ...
179                 ShapesStreifen1(modeNum,1).HE(stripNum,1) + dzp1d; % point
                        displacement + gvt displacement
180         end
181     end
182         % WL
183     [lineStreifenWL,~] = size(Streifen(1,1).WL);
184     for stripNum=1:length(GVTRefPoint(1,1).WL) % number of strips
185         for pointNum=1:lineStreifenWL
186             % SCALENE TRIANGLE
187             StreifenPunkt= Streifen(1,1).WL(pointNum,stripNum);
188             % side of triangle = length of the elastic axe in x direction
189             c= StreifenPunkt−GVTRefPoint(1,1).WL(1,stripNum);
190             % displacement in z direction = height of the scalene triangle.
191             dzp1d = c∗sin(ShapesStreifen1(modeNum,2).WL(stripNum,1));
192 % dxp1d = dzp1d∗tan(ShapesStreifen1(modeNum,2).WL(stripNum,1)); % displacement in x
      direction
193             % saving the displacements at each strip point for each modal form
194             ShapesStreifen2(modeNum,1).WL(pointNum,stripNum)= ...
195                 ShapesStreifen1(modeNum,4).WL(stripNum,1); %+ dxp1d; % point
                        displacement + gvt displacement
196             ShapesStreifen2(modeNum,2).WL(pointNum,stripNum)= ...
197                 0; % there's no displacement in y direction
198             ShapesStreifen2(modeNum,3).WL(pointNum,stripNum)= ...
199                 ShapesStreifen1(modeNum,1).WL(stripNum,1) + dzp1d; % point
                        displacement + gvt displacement
200         end
```

```
201     end
202         % VE
203     [lineStreifenVE,~] = size(Streifen(1,1).VE);
204     for stripNum=1:length(GVTRefPoint(1,1).VE) % number of strips
205             for pointNum=1:lineStreifenVE
206             % SCALENE TRIANGLE
207             StreifenPunkt= Streifen(1,1).VE(pointNum,stripNum);
208             % side of triangle = length of the elastic axe in x direction
209             c= StreifenPunkt−GVTRefPoint(1,1).VE(1,stripNum);
210             % displacement in z direction = height of the scalene triangle.
211             dzp1d = c∗sin(ShapesStreifen1(modeNum,2).VE(stripNum,1));
212             ShapesStreifen2(modeNum,1).VE(pointNum,stripNum)=
                    ShapesStreifen1(modeNum,4).VE(stripNum,1);% + dxp1d; % point
                    displacement + gvt displacement
213             ShapesStreifen2(modeNum,2).VE(pointNum,stripNum)= 0; % there's no
                    displacement in y direction
214             ShapesStreifen2(modeNum,3).VE(pointNum,stripNum)=
                    ShapesStreifen1(modeNum,1).VE(stripNum,1) + dzp1d; % point
                    displacement + gvt displacement
215             end
216     end
217
218 % % Correction in WL Displacements
219     ShapesStreifen2(modeNum,3).WL(:,1:3)= ShapesStreifen2(modeNum,3).WL(:,1:3);
220     ShapesStreifen2(modeNum,3).WL(:,4:6)=
            flipdim(ShapesStreifen2(modeNum,3).WL(:,4:6),2);
221 end
222 %% PLOT RESULTS INTERPOLATION 2
223 % ABC=1;
224 % % faktor=20;
225 % % for m=1:6 % mode number
226 % % Geometry
227 % surf(Streifen(1,1).wing, Streifen(1,2).wing, −Streifen(1,3).wing); hold on;
228 % surf(Streifen(1,1).HE, Streifen(1,2).HE, −Streifen(1,3).HE);
229 % surf(Streifen(1,1).VE, Streifen(1,3).VE, −Streifen(1,2).VE); alpha(0.0);
230 % % Modes
231 % surf(Streifen(1,1).wing + faktor∗ShapesStreifen2(m,1).wing, ...
232 % Streifen(1,2).wing, − Streifen(1,3).wing + faktor∗ShapesStreifen2(m,3).wing); hold on
233 % surf(Streifen(1,1).HE + faktor∗ShapesStreifen2(m,1).HE, ...
234 % Streifen(1,2).HE, − Streifen(1,3).HE + faktor∗ShapesStreifen2(m,3).HE);
235 % %
236 % surf(Streifen(1,1).VE + faktor∗ShapesStreifen2(m,1).VE, ...
```

```
237 % Streifen(1,3).VE + faktor*ShapesStreifen2(m,3).VE, -Streifen(1,2).VE);
238 % axis equal; grid on;
239 % xlabel 'x';ylabel 'y';zlabel 'z'; view(130,30);
240 % % end
241 %% 3. INTERPOLATION (GRIDDATA)
242 % Interpolations Function
243 % F.dxgrid = griddata(F.x , F.y , F.dx , F.xgrid , F.ygrid ,'v4')
244 % F.x, F.y and F.z must have the same size
245 %%%%% DATA
246 % F.x = Streifen(1,1).XXX % F.y = Streifen(1,2).XXX
247 % F.xgrid = Geo(1,1).XXX % F.ygrid = Geo(1,2).XXX
248 % F.dx = ShapesStreifen2(1,X).XXX
249 for modeNum=1:length(FileName)
250         % wing
251     ShapesTemp(modeNum,1).wing = griddata(Streifen(1,1).wing, Streifen(1,2).wing,
            ShapesStreifen2(modeNum,1).wing, GeoTemp(:,1).wing, GeoTemp(:,2).wing,'v4'); %
            x and y
252     ShapesTemp(modeNum,2).wing = griddata(Streifen(1,1).wing, Streifen(1,2).wing,
            ShapesStreifen2(modeNum,2).wing, GeoTemp(:,1).wing, GeoTemp(:,2).wing,'v4'); %
            y and z
253     ShapesTemp(modeNum,3).wing = griddata(Streifen(1,1).wing, Streifen(1,2).wing,
            ShapesStreifen2(modeNum,3).wing, GeoTemp(:,1).wing, GeoTemp(:,2).wing,'v4'); %
            z and y
254     % HE
255     ShapesTemp(modeNum,1).HE = griddata(Streifen(1,1).HE, Streifen(1,2).HE,
            ShapesStreifen2(modeNum,1).HE, GeoTemp(:,1).HE, GeoTemp(:,2).HE,'v4'); % x
            and y
256     ShapesTemp(modeNum,2).HE = griddata(Streifen(1,1).HE, Streifen(1,2).HE,
            ShapesStreifen2(modeNum,2).HE, GeoTemp(:,1).HE, GeoTemp(:,2).HE,'v4'); % y
            and z
257     ShapesTemp(modeNum,3).HE = griddata(Streifen(1,1).HE, Streifen(1,2).HE,
            ShapesStreifen2(modeNum,3).HE, GeoTemp(:,1).HE, GeoTemp(:,2).HE,'v4'); % z
            and y
258     % VE
259     ShapesTemp(modeNum,1).VE = griddata(Streifen(1,1).VE, Streifen(1,2).VE,
            ShapesStreifen2(modeNum,1).VE, GeoTemp(:,1).VE, GeoTemp(:,2).VE,'v4'); % x
            and y
260     ShapesTemp(modeNum,2).VE = griddata(Streifen(1,1).VE, Streifen(1,2).VE,
            ShapesStreifen2(modeNum,3).VE, GeoTemp(:,1).VE, GeoTemp(:,2).VE,'v4'); % y
            and z
261     ShapesTemp(modeNum,3).VE = griddata(Streifen(1,1).VE, Streifen(1,2).VE,
            ShapesStreifen2(modeNum,2).VE, GeoTemp(:,1).VE, GeoTemp(:,2).VE,'v4'); % z
```

```
        and y
% ShapesTemp(modeNum,1).VE = griddata(Streifen(1,1).VE, Streifen(1,2).VE,
    ShapesStreifen2(modeNum,1).VE, GeoTemp(:,1).VE, GeoTemp(:,2).VE,'v4'); % x and y
% ShapesTemp(modeNum,2).VE = griddata(Streifen(1,1).VE, Streifen(1,2).VE,
    ShapesStreifen2(modeNum,2).VE, GeoTemp(:,1).VE, GeoTemp(:,2).VE,'v4'); % y and z
% ShapesTemp(modeNum,3).VE = griddata(Streifen(1,1).VE, Streifen(1,2).VE,
    ShapesStreifen2(modeNum,3).VE, GeoTemp(:,1).VE, GeoTemp(:,2).VE,'v4'); % z and y

    % Wing let right
    ShapesTemp(modeNum,1).WLr = griddata(Streifen(1,1).WL(:,1:3),
        Streifen(1,2).WL(:,1:3), ShapesStreifen2(modeNum,1).WL(:,1:3),
        GeoTemp(:,1).WL(:,1:20), GeoTemp(:,2).WL(:,1:20),'v4'); % x and y
    ShapesTemp(modeNum,2).WLr = griddata(Streifen(1,1).WL(:,1:3),
        Streifen(1,2).WL(:,1:3), ShapesStreifen2(modeNum,3).WL(:,1:3),
        GeoTemp(:,1).WL(:,1:20), GeoTemp(:,2).WL(:,1:20),'v4'); % y and z
    ShapesTemp(modeNum,3).WLr = griddata(Streifen(1,1).WL(:,1:3),
        Streifen(1,2).WL(:,1:3), ShapesStreifen2(modeNum,2).WL(:,1:3),
        GeoTemp(:,1).WL(:,1:20), GeoTemp(:,2).WL(:,1:20),'v4'); % z and y
    % wing let left % (:,3).WL = Fx,Fz,dz,Fxgrid,Fzgrid
    ShapesTemp(modeNum,1).WLl = griddata(Streifen(1,1).WL(:,4:6),
        Streifen(1,2).WL(:,4:6), ShapesStreifen2(modeNum,1).WL(:,4:6),
        GeoTemp(:,1).WL(:,21:40), GeoTemp(:,2).WL(:,21:40),'v4'); % x and y
    ShapesTemp(modeNum,2).WLl = griddata(Streifen(1,1).WL(:,4:6),
        Streifen(1,2).WL(:,4:6), ShapesStreifen2(modeNum,3).WL(:,4:6),
        GeoTemp(:,1).WL(:,21:40), GeoTemp(:,2).WL(:,21:40),'v4'); % y and z
    ShapesTemp(modeNum,3).WLl = griddata(Streifen(1,1).WL(:,4:6),
        Streifen(1,2).WL(:,4:6), ShapesStreifen2(modeNum,2).WL(:,4:6),
        GeoTemp(:,1).WL(:,21:40), GeoTemp(:,2).WL(:,21:40),'v4'); % z and y

end
%% Verbindung vom Fluegel und Wing Let
if WL==1
    for count1=1:length(FileName) % number of modes
        % WingLet: Letzte Streifen rechts und erste Streifen links
        for count2=1:length(ShapesTemp(1,1).WLr)
            % x direction
            ShapesTemp(count1,1).WLr(:,count2) = ShapesTemp(count1,1).WLr(:,count2) +
                ShapesTemp(count1,1).wing(:,1);
            ShapesTemp(count1,1).WLl(:,count2) = ShapesTemp(count1,1).WLl(:,count2) +
                ShapesTemp(count1,1).wing(:,end);
            % z direction
```

```
285             ShapesTemp(count1,3).WLr(:,count2) = ShapesTemp(count1,3).WLr(:,count2) +
                    ShapesTemp(count1,3).wing(:,1);
286             ShapesTemp(count1,3).WLl(:,count2) = ShapesTemp(count1,3).WLl(:,count2) +
                    ShapesTemp(count1,3).wing(:,end);
287         end
288         % y direction
289         ShapesTemp(count1,2).wing(:,1) = ShapesTemp(count1,2).WLr(:,20) +
                ShapesTemp(count1,2).wing(:,1);
290         ShapesTemp(count1,2).wing(:,end) = ShapesTemp(count1,2).WLl(:, 1) +
                ShapesTemp(count1,2).wing(:,end);
291         % Corrections
292         if PODs==0 && count1==4 % mode 4, configuration with PODs
293             ShapesTemp(count1,2).wing(:,2)= ShapesTemp(count1,2).WLr(:,20) +
                    ShapesTemp(count1,2).wing(:,2);
294         end
295     end
296 end
297 %% Output Definitions
298 % Variable Symmetry
299 if PODs==0
300     Symmetry= {'symmetric'; 'anti-symmetric';'anti-symmetric';'symmetric'; ...
301         'anti-symmetric';'symmetric';'anti-symmetric';'symmetric';...
302         'anti-symmetric';'anti-symmetric'; 'symmetric';'symmetric'; ...
303         'anti-symmetric';'anti-symmetric'; 'symmetric';'symmetric';...
304         'anti-symmetric';'symmetric';'anti-symmetric';'anti-symmetric'; ...
305         'symmetric';'symmetric'};
306 elseif PODs==1
307     Symmetry= {'anty-symmetric';'symmetric';'anty-symmetric';'anty-symmetric'; ...
308         'anty-symmetric'; 'anty-symmetric';'anty-symmetric';'symmetric';...
309         'anty-symmetric';'anty-symmetric'; 'anty-symmetric';'anty-symmetric'; ...
310         'anty-symmetric';'anty-symmetric';'anty-symmetric'; 'anty-symmetric'; ...
311         'anty-symmetric';'symmetric';'anty-symmetric';'symmetric';'anty-symmetric';...
312         'anty-symmetric';'symmetric';'anty-symmetric';'symmetric';'symmetric'; ...
313         'anty-symmetric'; 'anty-symmetric';'symmetric';};
314 end
315
316 if WL==1
317     % Geo: saving wing and WL together
318     Geo(1,1).wing= [GeoTemp(1,1).WL(:,1:20) GeoTemp(1,1).wing
            GeoTemp(1,1).WL(:,21:end)]; Geo(1,1).wing(:,100)=[];
319     Geo(1,2).wing= [GeoTemp(1,3).WL(:,1:20) GeoTemp(1,2).wing
            GeoTemp(1,3).WL(:,21:end)]; Geo(1,2).wing(:,100)=[];
```

```
320     Geo(1,3).wing= [GeoTemp(1,2).WL(:,1:20) GeoTemp(1,3).wing
            GeoTemp(1,2).WL(:,21:end)]; Geo(1,3).wing(:,100)=[];
321     Geo(1,1).HE= GeoTemp(1,1).HE; Geo(1,1).HE(:,40)= [];
322     Geo(1,2).HE= GeoTemp(1,2).HE; Geo(1,2).HE(:,40)= [];
323     Geo(1,3).HE= GeoTemp(1,3).HE; Geo(1,3).HE(:,40)= [];
324     Geo(1,1).VE= GeoTemp(1,1).VE;
325     Geo(1,2).VE= -GeoTemp(1,2).VE;
326     Geo(1,3).VE= GeoTemp(1,3).VE;
327 elseif WL==0
328     % without wing let
329     Geo(1,1).wing= GeoTemp(1,1).wing; Geo(1,1).wing(:,80)=[];
330     Geo(1,2).wing= GeoTemp(1,2).wing; Geo(1,2).wing(:,80)=[];
331     Geo(1,3).wing= GeoTemp(1,3).wing; Geo(1,3).wing(:,80)=[];
332     Geo(1,1).HE= GeoTemp(1,1).HE; Geo(1,1).HE(:,40)= [];
333     Geo(1,2).HE= GeoTemp(1,2).HE; Geo(1,2).HE(:,40)= [];
334     Geo(1,3).HE= GeoTemp(1,3).HE; Geo(1,3).HE(:,40)= [];
335     Geo(1,1).VE= GeoTemp(1,1).VE;
336     Geo(1,2).VE= -GeoTemp(1,2).VE;
337     Geo(1,3).VE= GeoTemp(1,3).VE;
338 end
339 % Shapes: saving wing and WL together
340 for count1=1:length(FileName)
341     if WL==1
342         Shapes(count1,1).wing= [ShapesTemp(count1,1).WLr ShapesTemp(count1,1).wing
                ShapesTemp(count1,1).WLl];
343         Shapes(count1,2).wing= [ShapesTemp(count1,2).WLr ShapesTemp(count1,2).wing
                ShapesTemp(count1,2).WLl];
344         Shapes(count1,3).wing= [ShapesTemp(count1,3).WLr ShapesTemp(count1,3).wing
                ShapesTemp(count1,3).WLl];
345         Shapes(count1,1).HE = ShapesTemp(count1,1).HE;
346         Shapes(count1,2).HE = ShapesTemp(count1,2).HE;
347         Shapes(count1,3).HE = ShapesTemp(count1,3).HE;
348         Shapes(count1,1).VE = ShapesTemp(count1,1).VE;
349         Shapes(count1,2).VE = ShapesTemp(count1,3).VE;
350         Shapes(count1,3).VE = ShapesTemp(count1,2).VE;
351     elseif WL==0
352         % without winglet
353         Shapes(count1,1).wing= ShapesTemp(count1,1).wing;
354         Shapes(count1,2).wing= ShapesTemp(count1,2).wing;
355         Shapes(count1,3).wing= ShapesTemp(count1,3).wing;
356         Shapes(count1,1).HE = ShapesTemp(count1,1).HE;
357         Shapes(count1,2).HE = ShapesTemp(count1,2).HE;
```

```
358             Shapes(count1,3).HE = ShapesTemp(count1,3).HE;
359             Shapes(count1,1).VE = ShapesTemp(count1,1).VE;
360             Shapes(count1,2).VE = ShapesTemp(count1,3).VE;
361             Shapes(count1,3).VE = ShapesTemp(count1,2).VE;
362         end
363         % corrections in doubled strips
364         Shapes(count1,1).wing(:,100)= [];
365         Shapes(count1,2).wing(:,100)= [];
366         Shapes(count1,3).wing(:,100)= [];
367         Shapes(count1,1).HE(:,40) = [];
368         Shapes(count1,2).HE(:,40) = [];
369         Shapes(count1,3).HE(:,40) = [];
370     end
371 end
```

C.2 pitch_damper.m

Figure 82: Open loop block diagram implemented in MATLAB® Simulink.

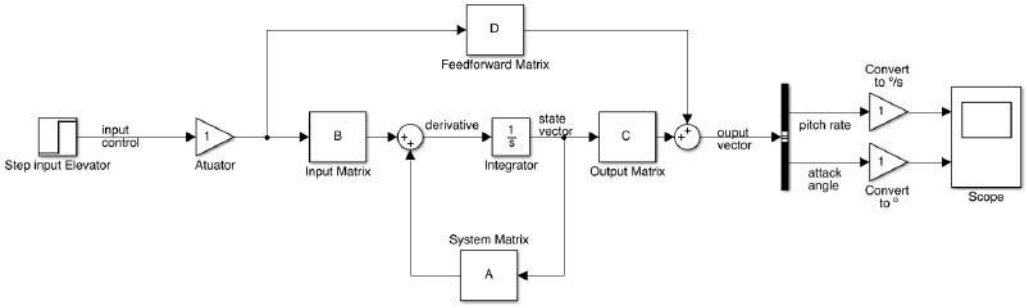

Source: Author.

Figure 83: Closed loop block diagram implemented in MATLAB® Simulink.

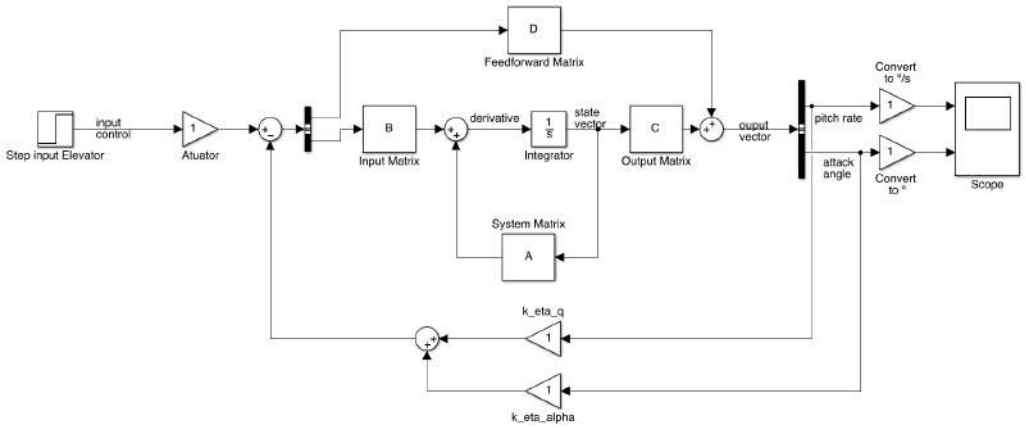

Source: Author.

Listing C.4: pitch_damper.m

```
1  %%%%%%%%%%%%%%%%%%%%%%%%%%%%%%%%%%%%%%%%%%%%%%%%%%%%%%%%%%%%%%%%%%%%%%%%%%%%
2  % % PITCH DAMPER DESIGN %
3  %%%%%%%%%%%%%%%%%%%%%%%%%%%%%%%%%%%%%%%%%%%%%%%%%%%%%%%%%%%%%%%%%%%%%%%%%%%%
4  close all; clear all; clc;
5  % pfad= 'insert your directory here';
6  %%%%%%%%%%%%%%%%%%%%%%%%%%%%%%%%%%%%%%%%%%%%%%%%%%%%%%%%%%%%%%%%%%%%%%%%%%%%
7  % FROM FLEXSIM
8  % STATE VARIABLES
9  % x= [
10 % V
11 % Theta
12 % q
```

```
% alpha
% H
% beta
% p
% phi
% r
% ]
%
% Control Variables
% u = [
% Shub = eta_F
% Querruder = xi
% Fluegelklappen = eta_k
% Hoehenruder = eta
% Seitenruder = zeta
% ]
%%%%%%%%%%%%%%%%%%%%%%%%%%%%%%%%%%%%%%%%%%%%%%%%%%%%%%%%%%%%%%%%%%%%%%%%%%%%
% % MODELS %
%%%%%%%%%%%%%%%%%%%%%%%%%%%%%%%%%%%%%%%%%%%%%%%%%%%%%%%%%%%%%%%%%%%%%%%%%%%%
% Model=1; % model 1 = LCSv8
% Model=2; % model 2 = ohne PODs korrigiert
% Model=3; % model 3 = ohne PODs
% Model=4; % model 4 = mit PODs korrigiert
Model=5; % model 5 = mit PODs
%%%%%%%%%%%%%%%%%%%%%%%%%%%%%%%%%%%%%%%%%%%%%%%%%%%%%%%%%%%%%%%%%%%%%%%%%%%%
if Model==1 % LCSv8 elev 1deg
    state_space_name_rigid = 'State_space_rigid_lcsv8_elev1deg.mat'; % rigid
    state_space_name_flex = 'State_space_flex_lcsv8_elev1deg.mat'; % flex
    disp(['Model Nr.: ', Model])
    disp(['Modelo rigido: ',state_space_name_rigid])
    disp(['Modelo elastico: ',state_space_name_flex])
elseif Model==2 % ECARY ES15 ohne PODs korrigiert
    state_space_name_rigid = 'State_space_rigid_noPODsnoWL_elev1deg_corriged.mat';
        % rigid
    state_space_name_flex = 'State_space_flex_noPODsnoWL_elev1deg_corriged.mat'; %
        flex
    disp(['Model Nr.: ',Model])
    disp(['Modelo rigido: ',state_space_name_rigid])
    disp(['Modelo elastico: ',state_space_name_flex])
elseif Model==3 % ECARY ES15 ohne PODs
    state_space_name_rigid = 'State_space_rigid_noPODsnoWL_elev1deg.mat'; % rigid
    state_space_name_flex = 'State_space_flex_noPODsnoWL_elev1deg.mat'; % flex
```

```
53      disp(['Model Nr.: ',Model])
54      disp(['Modelo rigido: ',state_space_name_rigid])
55      disp(['Modelo elastico: ',state_space_name_flex])
56  %elseif Model==4
57  % state_space_name_rigid = 'State_space_rigid_noPODsnoWL_elev1deg.mat'; % rigid
58  % state_space_name_flex = 'State_space_flex_noPODsnoWL_elev1deg.mat'; % flex
59  % disp(['Model Nr.: ',Model])
60  % disp(['Modelo rigido: ',state_space_name_rigid])
61  % disp(['Modelo elastico: ',state_space_name_flex])
62  elseif Model==5
63      state_space_name_rigid = 'State_space_rigid_PODsnoWL_elev1deg.mat'; % rigid
64      state_space_name_flex = 'State_space_flex_PODsnoWL_elev1deg.mat'; % flex
65      disp(['Model Nr.: ',Model])
66      disp(['Modelo rigido: ',state_space_name_rigid])
67      disp(['Modelo elastico: ',state_space_name_flex])
68  end
69  %%%%%%%%%%%%%%%%%%%%%%%%%%%%%%%%%%%%%%%%%%%%%%%%%%%%%%%%%%%%%%%%%%%%%%%%%%%%
70  %% LOAD SYSTEM MATRICES
71  %%%%%%%%%%%%%%%%%%%%%%%%%%%%%%%%%%%%%%%%%%%%%%%%%%%%%%%%%%%%%%%%%%%%%%%%%%%%
72  % Load System Matrices
73  %state_space_name = 'State_space_rigid_lcsv8_elev1deg'; % rigid
74  load([pfad,state_space_name_rigid])
75  %
76  % System Matrix A
77  temp= Lin_Model(1,1);
78  A= cell2mat(temp);
79  % System Matrix B
80  temp= Lin_Model(1,2);
81  B= cell2mat(temp);
82  % System Matrix C
83  C=eye(length(A));
84  % System Matrix D
85  [m,n]= size(B);
86  D=zeros(m,n);
87  %% FULL RIGIB BODY (RB) AIRCRAFT
88  % State-space system
89  SS_rigid=ss(A,B,C,D);
90  % pzmap
91  f11=figure();
92  pzmap(SS_rigid); legend 'FULL RIGIB BODY (RB) AIRCRAFT'; grid on;
93  % System Characteristics
94  [wn_RB,D_RB,poles_RB]=damp(SS_rigid);
```

```
95  %% RB LONGITUDINAL MOTION APPROXIMATION (LB)
96  A_LB(1,:)= A(1,1:4); % Geschwindigkeit
97  A_LB(2,:)= A(2,1:4); % Theta
98  A_LB(3,:)= A(3,1:4); % q
99  A_LB(4,:)= A(4,1:4); % alpha
100 %
101 B_LB(1:4,1)= B(1:4,1); % Shub
102 B_LB(1:4,2)= B(1:4,4); % Hoehenruder
103 %
104 C_LB= eye(4,4);
105 D_LB= zeros(4,2);
106 % State Space Model
107 SS_LB_rigid = ss(A_LB,B_LB,C_LB,D_LB);
108 % Transfer Function
109 TF_LB_rigid = tf(SS_LB_rigid);
110 % TFs: Input 1= eta_f
111 % Input 2= eta
112         %
113 % Output1= q
114 % Output2= a = Alpha
115 % Output3= V
116 % Output4= t = theta
117 % eta
118 F_q_eta = TF_LB_rigid(3,2);
119 F_a_eta = TF_LB_rigid(4,2);
120 F_V_eta = TF_LB_rigid(1,2);
121 F_t_eta = TF_LB_rigid(2,2);
122 %
123 % Characteristische Polynom ableiten
124 Charpol_LB = poly(A_LB);
125 % Pollstellen: 1 und 2= Phugoid (PH) (V und Theta)
126 % 3 und 4= Anstelwinkelschwingung (AS) (q und Alpha)
127 pole_LB = roots(Charpol_LB);
128 % PN-Diagramm
129 f2=figure();
130 pzmap(SS_LB_rigid); grid on; legend(' RB Longitudinal Motion Aproximation')
131 %
132 % Natural Frequency and Damping
133 % [Wn,zeta] = damp(sys). Wn = vector with natural frequencies
134 % Zeta = vector with damping ratios
135 [wn_RB_LB,D_RB_LB,P_LB_RB] = damp(SS_LB_rigid);
136 nfFreqAS = wn_RB_LB(3);
```

```
dampAS = D_RB_LB(3);
%
%%%%%%%%%%%%%%%%%%%%%%%%%%%%%%%%%%%%%%%%%%%%%%%%
%%      SHORT PERIOD APPROXIMATION      %
%%%%%%%%%%%%%%%%%%%%%%%%%%%%%%%%%%%%%%%%%%%%%%%%
A_LB_AS(1,1:2)= A_LB(3,3:4);
A_LB_AS(2,1:2)= A_LB(4,3:4);
B_LB_AS = B_LB(3:4,2);
C_LB_AS = eye(size(A_LB_AS));
D_LB_AS = zeros(size(B_LB_AS));
% State-space
SS_LB_AS_Rigid = ss(A_LB_AS,B_LB_AS,C_LB_AS,D_LB_AS);
% Transfer Functions
TF_LB_AS_Rigid = tf(SS_LB_AS_Rigid);
% eta x q
F_q_eta_AS_rigid = TF_LB_AS_Rigid(1);
F_alpha_AS_rigid = TF_LB_AS_Rigid(2);
% step(F_q_eta,'b',F_q_eta_AS_rigid,'r'); % compare the Short period
% approximation
%%%%%%%%%%%%%%%%%%%%%%%%%%%%%%%%%%%%%%%%%%%%%%%%
%%        STEUERBARKEIT        %
%%%%%%%%%%%%%%%%%%%%%%%%%%%%%%%%%%%%%%%%%%%%%%%%
%
Q_S = [B_LB_AS, A_LB_AS*B_LB_AS];
Steuerbarkeit = det(Q_S); % Ist ungleich Null, deswegen ist das System Steuerbar
% Regelungsnormalform
rnf_LB_AS = canon(SS_LB_AS_Rigid,'companion');
%
%%%%%%%%%%%%%%%%%%%%%%%%%%%%%%%%%%%%%%%%%%%%%%%%
%% POLE PLACEMENT - SHORT PERIOD APPROXIMATION %
%%%%%%%%%%%%%%%%%%%%%%%%%%%%%%%%%%%%%%%%%%%%%%%%
% Desired damping and frequency
w0_AS_ziel = 2.500; % rad/s
D_AS_ziel = 0.707; % Find the reference
% Roots of a 2nd order system with the desired damping and frequency values
p_AS = roots([1 2*D_AS_ziel*w0_AS_ziel w0_AS_ziel^2]);
% Pole placement
kT = place(A_LB_AS,B_LB_AS,p_AS);
% K-values
k_eta_q = kT(1);
k_eta_alpha = kT(2);
%
```

```
%%%%%%%%%%%%%%%%%%%%%%%%%%%%%%%%%%%%%%%%%%%%%
%% MODIFIED RB SHORT PERIOD APPROXIMATION (CLOSED LOOP)
%%%%%%%%%%%%%%%%%%%%%%%%%%%%%%%%%%%%%%%%%%%%%
K_LB_AS_Rigid = zeros(size(B_LB_AS))';
K_LB_AS_Rigid(1) = -kT(1);
K_LB_AS_Rigid(2) = -kT(2);
% Modified System Matrices
A_LB_AS_mod = A_LB_AS-B_LB_AS*K_LB_AS_Rigid;
B_LB_AS_mod = B_LB_AS;
C_LB_AS_mod = C_LB_AS;
D_LB_AS_mod = D_LB_AS;
% State Space of modified system
SS_LB_AS_rigid_mod = ss(A_LB_AS_mod,B_LB_AS_mod,C_LB_AS_mod,D_LB_AS_mod);
% Transfer Function
TF_LB_AS_rigid_mod = tf(SS_LB_AS_rigid_mod);
%
F_q_eta_AS_rigid_mod = TF_LB_AS_rigid_mod(1);
F_alpha_eta_AS_rigid_mod = TF_LB_AS_rigid_mod(2);
% step(F_q_eta,'b',F_q_eta_AS_rigid,'r',F_q_eta_AS_rigid_mod,'m'); % compare the Short period
%%%%%%%%%%%%%%%%%%%%%%%%%%%%%%%%%%%%%%%%%%%%%
%% MODIFIED RB LONGITUDINAL APPROXIMATION (CLOSED LOOP)
%%%%%%%%%%%%%%%%%%%%%%%%%%%%%%%%%%%%%%%%%%%%%
K_LB_Rigid = zeros(size(B_LB))';
K_LB_Rigid(2,3) = -kT(1); %kT(1); %-kT(1); %
K_LB_Rigid(2,4) = -kT(2); %?kT(2); %-kT(2); %
% Modified System Matrices
A_LB_mod = A_LB-B_LB*K_LB_Rigid;
B_LB_mod = B_LB;
C_LB_mod = C_LB;
D_LB_mod = D_LB;
% State Space of modified system
SS_LB_rigid_mod = ss(A_LB_mod,B_LB_mod,C_LB_mod,D_LB_mod);
% Transfer Function
TF_LB_rigid_mod = tf(SS_LB_rigid_mod);
%
F_q_eta_rigid_LB_mod = TF_LB_rigid_mod(3,2);
F_alpha_eta_rigid_LB_mod = TF_LB_rigid_mod(4,2);
% step(F_q_eta,'b',F_q_eta_AS_rigid,'r',F_q_eta_rigid_LB_mod,'m'); % compare the Short period
%%%%%%%%%%%%%%%%%%%%%%%%%%%%%%%%%%%%%%%%%%%%%
%% MODIFIED FULL RIGIB BODY (RB) AIRCRAFT
```

```
%%%%%%%%%%%%%%%%%%%%%%%%%%%%%%%%%%%%%%%%%%%%%%%
K_Rigid = zeros(size(B))';
K_Rigid(4,3) = -kT(1);
K_Rigid(4,4) = -kT(2);
% Modified System Matrices
A_Rigid_mod = A-B*K_Rigid;
B_Rigid_mod = B;
C_Rigid_mod = C;
D_Rigid_mod = D;
% State Space of modified system
SS_rigid_mod = ss(A_Rigid_mod,B_Rigid_mod,C_Rigid_mod,D_Rigid_mod);
% Transfer Function
TF_rigid_mod = tf(SS_rigid_mod);
%
F_q_eta_rigid_mod = TF_rigid_mod(3,4);
F_alpha_eta_rigid_mod = TF_rigid_mod(4,4);
% step(F_q_eta,'b',F_q_eta_AS_rigid,'r',F_alpha_eta_rigid_mod,'m'); % compare the Short period
%
%
%%%%%%%%%%%%%%%%%%%%%%%%%%%%%%%%%%%%%%%%%%%%%%%
% % FLEXIBLE AIRCRAFT       %
%%%%%%%%%%%%%%%%%%%%%%%%%%%%%%%%%%%%%%%%%%%%%%%
%
%
%%%%%%%%%%%%%%%%%%%%%%%%%%%%%%%%%%%%%%%%%%%%%%%
%% LOAD FLEXIBLE AIRCRAFT SYSTEM MATRICES %
%%%%%%%%%%%%%%%%%%%%%%%%%%%%%%%%%%%%%%%%%%%%%%%
%state_space_name = 'State_space_flex_lcsv8_elev1deg.mat'; % flex
load([pfad,state_space_name_flex])
% System Matrix
A_flex = Lin_Model{1};
B_flex = Lin_Model{2};
C_flex = eye(size(A_flex));
D_flex = zeros(size(B_flex));
%%%%%%%%%%%%%%%%%%%%%%%%%%%%%%%%%%%%%%%%%%%%%%%
%% FULL FLEXIBLE (FLEX) AIRCRAFT %
%%%%%%%%%%%%%%%%%%%%%%%%%%%%%%%%%%%%%%%%%%%%%%%
%
% State-space system
SS_flex=ss(A_flex,B_flex,C_flex,D_flex);
%
```

```
% TF_flex=tf(SS_flex); % OVERFLOW !!!!!
% pzmap
f11=figure();
pzmap(SS_flex); legend 'FULL FLEXIBLE (FLEX) AIRCRAFT'; grid on;
% System Characteristics
[wn_Flex,D_Flex,poles_Flex]=damp(SS_flex);
%%%%%%%%%%%%%%%%%%%%%%%%%%%%%%%%%%%%%%%%%%%%%%%%%%%%%%%%%%%%%%%%
%% FLEX LONGITUDINAL MOTION APPROXIMATION (LB) %
%%%%%%%%%%%%%%%%%%%%%%%%%%%%%%%%%%%%%%%%%%%%%%%%%%%%%%%%%%%%%%%%
A_flex_LB= A_flex(1:4,1:4);
B_flex_LB(1:4,1)= B_flex(1:4,1);
B_flex_LB(1:4,2)= B_flex(1:4,4);
C_flex_LB= eye(size(A_flex_LB));
D_flex_LB= zeros(size(B_flex_LB));
%
SS_flex_LB= ss(A_flex_LB,B_flex_LB,C_flex_LB,D_flex_LB);
%
TF_flex_LB= tf(SS_flex_LB);
F_eta_q_flex_LB= TF_flex_LB(3,2);
F_eta_alpha_flex_LB= TF_flex_LB(4,2);
%
%%%%%%%%%%%%%%%%%%%%%%%%%%%%%%%%%%%%%%%%%%%%%%%%%%%%%%%%%%%%%%%%
%% FLEX SHORT PERIOD APPROXIMATION (AS) %
%%%%%%%%%%%%%%%%%%%%%%%%%%%%%%%%%%%%%%%%%%%%%%%%%%%%%%%%%%%%%%%%
A_flex_LB_AS(1,1:2)= A_flex_LB(3,3:4);
A_flex_LB_AS(2,1:2)= A_flex_LB(4,3:4);
B_flex_LB_AS= B_flex_LB(3:4,2);
C_flex_LB_AS= eye(size(A_flex_LB_AS));
D_flex_LB_AS= zeros(size(B_flex_LB_AS));
%
SS_flex_LB_AS= ss(A_flex_LB_AS,B_flex_LB_AS,C_flex_LB_AS,D_flex_LB_AS);
%
TF_flex_LB_AS= tf(SS_flex_LB_AS);
F_eta_q_flex_LB_AS= TF_flex_LB_AS(1);
F_eta_alpha_flex_LB_AS= TF_flex_LB_AS(2);
%
% step(F_q_eta_AS_rigid,'b',F_eta_q_flex_LB_AS,'r',5);
%%%%%%%%%%%%%%%%%%%%%%%%%%%%%%%%%%%%%%%%%%%%%%%%%%%%%%%%%%%%%%%%
%% FLEX STEUERBARKEIT
%%%%%%%%%%%%%%%%%%%%%%%%%%%%%%%%%%%%%%%%%%%%%%%%%%%%%%%%%%%%%%%%
%
Q_S_flex_AS = [B_flex_LB_AS, A_flex_LB_AS*B_flex_LB_AS];
```

```
Steuerbarkeit_flex = det(Q_S_flex_AS); % Ist ungleich Null, deswegen ist das System Steuerbar
% Regelungsnormalform
rnf_LB_AS = canon(SS_flex_LB_AS,'companion');
%
%%%%%%%%%%%%%%%%%%%%%%%%%%%%%%%%%%%%%%%%%%%%%%%%%%
%% FLEX POLEPLACEMENT - POLLVORGABE
%%%%%%%%%%%%%%%%%%%%%%%%%%%%%%%%%%%%%%%%%%%%%%%%%%
% SAME FREQUENCY AND DAMPING DESIRED VALUES AS IN THE RIGID AIRCRAFT
% Pole placement
kT_flex = place(A_flex_LB_AS,B_flex_LB_AS,p_AS);
% K-values
k_eta_q_flex = kT_flex(1);
k_eta_alpha_flex = kT_flex(2);
%
%%%%%%%%%%%%%%%%%%%%%%%%%%%%%%%%%%%%%%%%%%%%%%%%%%
%% MODIFIED FLEX SHORT PERIOD APPROXIMATION
%%%%%%%%%%%%%%%%%%%%%%%%%%%%%%%%%%%%%%%%%%%%%%%%%%
A_flex_LB_AS_mod= A_flex_LB_AS - B_flex_LB_AS*-kT_flex;
B_flex_LB_AS_mod= B_flex_LB_AS;
C_flex_LB_AS_mod= C_flex_LB_AS;
D_flex_LB_AS_mod= D_flex_LB_AS;
%
SS_flex_LB_AS_mod= ss(A_flex_LB_AS_mod,B_flex_LB_AS_mod,C_flex_LB_AS_mod,D_flex_LB_AS_mod);
%
TF_flex_LB_AS_mod= tf(SS_flex_LB_AS_mod);
F_eta_q_flex_LB_AS_mod= TF_flex_LB_AS_mod(1);
```